

AFIT/GE/ENG/97D-04

OPTIMIZED DESIGN METHODOLOGY OF CAVITY-BACKED
MICROSTRIP ANTENNAS WITH DIELECTRIC OVERLAYS

THESIS

Douglas Joseph Hermes
First Lieutenant, USAF

AFIT/GE/ENG/97D-04

DFIC QUALITY INSPECTED 3

Approved for public release; distribution unlimited

19980127 071

The views expressed in this thesis are those of the author and do not reflect the official policy or position of the Department of Defense or the United States Government.

AFIT/GE/ENG/97D-04

OPTIMIZED DESIGN METHODOLOGY OF CAVITY-BACKED
MICROSTRIP ANTENNAS WITH DIELECTRIC OVERLAYS

THESIS

Presented to the Faculty of the School of Engineering
of the Air Force Institute of Technology
Air University
In Partial Fulfillment of the
Requirements for the Degree of
Master of Science in Electrical Engineering

Douglas Joseph Hermes, B.S.E.E.

First Lieutenant, USAF

December 1997

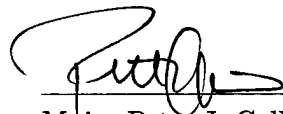

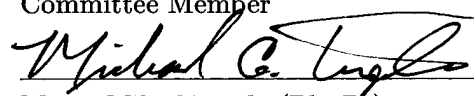
Approved for public release; distribution unlimited

OPTIMIZED DESIGN METHODOLOGY OF CAVITY-BACKED
MICROSTRIP ANTENNAS WITH DIELECTRIC OVERLAYS

Douglas Joseph Hermes, B.S.E.E.

First Lieutenant, USAF

Approved:

	<u>1 DEC 97</u>
Major Peter J. Collins (Ph. D.)	Date
Thesis Advisor	
	<u>1 Dec 97</u>
Dr. William P. Baker	Date
Committee Member	
	<u>1 Dec 97</u>
Major Mike Temple (Ph. D.)	Date
Committee Member	

Acknowledgements

I would like to thank my thesis committee members: my advisor Major Peter Collins, and other members Dr. William Baker and Major Mike Temple for their motivation and direction throughout this research process. This research was sponsored by Dr. Stephen Schneider from the Wright Laboratory Advanced RF Technology Branch (WL/AAMP) at Wright Patterson AFB, OH. I thank Dr. Schneider for his support, his technical guidance, and the use of the Radiation and Scattering Compact Antenna Laboratory (RASCAL) facility. I also thank James Mudd from WL/AAMP and John Meher from WL/AAMP and Mission Research Corporation for their technical expertise in the design, construction, and testing of the optimized antenna design. Thanks also to Ed Sandor of Rogers Corporation for supplying dielectric material used in the construction of an optimized antenna design. Thanks also to Major Edward Pohl for his help in Response Surface Methodology techniques and to Captain Kelce Wilson for his help in cubic splines empirical modeling. Finally, I am most thankful to my wife, Ruth, for her patience and understanding throughout the last 18 months of study and research. Without each person's assistance this research would not have been a success.

Douglas Joseph Hermes

Table of Contents

	Page
Acknowledgements	iii
List of Figures	viii
List of Tables	xiii
Abstract	xv
 I. Introduction	 1-1
1.1 Problem Statement	1-1
1.2 Assumptions	1-2
1.3 Scope	1-2
1.4 Resources	1-3
1.5 Overview	1-3
 II. Background	 2-1
2.1 Introduction	2-1
2.2 Dielectric Overlay Effects	2-1
2.2.1 Resonant Frequency	2-1
2.2.2 Antenna Gain	2-2
2.2.3 Frequency Bandwidth	2-6
2.2.4 Input Impedance and Input Impedance Bandwidth	2-6
2.3 Cavity Effects	2-7
2.3.1 Method Of Moments Analysis Of Cavity-Backed Antennas	2-7
2.3.2 Hybrid Finite Element Method Analysis Approach	2-8
2.4 Application Of Designed Experiments, Antenna Modeling, and Parameter Optimization	2-9
2.5 Summary	2-12

	Page
III. Research Methodology	3-1
3.1 RSM Tasks	3-1
3.2 Experiment Development	3-1
3.2.1 Input Variables	3-2
3.2.2 Variable Screening Procedure	3-2
3.2.3 Variable Levels	3-3
3.2.4 Experimental Designs	3-3
3.2.5 System Response and Measurement	3-6
3.3 System Modeling	3-8
3.3.1 Mechanistic Modeling	3-8
3.3.2 Empirical Modeling	3-9
3.3.3 Cubic Splines	3-9
3.3.4 Model Adequacy	3-13
3.4 Analysis of Variance	3-14
3.4.1 Test Hypotheses	3-17
3.4.2 Statistical Analysis	3-17
3.4.3 Example Analysis of Variance Test	3-20
3.5 Optimization Procedures	3-22
3.5.1 Quadratic Optimization Method	3-22
3.5.2 Simplex Method	3-25
3.6 Closing Comments	3-26
IV. Optimized Design Methodology Development	4-1
4.1 Experiment Development	4-1
4.1.1 Input Variables	4-1
4.1.2 Variable Screening Procedure	4-3
4.1.3 Variable Levels	4-3
4.1.4 System Response	4-6

	Page
4.1.5 Experimental Design	4-6
4.1.6 Hybrid Finite Element Method Measurements . . .	4-7
4.2 Average Antenna Gain Empirical Modeling	4-7
4.2.1 Cubic Splines Empirical Modeling	4-8
4.2.2 Least Squares Empirical Modeling	4-9
4.2.3 Average Antenna Gain Model Adequacy	4-10
4.3 Analysis of Variance	4-17
4.3.1 Frequency Effects ANOVA Test	4-17
4.3.2 Full Effects ANOVA Test	4-18
4.4 Optimization Procedures	4-20
4.5 Additional System Response Modeling Possibilities	4-24
4.5.1 Input Impedance Modeling	4-27
4.5.2 Average Antenna Gain Modeling Near the Cavity Ground Plane	4-28
4.6 Closing Comments	4-38
V. Optimized Design Methodology Implementation	5-1
5.1 Experiment Development	5-1
5.1.1 Design Methodology Input Variable Levels	5-1
5.1.2 Measured Responses	5-3
5.1.3 Experimental Design	5-6
5.2 Average Antenna Gain and Input Impedance Modeling . . .	5-6
5.2.1 Average Antenna Gain Model Adequacy	5-7
5.2.2 Antenna Input Impedance Model Adequacy	5-8
5.3 Average Antenna Gain and Antenna Input Impedance Opti- mization	5-18
5.4 Compact Range Validation of Designed Cavity-Backed Microstrip Antenna With Dielectric Overlays	5-25
5.5 Closing Comments	5-27

	Page
VI. Conclusion	6-1
6.1 Summary and Conclusions	6-1
6.2 Recommendations	6-3
Bibliography	BIB-1
Vita	VITA-1

List of Figures

Figure		Page
2.1.	Microstrip Antenna With Dielectric Superstrate Geometry	2-2
2.2.	Hertzian Electric Dipole (HED) Embedded In Substrate With Multiple Superstrates	2-4
2.3.	Equivalent Transmission Line Model	2-4
2.4.	Microstrip Antenna With Superstrate Layer	2-5
2.5.	Geometry Of Cavity-Backed Aperture Antenna With Overlays . . .	2-8
2.6.	Multi-layer Microstrip Patch Antenna	2-10
3.1.	Central Composite Design For $k = 3$	3-6
3.2.	Normal Probability Plot of Least Squares System Response Model	3-14
3.3.	Plot of Residuals Versus Fitted Values	3-15
3.4.	Plot of Residuals Versus Individual Variable Parameter	3-15
3.5.	System Graphical Surface Response	3-23
3.6.	Expansion of Simplex Constraint Equations Towards an Optimal Solution	3-26
4.1.	Antenna Configuration	4-2
4.2.	Smith Chart Analysis of Input Admittance Values With First and Second Superstrate Dielectric Relative Permittivities Equal to 1.0 ($\epsilon_{r1} = \epsilon_{r2} = 1.0$)	4-5
4.3.	Smith Chart Analysis of Input Admittance Values With First and Second Superstrate Dielectric Relative Permittivities Equal to 8.0 ($\epsilon_{r1} = \epsilon_{r2} = 8.0$)	4-5
4.4.	Normal Probability Plots of Cubic Spline and Least Squares System Response Models	4-11
4.5.	Cubic Spline and Least Squares Residuals Versus Fitted Values . .	4-12
4.6.	Cubic Spline and Least Squares Residuals Versus Frequency Values	4-13

Figure		Page
4.7.	Cubic Spline and Least Squares Residuals Versus First Layer Relative Permittivity Values	4-14
4.8.	Cubic Spline and Least Squares Residuals Versus Second Layer Relative Permittivity Values	4-15
4.9.	Cubic Spline and Least Squares Residuals Versus First Layer Thickness Values	4-16
4.10.	Optimization Process Flow Chart	4-22
4.11.	Optimized Antenna Pattern	4-23
4.12.	First Layer Relative Permittivity and Frequency Effects Near the Optimized Location	4-24
4.13.	Second Layer Relative Permittivity and Frequency Effects Near the Optimized Location	4-25
4.14.	First Layer Thickness and Frequency Effects Near the Optimized Location	4-25
4.15.	First and Second Layer Relative Permittivity Effects Near the Optimized Location	4-26
4.16.	First Layer Thickness and Second Layer Relative Permittivity Effects Near the Optimized Location	4-26
4.17.	First Layer Relative Permittivity and Thickness Effects Near the Optimized Location	4-27
4.18.	Normal Probability Plots of Cubic Spline Input Impedance Residuals	4-29
4.19.	Cubic Spline Impedance Residuals Versus Fitted Values	4-30
4.20.	Cubic Spline Impedance Residuals Versus Frequency Values	4-31
4.21.	Cubic Spline Impedance Residuals Versus First Layer Relative Permittivity Values	4-32
4.22.	Cubic Spline Impedance Residuals Versus Second Layer Relative Permittivity Values	4-33
4.23.	Cubic Spline Impedance Residuals Versus First Layer Thickness Values	4-34
4.24.	Cubic Spline Normal Probability Plot of Residuals Near Ground Plane	4-35
4.25.	Cubic Splines Residuals Near Ground Plane Versus Fitted Values .	4-36

Figure		Page
4.26.	Cubic Splines Residuals Near Ground Plane Versus Frequency Values	4-36
4.27.	Cubic Spline Residuals Near Ground Plane Versus First Layer Relative Permittivity Values	4-37
4.28.	Cubic Spline Residuals Near Ground Plane Versus Second Layer Relative Permittivity Values	4-37
4.29.	Cubic Spline Residuals Near Ground Plane Versus First Layer Thickness Values	4-38
5.1.	Scaled Antenna Design	5-2
5.2.	Scaled Antenna Smith Chart Analysis of Input Impedance Values With First and Second Superstrate Dielectric Relative Permittivities Equal to 1.0 ($\epsilon_{r1} = \epsilon_{r2} = 1.0$)	5-4
5.3.	Scaled Antenna Smith Chart Analysis of Input Impedance Values With First and Second Superstrate Dielectric Relative Permittivities Equal to 10.0 ($\epsilon_{r1} = \epsilon_{r2} = 10.0$)	5-5
5.4.	Average Antenna Gain Empirical Model Normal Probability Plots of Residuals	5-8
5.5.	Average Antenna Gain Empirical Model Residuals Versus Fitted Values	5-9
5.6.	Average Antenna Gain Empirical Model Residuals Versus Frequency Values	5-9
5.7.	Average Antenna Gain Empirical Model Residuals Versus First Layer Relative Permittivity Values	5-10
5.8.	Average Antenna Gain Empirical Model Residuals Versus Second Layer Relative Permittivity Values	5-10
5.9.	Average Antenna Gain Empirical Model Residuals Versus First Layer Thickness Values	5-11
5.10.	Antenna Input Impedance Empirical Model Normal Probability Plots of Residuals	5-12
5.11.	Antenna Input Impedance Empirical Model Residuals Versus Fitted Values	5-13

Figure		Page
5.12.	Antenna Input Impedance Empirical Model Residuals Versus Frequency Values	5-14
5.13.	Antenna Input Impedance Empirical Model Residuals Versus First Layer Relative Permittivity Values	5-15
5.14.	Antenna Input Impedance Empirical Model Residuals Versus Second Layer Relative Permittivity Values	5-16
5.15.	Antenna Input Impedance Empirical Model Residuals Versus First Layer Thickness Values	5-17
5.16.	Antenna Radiation Pattern (Frequency = 1.2 GHz, First Superstrate Dielectric Layer Permittivity = Second Superstrate Dielectric Layer Relative Permittivity = 2.0)	5-19
5.17.	Antenna Radiation Pattern (Frequency = 1.4 GHz, First Superstrate Dielectric Layer Permittivity = Second Superstrate Dielectric Layer Relative Permittivity = 10.0)	5-19
5.18.	Optimization Starting Radiation Pattern	5-20
5.19.	Optimized Antenna Design Radiation Pattern	5-21
5.20.	First Layer Relative Permittivity and Frequency Effects Near the Optimized Location	5-21
5.21.	Second Layer Relative Permittivity and Frequency Effects Near the Optimized Location	5-22
5.22.	First Layer Thickness and Frequency Effects Near the Optimized Location	5-22
5.23.	First and Second Layer Relative Permittivity Effects Near the Optimized Location	5-23
5.24.	First Layer Thickness and Second Layer Relative Permittivity Effects Near the Optimized Location	5-23
5.25.	First Layer Relative Permittivity and Thickness Effects Near the Optimized Location	5-24
5.26.	Constructed Antenna	5-26
5.27.	Predicted Radiation Pattern for the Constructed Antenna Design .	5-27

Figure		Page
5.28.	Electric Field with Phi Polarization ($\phi = 0$ <i>degress</i>)	5-28
5.29.	Electric Field with Theta Polarization ($\phi = 0$ <i>degress</i>)	5-29
5.30.	Electric Field with Phi Polarization ($\phi = 90$ <i>degress</i>)	5-30
5.31.	Electric Field with Theta Polarization ($\phi = 90$ <i>degress</i>)	5-31

List of Tables

Table		Page
2.1.	First Resonance Condition	2-3
2.2.	Second Resonance Condition	2-3
2.3.	GRS Model Fixed Parameters	2-11
2.4.	GRS Variable Ranges	2-11
2.5.	Optimum GRS Antenna Design	2-11
3.1.	Two Factor, Three Level, Full Factorial Design	3-4
3.2.	Full Factorial Design with Two Variables, Three Levels, and m Replicates	3-5
3.3.	General Two Variable Full Factorial Design	3-16
3.4.	Degrees of Freedom	3-19
3.5.	ANOVA Table for the Two-Factor Factorial Experiment	3-20
3.6.	Experiment Data for Example ANOVA Test	3-20
3.7.	Example ANOVA Results	3-21
4.1.	Constant Antenna Design Parameters	4-3
4.2.	Variable Antenna Design Parameters	4-6
4.3.	Full Factorial Design	4-7
4.4.	Model Adequacy Test Variable Levels	4-10
4.5.	Model Adequacy Test Cases	4-10
4.6.	Mean and Standard Deviation Values of Cubic Spline and Least Squares Residuals	4-11
4.7.	Frequency ANOVA Test Variable Levels	4-18
4.8.	Cubic Spline Empirical Model Frequency ANOVA Test Results	4-18
4.9.	HFEM Frequency ANOVA Test Results	4-18
4.10.	Full ANOVA Test Variable Levels	4-19

Table		Page
4.11.	Full ANOVA Test Results	4-20
4.12.	Initial Optimized Location Guess	4-21
4.13.	Optimized Antenna Design	4-21
4.14.	Real and Imaginary Impedance Residual Means and Standard Deviations	4-28
4.15.	Average Antenna Gain Cubic Spline Model Residual Mean And Residual Standard Deviation Values Near Ground Plane	4-35
5.1.	Scaled Constant Antenna Design Parameters	5-2
5.2.	Scaled Variable Antenna Design Parameters	5-4
5.3.	Scaled Antenna Full Factorial Design	5-6
5.4.	Scaled Antenna Model Adequacy Test Variable Levels	5-6
5.5.	Scaled Antenna Model Adequacy Test Cases	5-7
5.6.	Average Antenna Gain Empirical Model Residual Mean And Residual Standard Deviation Values	5-8
5.7.	Real and Imaginary Antenna Input Impedance Empirical Model Mean Residual and Residual Standard Deviations Values	5-11
5.8.	Optimization Starting Point	5-18
5.9.	Optimized Antenna Design	5-20
5.10.	Constructed Antenna Design Parameters	5-25

Abstract

The optimized design methodology implemented in this research employs a design methodology, namely Response Surface Methodology (RSM), that is relatively new to the electromagnetics field. The design methodology used a full factorial designed experiment, a Hybrid Finite Element Method (HFEM) analysis code, a cubic spline empirical model, an Analysis of Variance (ANOVA) test, and a simplex optimization code to successfully measure, predict, analyze, and optimize average antenna gain and antenna input impedance for a cavity-backed microstrip antenna with dielectric overlays. Using the antenna operating frequency, the relative permittivities of two dielectric superstrate layers, and the thickness of a single dielectric superstrate layer as experiment variables, the full factorial designed experiment used a HFEM analysis code to determine average antenna gain and antenna input impedance for five levels of each experiment variable. Based on HFEM results from the full factorial designed experiment, a cubic spline empirical model successfully predicted average antenna gain and input impedance values for variable combinations within the experiment variable limits. The ANOVA test determined the impact each design variable introduced on the average antenna gain and indicated the areas of greatest concern during manufacturing and testing phases. Using simplex optimization, an optimized, realizable antenna design with minimum average antenna gain above the antenna bore sight and a target input impedance of 50 ohms was located within two minutes that agreed within approximately 4.0 percent to HFEM values determined from design validation tests, while measured results from the constructed optimized antenna design closely replicated the predicted antenna patterns and the predicted input impedance value. The design methodology eliminated the need of numerous and costly antenna builds by applying straight-forward RSM techniques and saved countless man hours. The significant time savings found using this optimized design methodology demonstrates the power of RSM and motivates its application to other electromagnetic design problems.

OPTIMIZED DESIGN METHODOLOGY OF CAVITY-BACKED MICROSTRIP ANTENNAS WITH DIELECTRIC OVERLAYS

I. Introduction

Proven through the years, antenna design generally follows two principle paths: either original research or existing antenna scaling. In general, both antenna design approaches require in-depth modeling and testing that use established numerical methods such as Method of Moments (MoM) or Finite Element Method (FEM) validation prior to antenna construction. Following the construction of a physical antenna, additional verification of the antenna's operational characteristics using antenna chamber measurements usually completes the overall antenna design procedure. This process demands large amounts of time and computational effort as well as expensive prototype builds. A need exists in the antenna design field for a new design methodology that maintains antenna design accuracy while providing fast, accurate antenna designs. Response Surface Methodology (RSM) and designed experiments offer a solution. This research applies the principles of RSM and develops an optimized antenna design methodology that uses Hybrid Finite Element Method (HFEM) predictions, designed experiments, empirical modeling, Analysis of Variance (ANOVA) tests, and simplex optimization. The design methodology is illustrated by applying the principles of dielectric loading to a cavity-backed microstrip antenna and determines an optimized antenna design within minutes rather than days without using older, time consuming antenna design approaches.

1.1 Problem Statement

This research is tasked to develop an optimized antenna design methodology that uses RSM techniques and to illustrate its application on a cavity-backed microstrip antenna by employing the principles of dielectric loading. The general antenna configuration includes:

- A rectangular cavity with constant dimensions,

- A rectangular radiating aperture with constant feed pin location that is immersed in a dielectric substrate with constant relative permittivity,
- Two dielectric superstrate layers.

The optimized design methodology's goal is an optimized antenna design in minutes rather than the days typically required using traditional antenna design approaches.

1.2 Assumptions

Assumptions prior to beginning research progress include:

1. The ability to accurately predict antenna pattern shape and antenna gain using a HFEM code,
2. The ability to control antenna pattern shape, antenna gain, and antenna input impedance using dielectric overlays,
3. The ability to sufficiently sample antenna gain and antenna input impedance values using designed experiments,
4. The ability to empirically model average antenna gain and antenna input impedance.

1.3 Scope

While the design methodology developed here could be applied to any electromagnetic design problem, for the purposes of illustration, only a cavity-backed microstrip antenna design problem will be examined. The methodology design problem accomplishes the following objectives:

1. Develops an optimized design methodology based on HFEM code results describing a cavity-backed microstrip antenna with dielectric overlays.
2. Creates an empirical model that accurately describes the antenna gain results and input impedance in a region of interest.
3. Validates the empirical model within the region of interest.

4. Applies the principles of ANOVA testing to determine the effects of experiment variables on antenna gain thereby indicating the antenna gain's sensitivity to variation in experiment variable levels.
5. Applies an optimization routine to the empirical model to locate and define an optimized antenna configuration in the desired region of interest.
6. Validates the empirical model based optimized antenna design by comparing predicted model results with HFEM code results and constructed antenna measurements of identical antenna configurations.

1.4 Resources

Resources necessary for the research accomplishment include:

1. An HFEM code that specifically accommodates the analysis of cavity-backed microstrip antennas,
2. A computer resource capable of performing large numbers of HFEM code predictions within a short period time,
3. A compact anechoic range facility for designed antenna measurements.

1.5 Overview

This document contains a review of the recent significant work performed in the area of dielectric loading, the theory behind RSM and designed experiments, the development of an optimized design methodology, and the optimized design methodology applied to a realizable antenna design with both predicted and measured antenna results. Chapter II reviews current literature available in the area of dielectric loading effects of microstrip antennas, antenna analysis techniques using MoM and HFEM codes, and an original attempt of microstrip antenna optimization using an adapted form of RSM and designed experiments. Chapter III provides the theory behind the optimized design methodology developed later in Chapter IV. Chapter IV develops the optimized design methodology using a specific antenna configuration and validates the design methodology using standard designed experiments techniques and HFEM results. Chapter V applies the design

methodology previously developed in Chapter IV to a realizable antenna design using a common substrate dielectric constant and designs an optimized antenna. Chapter V then validates the designed antenna using two approaches: HFEM code validation and measured antenna parameter validation. Chapter VI draws conclusions from the results found in the previous chapters and recommends areas where this design methodology is applicable.

II. Background

2.1 Introduction

The optimized design methodology developed in Chapter IV and applied in Chapter V uses the principles of dielectric overlays on a cavity-backed microstrip antenna to control antenna gain and input impedance with the added effect of controlling the antenna radiation pattern. Chapters IV and V directly apply the dielectric overlay effects described in Section 2.2 to an optimized design methodology development by using an analysis technique similar to those described in Section 2.3. Section 2.4 introduces an initial optimization example applying an adapted form of Response Surface Methodology (RSM) and designed experiments to microstrip antenna design. In a similar fashion, the optimized design methodology of Chapter IV applies a form of RSM to a cavity-backed microstrip antenna with dielectric overlays making Sections 2.2, 2.3, and 2.4 directly applicable.

2.2 Dielectric Overlay Effects

According to the effects of Snell's Law, image theory, and boundary conditions, dielectric overlays strongly influence antenna frequency, gain, input impedance, input impedance bandwidth, and frequency bandwidth [1–4, 6, 11, 12, 17, 18, 21]. For example, an optimized selection of superstrate permittivity or permeability accompanied by an optimized selection of superstrate thickness positively affects antenna gain while negatively affecting other antenna properties [2, 11, 21].

2.2.1 Resonant Frequency. Using the general microstrip antenna design displayed in Figure 2.1, Bahl demonstrated that loading a microstrip antenna with a dielectric superstrate altered the antenna's resonant frequency [3]. The absolute resonant frequency change increased with operating frequency, superstrate permittivity, and the superstrate thickness where the fractional resonant frequency change relative to the unloaded case can be calculated using Equation (2.1) for a fixed superstrate thickness [3].

$$\frac{\Delta f_r}{f_r} = \frac{f_r(d=0) - f_r(d)}{f_r(d=0)} \quad (2.1)$$

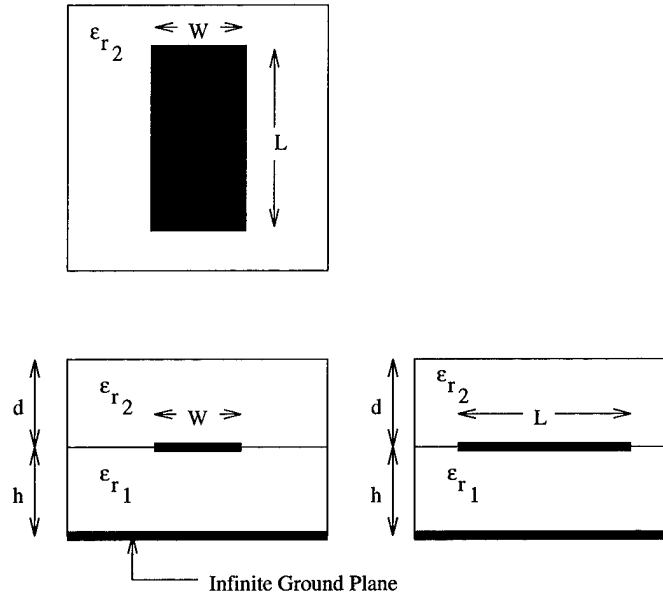


Figure 2.1 Microstrip Antenna With Dielectric Superstrate Geometry

In Equation (2.1), $f_r(d = 0)$ and $f_r(d)$ represent the unloaded resonant frequency case and the loaded resonant frequency case respectively. Equation (2.2) provides a first order resonant frequency change in terms of effective permittivity values

$$\frac{\Delta f_r}{f_r} = \frac{\sqrt{\epsilon_e} - \sqrt{\epsilon_{eo}}}{\sqrt{\epsilon_o}} \quad (2.2)$$

where ϵ_{eo} and ϵ_e represent the effective permittivity without superstrate loading and the effective permittivity with superstrate loading respectively for a fixed superstrate thickness. Bahl observed that the antenna's operating frequency decreased as the superstrate's permittivity increased and as the superstrate's thickness increased [3].

2.2.2 Antenna Gain. Printed circuit antennas suffer from the disadvantage of low antenna gain. Using Green's functions and contour integration, Alexopoulos derived that dielectrically loading an embedded Hertzian dipole with a single dielectric superstrate affects the resulting antenna gain [2]. Specifically, the proper choices of dielectric constants and thicknesses for the substrate and superstrate layers increased the antenna gain and led to the development of two resonance conditions. Tables 2.1 and 2.2 list the details for

Superstrate thickness	0.25λ
Substrate thickness	0.50λ
Dipole location	Substrate center
Permittivity	$\epsilon_{superstrate} \gg \epsilon_{substrate}$

Table 2.1 First Resonance Condition

Superstrate thickness	0.25λ
Substrate thickness	0.25λ
Dipole location	Substrate/superstrate interface
Permeability	$\mu_{superstrate} \gg \mu_{substrate}$

Table 2.2 Second Resonance Condition

each condition. Application of the resonance conditions led to the development of a simple transmission line model for quick and accurate gain calculations.

Extending the ideas developed by Alexopoulos, Yang introduced a transmission line model describing an embedded Hertzian dipole antenna covered with multiple superstrate layers [21]. Figure 2.3 illustrates the transmission line model describing the antenna design of Figure 2.2. From a ray optics perspective, rays emanating from the antenna and incident upon the interface of different media will bend according to Snell's Law. With a transmission line analysis, Yang found that the proper arrangement of multiple layer parameters bent transmitted rays in a prescribed direction. The antenna design used by Yang displayed in Figure 2.2 assumes an infinite ground plane, k superstrate layers, and infinite dielectric layers in length and width. Using the resonance conditions established by Alexopoulos for the single layer superstrate design, Yang noticed that when using configurations of multiple superstrate layers, the alternation of layers of large permittivity with layers of large permeability yields desired high antenna gain. Specifically, in the case of the first resonant condition, the even numbered layers have large permittivity values, and the odd numbered layers have large permeability values. In the case of the second resonant condition, the even numbered layers have large permeability values, and the odd numbered layers have large permittivity values. When resonant conditions are satisfied and layer parameters are met, the high gain condition described by the transmission line model corresponds to the maximum voltage transfer from the incident voltage wave V_{in} to the line voltage of the substrate V_1 , at a prescribed incident angle θ [21]. For the first res-

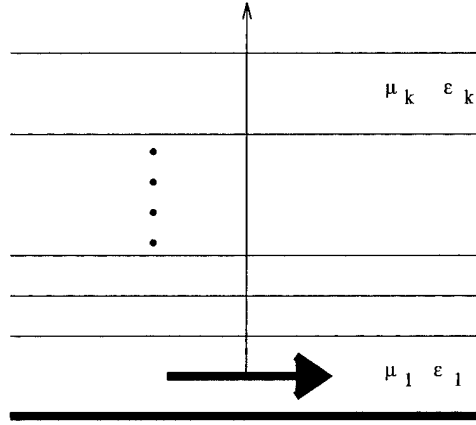


Figure 2.2 Hertzian Electric Dipole (HED) Embedded In Substrate With Multiple Superstrates

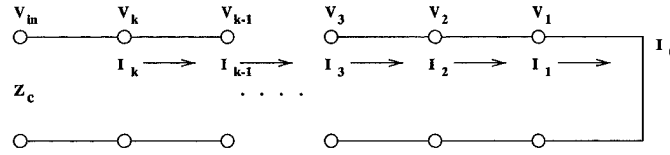


Figure 2.3 Equivalent Transmission Line Model

onant condition at a prescribed incident angle θ , the maximum voltage transfer for $2k + 1$ layers is described by

$$V_1 = V_{in} \frac{Z_{c1} Z_{c3} Z_{c5} \cdots Z_{c(2k+1)}}{Z_{c0} Z_{c2} Z_{c4} \cdots Z_{c(2k)}}, \quad (2.3)$$

while

$$V_1 = V_{in} \frac{Z_{c1} Z_{c3} Z_{c5} \cdots Z_{c(2k-1)}}{Z_{c2} Z_{c4} \cdots Z_{c(2k)}} \quad (2.4)$$

describes the maximum voltage transfer for $2k$ layers. In Equations (2.3) and (2.4), Z_{ci} is the characteristic impedance of layer i for $i = 0, 1, 2, \dots, k$. Likewise, in the case of the second resonant condition at a prescribed incident angle θ , the maximum voltage transfer for $2k + 1$ layers is described by

$$V_1 = V_{in} \frac{Z_{c2} Z_{c4} Z_{c6} \cdots Z_{c(2k)}}{Z_{c3} Z_{c5} Z_{c7} \cdots Z_{c(2k+1)}}, \quad (2.5)$$

while

$$V_1 = V_{in} \frac{Z_{c2} Z_{c4} Z_{c6} \cdots Z_{c(2k)}}{Z_{c0} Z_{c3} Z_{c5} \cdots Z_{c(2k-1)}} \quad (2.6)$$

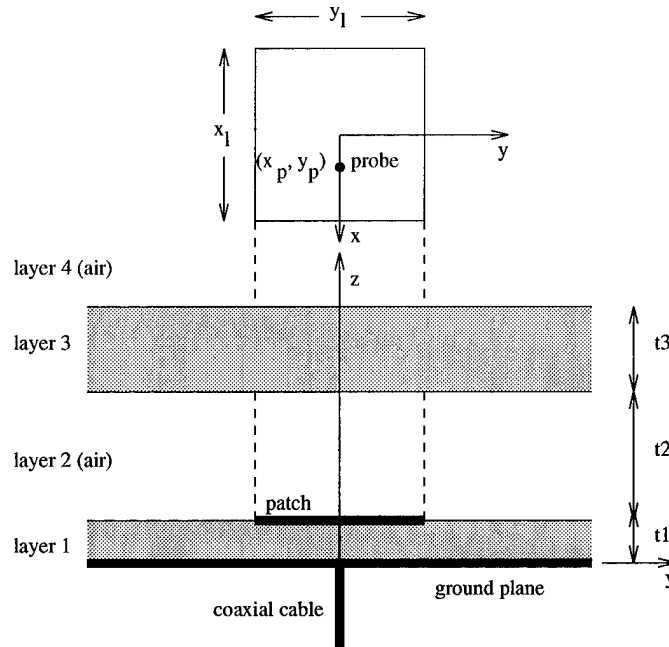


Figure 2.4 Microstrip Antenna With Superstrate Layer

describes the maximum voltage transfer for $2k$ layers.

Using a Method of Moments (MoM) approach as opposed to a transmission line model, Shen devised another antenna design technique for antennas with dielectric superstrates [17]. Consider the antenna displayed in Figure 2.4. Shen discovered that using a superstrate layer with a quarter wavelength thickness, a high relative permittivity ϵ_r in layer three, and adjusting t_2 led to high antenna gain. Shen observed that the antenna gain first increased with the distance t_2 to a maximum value, G_{max} , at a resonant distance, t_{2r} . For every t_3 , a corresponding t_{2r} and G_{max} exists that are functions of the t_3 plate thickness. Generally, as t_3 increases, t_{2r} decreases, and G_{max} occurs when t_3 is $\frac{\lambda_3}{4}$. The thickness t_1 is not of immense importance since the thickness of layer 2 may be adjusted to account for negative effects introduced by layer one. For initial considerations and assuming no superstrate loading, the initial antenna design defines the thickness of layer one. In summary, the key resonance condition is the electrical thickness of t_3 , and the final resonance condition can be tuned by adjusting the value of t_2 .

2.2.3 Frequency Bandwidth. A major limitation in antenna designs implementing dielectric loading is the frequency bandwidth. According to Shen and Yang, antenna frequency bandwidth decreases as antenna gain increases [17, 21]. In other words, the frequency bandwidth continues to decrease with the addition of gain enhancing superstrate layers. Shen defines the half power frequency bandwidth as

$$\frac{\Delta f_{0.5G}}{f_0} = \frac{(f_2 - f_1) |_{G=0.5G_{max}}}{f_0} \quad (2.7)$$

where G is the antenna gain and f is the frequency.

2.2.4 Input Impedance and Input Impedance Bandwidth. A second limitation to the application of dielectric superstrates used for gain enhancement is the input impedance. Soares noticed that in an antenna configuration with a single dielectric superstrate, the antenna's input impedance dramatically decreased as the antenna's superstrate permittivity increased [18]. The only way to maintain an adequate input impedance level is to reduce antenna gain when implementing dielectric superstrates for gain enhancement [17].

In comparison with the frequency bandwidth, the addition of superstrate layers reduces the antenna's input impedance bandwidth from original levels without dielectric loading and causes the input impedance bandwidth to become even more restrictive than the frequency bandwidth [17, 18]. Shen defines the input impedance bandwidth as

$$\frac{\Delta f_{0.69R_r}}{f_r} = \frac{(f_2 - f_1) |_{R=0.69R_r}}{f_r} \quad (2.8)$$

where R is the input impedance at $0.69R_r$, R_r is the resonant input impedance, and f is the frequency at specific R values. When matched at resonance, the impedance bandwidth using the impedance coefficient, 0.69, has a return loss below -10 dB. The consequences of dramatic input impedance level changes demand that input impedance requirements be maintained throughout the entire antenna design process.

2.3 Cavity Effects

In the case of microstrip antennas, the frequency bandwidth limits their usefulness. Thick substrate layers circumvent this problem but create the additional problem of surface wave propagation. In the case of cavity-backed microstrip antennas, the microstrip antenna employs a metallic cavity to enclose the antenna and suppress surface waves [6]. In addition to substrate mode elimination, the metallic cavity serves as a heat sink and improves heat dissipation [6]. Analysis of cavity-backed aperture antennas performed using the Method of Moments (MoM) and a Hybrid Finite Element Method (HFEM) are discussed in the following sections.

2.3.1 Method Of Moments Analysis Of Cavity-Backed Antennas. Due largely to the development of high speed computers with enormous computational capabilities, complex antenna designs can be solved, modeled, and optimized by the implementation of MoM. In their analyses, Biebl and Lee *et al.* demonstrated the principles behind MoM analysis of cavity-backed aperture antennas [4,11]. Using the aperture antenna with multiple layers in Figure 2.5, Biebl implemented MoM to analyze the effects of multiple dielectric overlays on an aperture antenna. Lee on the other hand studied an antenna with a single dielectric overlay using MoM. Both Biebl and Lee divided the antenna into two regions, the cavity region and the superstrate region. In the cavity region, dyadic Green's functions applied in the spatial domain corresponded to the physical design and shape of the cavity itself [11]. Similarly, in the superstrate region, dyadic Green's functions applied in the spectral domain accounted for the radiating field that traveled through the dielectric overlays and into free space beyond. By modeling the superstrate region as a series connection of transmission lines and the cavity region as a waveguide, MoM solved the respective regional integral equations based on dyadic Green's functions and determined the resulting solution by applying a weighted series summation. In the superstrate region, the dyadic Green's function accounted for wave impedance's for both the transverse magnetic mode and the transverse electric mode, and in the cavity region, the wave propagation constant, the attenuation factor, and ohmic power losses. The MoM solution was only valid for operating frequencies greater than the cavity cutoff frequency. With MoM, the double in-

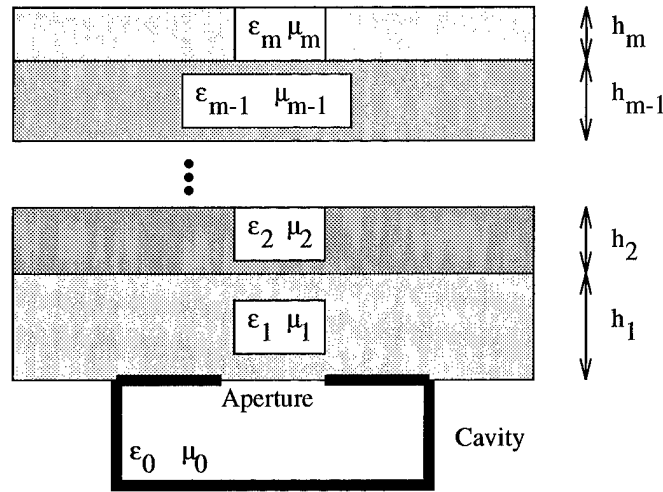


Figure 2.5 Geometry Of Cavity-Backed Aperture Antenna With Overlays

tegral dyadic Green's function was solved directly without the introduction of asymptotic approximation techniques.

Using the MoM technique, the effects of dielectric loading of cavity-backed antennas coincided well with dielectric overlay effects on printed circuit antennas. Lee observed that as the permittivity of the single superstrate layer increased, the resonant frequency and the input impedance of the cavity-backed aperture antenna decreased. In the same fashion, as the thickness of the single superstrate layer increased, the resonant frequency and the input impedance of the cavity-backed aperture antenna decreased. The superstrate permittivity and thickness effects of the cavity-backed aperture antenna are dual effects of the printed circuit antenna with dielectric overlays.

2.3.2 Hybrid Finite Element Method Analysis Approach. Cheng *et al.* [6] applied a hybrid analysis technique to a complex cavity-backed microstrip antenna with dielectric overlays that emphasized the positive attributes of both MoM and Finite Element Method (FEM) principles known as the Hybrid Finite Element Method (HFEM) and proved superior to the pure MoM analysis procedure. As in the MoM procedure, the hybrid technique established two analysis regions, the superstrate region and the cavity region. Although computationally efficient in solving spatially unbounded problems, MoM is applicable only to a few specific cavity configurations with known Green's functions. Similarly, FEM is

useful only for bounded regions of known volume and is unreliable for unbounded volumes. Consequently, Cheng applied MoM to solve the dyadic Green's functions for the spectral domain in the superstrate region and FEM to solve the electromagnetic field distributions due to the physical complexities of the cavity region. FEM divided the cavity configuration into discrete volumetric portions and analyzed each individual portion separately. Upon completion of the individual portion analysis, the FEM code summed the individual electromagnetic solutions and determined the net cavity solution. The overall antenna solution combined both regional solutions obtained from MoM and FEM and satisfied the tangential boundary conditions. Specifically, the tangential field components resulting from the MoM spectral solution of the superstrate region equaled the tangential field components resulting from the FEM spatial solution of the cavity region at the boundary separating the two regions.

2.4 *Application Of Designed Experiments, Antenna Modeling, and Parameter Optimization*

Due to the effects and limitations of dielectric overlays, the design of microstrip antennas with single or multiple dielectric overlays requires numerous tests, builds, and measurements. A new design approach used by Moosbrugger *et al.* [15] implemented a design methodology composed of several prototype antennas, a Global Response Surface (GRS) model, and a parameter optimization routine. From the antenna design in Figure 2.6, the design methodology used antenna frequency, resonant patch length L_r , and dielectric layer separation S as experimental input parameters and driven patch input impedance as the experimental measured response. The remaining physical parameters labeled in Figure 2.6 remained fixed values and are listed in Table 2.3. Using five resonant patch lengths, four layer separation distances, and 31 frequencies, the design methodology created a $5 \times 4 \times 31$ full factorial designed experiment where full factorial designed experiments measure the system response at each possible combination of the input variables. In this case, the full factorial designed experiment measured the antenna input impedance for each of the resulting 620 ($5 \times 4 \times 31$) antenna configurations. Table 2.4 lists the ranges for the experimental variables. Based upon the completed impedance measurements set,

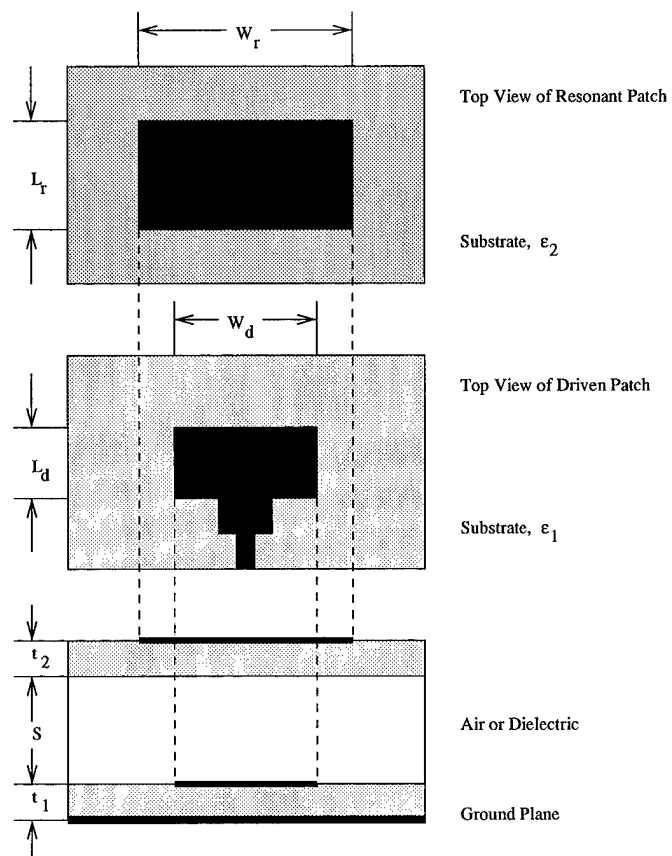


Figure 2.6 Multi-layer Microstrip Patch Antenna

Parameter	Fixed Value
ϵ_1	2.33
ϵ_2	2.55
t_1	1.2mm
t_2	0.8mm
L_d	38mm
W_d	50mm
W_r	50mm

Table 2.3 GRS Model Fixed Parameters

Parameter	Symbol	Range
Resonant patch length	L_r	38.1mm to 46.1mm
Dielectric layer separation	S	5.1mm to 10.1mm
Frequency	f	2.3GHz to 2.9GHz

Table 2.4 GRS Variable Ranges

the implementation of a GRS model used a cubic spline algorithm to predict driven patch impedance values at various variable value combinations within the experimental limitations of frequency, layer separation, and resonant patch length. The additional application of a simplex method optimization routine allowed the GRS model to locate optimum impedance and corresponding variable values in specific frequency ranges. Table 2.5 describes an optimized antenna configuration completed using this design methodology where each variable value is within its range limits. A fabricated antenna constructed from the Table 2.5 design agreed extremely well with predicted GRS impedance and return loss values. The design methodology described here required less than two minutes to locate an optimized antenna design since the GRS cubic spline antenna model required less than one second for impedance determination. Moosbrugger *et al.* demonstrated that under controlled conditions antenna design speed is greatly improved while maintaining design accuracy.

Parameter	Symbol	Value
Resonant patch length	L_r	41.30mm
Dielectric layer separation	S	7.12mm
Frequency	f	2.5GHz to 2.7GHz
Driven patch input impedance	Z_{opt}	20 Ω

Table 2.5 Optimum GRS Antenna Design

2.5 Summary

The effects of dielectric superstrate layers on printed circuit antennas as well as cavity-backed antennas must be included in the final antenna configuration. The selection of dielectric superstrate and substrate permittivity and thickness values strongly affect antenna resonant frequency, gain, input impedance, and frequency bandwidth in different ways. Proven by transmission line theory, MoM techniques, and HFEM procedures, the proper selection of dielectric constants and thickness for superstrate layers improves antenna gain while decreasing the antenna's resonant frequency, input impedance, and frequency bandwidth. To reduce the difficulties encountered during the antenna design phase, a new antenna design methodology was introduced that corresponds well with established antenna design methods and requires only seconds for completion. The design methodology developed in Chapter IV incorporates the basic design methodology outlined in Section 2.4 but uses rigorous HFEM code solutions instead of multiple, expensive antenna builds to determine antenna response data.

III. Research Methodology

Response Surface methodology (RSM) comprises a set of statistical techniques for empirical model building and model exploitations. By careful design and analysis of experiments, it seeks to relate a response, or output variable, to the levels of a number of predictors, or input variables, that affect it [5].

In the development of an optimized design methodology for cavity-backed microstrip antennas with dielectric overlays, this chapter develops the theory of RSM including designed experiments, system modeling, and system optimization used throughout this research.

3.1 RSM Tasks

The opening quote from Box and Draper outlines the key RSM design methodology tasks that include:

1. Design a series of experiments that yields reliable measurements of the system response of interest in a region under consideration.
2. Determine an empirical model that accurately describes the system response.
3. Analyze the system response in relation to the effects introduced by input variables and interactions among variables.
4. Search for the optimal levels of the input variables that produce a desired system response.

When properly completed, the four tasks produce an optimized design methodology yielding reliable predicted system responses over the region of interest.

3.2 Experiment Development

In response to the first RSM task, the establishment of a designed experiment, Box and Draper list five specific initial questions that include [5]:

1. Which variables should be studied?
2. How shall qualitative variables be chosen?

3. At which levels of a given input variable should experiments be run?
4. What experimental arrangement should be used?
5. How should the response be measured?

This section addresses each question and provides solutions that directly apply to the development of an optimized design methodology.

3.2.1 Input Variables. The first question of Section 3.2 seeks the compilation of a set of applicable input variables that directly impacts the system under consideration. The first attempt, usually a brainstorming session with all interested parties followed by a variable screening procedure, applies working knowledge of the system to develop a complete variable list [5]. The system under consideration described by

$$\eta = f(\xi_1, \xi_2, \dots, \xi_k) \quad (3.1)$$

contains the function, f , with k input variables, ξ . The function, f , often contains a large group of input variables with strong impacts as well as variables with weak impacts. The proper selection of input variables found here helps develop later an empirical system model that emphasizes strong input variables over weaker input variables thereby reducing the empirical model complexity [7]. Throughout the experiment, the experimenter must remain flexible and continuously review the variable selection in the event previously unconsidered variables strongly influence system responses.

3.2.2 Variable Screening Procedure. The second question of Section 3.2 complements the selection of system input variables by providing a means of eliminating nonessential variables with weak system impacts thereby keeping the number of useful variables to a manageable number. As in the variable selection stage, the first attempt of list reduction usually applies system operating knowledge. Technical knowledge given by experts often provides the simplest approach towards reducing the variable list to critical factors, and expert technical knowledge potentially uncovers variables overlooked during brainstorming sessions. The second variable list reduction technique, a two-level full factorial designed experiment, tests the effects of input levels and their functional impacts and quickly decides

the necessity of retaining particular variables in the experiment [5]. Discussed in a later section, full factorial designed experiments provide an excellent experimental design for the gathering of system responses in a systematic fashion. Here, in the variable screening process the two-level full factorial designed experiment tests the system response at two separate levels of each variable used in the experiment. For a total of n variables in the experiment, all possible variable combinations are implemented and their responses recorded for a total of 2^n possible variable combinations and measured responses. To shrink the size of the screening experiment, a two-level full factorial designed experiment of only the variables in doubt could be performed to discover variable relationships to experimental system responses.

3.2.3 Variable Levels. The third question of Section 3.2 seeks an appropriate number of variable levels and precludes the experimental design selection used for gathering system response data. In addition, the number of variable levels chosen here directly impacts both the empirical model accuracy used to predict system responses and the time required to gather the entire set of measured system responses. In particular, as the number of variable levels increase, the size of the experiment increases, and the time necessary for experiment completion drastically increases. On the other hand, the accuracy of an empirical system model based on an experiment including three or more variable levels per variable far exceeds the accuracy of a similar empirical model that describes the same system and uses only two variable levels [14]. The mathematical model using a greater number of variable levels precisely determines system responses due to variable changes more accurately than models using fewer variable levels. An experimenter must reach a decision concerning the number of variable levels and the time expense necessary for an accurate experimental result.

3.2.4 Experimental Designs. In response to the fourth question of Section 3.2, two common experimental designs used in RSM experiments include the full factorial designed experimental and the central composite designed experiment. Of these designs, the central composite design remains the most widely used despite numerous advantages offered by the full factorial design [14].

Variable 1	Variable 2	Response
1a	2a	1
1a	2b	2
1a	2c	3
1b	2a	4
1b	2b	5
1b	2c	6
1c	2a	7
1c	2b	8
1c	2c	9

Table 3.1 Two Factor, Three Level, Full Factorial Design

3.2.4.1 Full Factorial Designed Experiments. Full factorial designed experiments are detail oriented and highly accurate regardless of system response smoothness or roughness. Furthermore, full factorial designs consider the system response for each input variable level as well as responses caused by variable interaction by investigating system responses for all possible variable level combinations. For example, in the case of the system described in Table. 3.1 with two input variables using three levels each, a complete full factorial experiment compiles a total of 3^2 measured system responses, one for each variable combination. full factorial designs are extendible to any number of input variables with the unfortunate cost of an increased number of measured responses and an increased time requirement for experiment completion [13]. Montgomery lists several advantages of full factorial designed experiments over all other forms of experimental designs that include [14]:

1. More efficient than a one factor at a time experiment,
2. Necessary when variable interactions are present to avoid misleading conclusions,
3. Allows the effects of a factor to be estimated at several levels of the other factors, yielding conclusions valid over a range of conditions,
4. Allows multitudes of comparisons to be performed and so facilitate model creation and criticism,
5. Provides highly efficient estimates of constants whose variances are small,
6. Leads to simple calculations.

Variable One	Variable Two		
	1a	1b	1c
2a	$1a_12a_1$	$1b_12a_1$	$1c_12a_1$
	$1a_22a_2$	$1b_22a_2$	$1c_22a_2$
	\vdots	\vdots	\vdots
	$1a_m2a_m$	$1b_m2a_m$	$1c_m2a_m$
2b	$1a_12b_1$	$1b_12b_1$	$1c_12b_1$
	$1a_22b_2$	$1b_22b_2$	$1c_22b_2$
	\vdots	\vdots	\vdots
	$1a_m2b_m$	$1b_m2b_m$	$1c_m2b_m$
2c	$1a_12c_1$	$1b_12c_1$	$1c_12c_1$
	$1a_22c_2$	$1b_22c_2$	$1c_22c_2$
	\vdots	\vdots	\vdots
	$1a_m2c_m$	$1b_m2c_m$	$1c_m2c_m$

Table 3.2 Full Factorial Design with Two Variables, Three Levels, and m Replicates

In general, m replicates of the experiment are performed for nondeterministic systems providing m measured system responses for each variable combination [14]. Assuming system responses with normally distributed random systematic error, m replicates provide a means of determining the expected system response for each variable level combination. Table 3.2 indicates a typical full factorial design using m replicates with two variables each having three levels.

3.2.4.2 Central Composite Designed Experiments. Central composite designed experiments establish strategic measurement locations by enclosing the system response space with system measurements and by including repeated system measurements central to the system space. Figure 3.1 represents a typical central composite design used to gather system response measurements using only three input variables. Central composite designs strongly reduce the required number of measurements for systems with smooth responses and are generally used to create second order empirical models [13]. Therefore, central composite designs offer little help in modeling systems with sharp transitions or discontinuities since an insufficient number of measurements are available to accurately characterize the system performance throughout the entire range of each input variable.

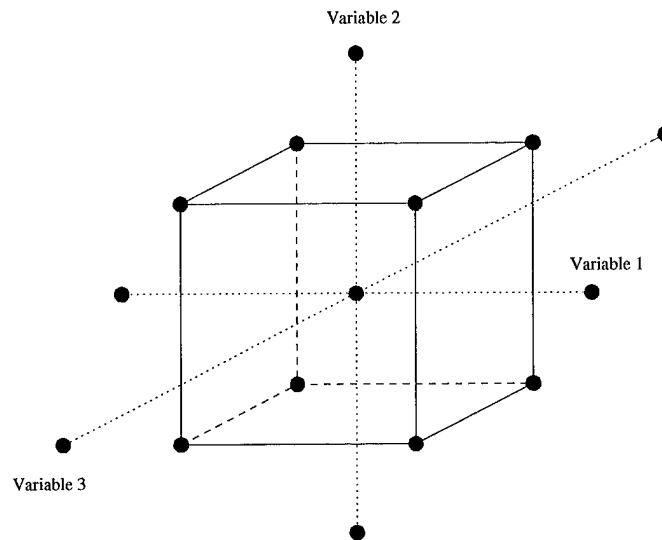


Figure 3.1 Central Composite Design For $k = 3$

Mason lists the steps needed to construct a central composite designed experiment with k input variables [13].

1. Construct a complete 2^k full factorial designed experiment with high and low variable levels depending on the need for efficiency and the ability to ignore system variable interaction.
2. Add $2k$ axial test points along the coordinate axes.
3. Add multiple repeat observations at the experimental design center.

3.2.5 System Response and Measurement. The fifth question of Section 3.2 determines the desired system response and the means by which the response is measured. The system response, often called the main effect, is generally the easiest to determine since the main effect is usually the reason for conducting the experiment. Once again, system or functional knowledge is useful in the determination of an appropriate main effect. In the case of antenna design, antenna gain or input impedance are excellent main effect choices. Furthermore, in the case of a cavity-backed microstrip antenna with dielectric overlays, the Hybrid Finite Element Method (HFEM) is the method of choice to predict antenna responses. The HFEM method is an adapted version of the Finite Element Method (FEM)

that applies boundary conditions linking internal antenna cavity space to external cavity space.

3.2.5.1 Hybrid Finite Element Method. According to Jin, the HFEM method incorporates the advantages of integral equation methods and FEM methods to solve electromagnetic problems composed of bounded and unbounded regions such as cavity-backed aperture antennas [10]. The general principle of the technique introduces a fictitious boundary separating the cavity region from the unbounded region. Interior to the cavity, the HFEM method formulates electric and magnetic field solutions, whereas in the exterior region HFEM uses integral equations to determine field solutions. At the fictitious boundary, field continuity conditions connect the fields in the two regions, leading to a coupled system for the solution of interior and exterior fields. In the external region, the HFEM method applies the well known vector wave equation, the dyadic Green's function, and the Sommerfield radiation condition to determine electric and magnetic field quantities at a distance r from the fictitious boundary as well as located on the boundary. Since the tangential electric and magnetic fields must be continuous across the boundary, field quantities just above the cavity boundary equal those just below the boundary. Section 3.2.5.2 develops the general FEM approach used within the cavity.

3.2.5.2 Finite Element Method. This section follows the general FEM development used by Jin [10]. FEM analysis replaces an entire spatial domain by a number of sub domains in which an unknown function is represented by simple interpolation functions with unknown coefficients. FEM analysis includes the four basic steps:

1. Discretization of the domain,
2. Selection of interpolation functions,
3. Formulation of system equations,
4. Solution of the system of equations.

The first and perhaps the most important step, discretization of the domain Ω , affects computer storage requirements, computational time, and accuracy of the numerical results. Depending on the domain shape, FEM partitions the domain using common ele-

ment shapes such as line segments, triangles, triangular prisms, or rectangular bricks and seeks to find individual solutions relative to each discrete element. The second step selects an interpolation function that provides an approximation of the unknown solution within each element. The interpolation functions of each element are usually selected to be a polynomial of first or second order since higher order polynomials usually result in a more complicated composite interpolation function formulation. The third step formulates a system of equations by using the Rayleigh-Ritz or the Galerkin methods and then sums the elemental equations over all elements to obtain the final form of the system of equations. Next, Neumann and Dirichlet boundary conditions are applied to each discrete element thus completing the system of equations. The final step, solving the system of equations, provides an approximation to the fields in the problem domain Ω for which the desired antenna parameters such as gain, input impedance, and radiation patterns can be measured.

3.3 System Modeling

The second task in the design methodology development, system response modeling, allows the experimenter to gain an understanding of the system under study and provides a means to predict system responses for differing input variable levels. A model of the system response, η , composed of Φ input variables and Θ constants takes on the general form

$$\eta = g(\Phi, \Theta) + \epsilon \quad (3.2)$$

$$\Phi = [\xi_1, \xi_2, \dots, \xi_k] \quad (3.3)$$

$$\Theta = [\theta_1, \theta_2, \dots, \theta_k] \quad (3.4)$$

where the error, ϵ , is desired to be as small as possible [5]. Mathematical models are of two forms, the mechanistic and the empirical models.

3.3.1 Mechanistic Modeling. Box and Draper refer to the mechanistic model as the true system functional form based on initial-value and boundary-value problems such as Neumann and Dirichlet equations [5]. Mechanistic models use known physical properties

to scientifically describe the complex performance and responses produced by the system under study. Mechanistic models are of the general form

$$\eta = f(\Phi, \Theta) \quad (3.5)$$

where the function f incorporates all known physical properties and provides an exact solution. HFEM is an example of a mechanistic model.

3.3.2 Empirical Modeling. In the absence of scientific or physical knowledge of a system or burdened with extremely complex mechanistic models, Box and Draper prefer empirical system models [5]. An empirical model closely approximates the true, mechanistic model and takes on the following form:

$$\eta = f(\Phi, \Theta) \approx g(\Phi, \Theta) + \epsilon \quad (3.6)$$

where the error, ϵ , is kept as small as possible. Two common techniques for empirical model building include least squares and cubic splines. Least squares curve fitting is widely understood and therefore, is not developed in this chapter. The interested reader is referred to experimental design and linear algebra textbooks such as Montgomery and Strang which thoroughly develop least squares curve fitting [14, 19].

3.3.3 Cubic Splines. This section follows the cubic spline development of Gerald and Wheatley [9]. Cubic splines fit functions with local irregularities without violent misbehavior and retain smoothness in regions of functional smoothness. In the development of cubic splines, a set of cubics pass through a set of measured data points fitting a new cubic to each interval between data points. For the pair of cubics that join at each data point, a requirement exists that the slope and curvature of each cubic equal the slope and curvature of the joining cubic at the data point. The cubic for the i th interval, which lies between the points (x_i, y_i) and (x_{i+1}, y_{i+1}) takes the form

$$y = a_i(x - x_i)^3 + b_i(x - x_i)^2 + c_i(x - x_i) + d_i . \quad (3.7)$$

Since it fits at the two endpoints of the interval,

$$y_i = a_i(x_i - x_i)^3 + b_i(x_i - x_i)^2 + c_i(x_i - x_i) + d_i = d_i ; \quad (3.8)$$

$$\begin{aligned} y_{i+1} &= a_i(x_{i+1} - x_i)^3 + b_i(x_{i+1} - x_i)^2 + c_i(x_{i+1} - x_i) + d_i \\ &= a_i h_i^3 + b_i h_i^2 + c_i h_i + d_i \end{aligned} \quad (3.9)$$

where

$$h_i = x_{i+1} - x_i . \quad (3.10)$$

To fulfill the slope and curvature requirement for joining cubics, Equations (3.11) and (3.12) provide the first and second derivatives of Equation (3.7) in the i th interval.

$$y' = 3a_i(x - x_i)^2 + 2b_i(x - x_i) + c_i \quad (3.11)$$

$$y'' = 6a_i(x - x_i) + 2b_i \quad (3.12)$$

Writing the equations in terms of the second derivatives of the interpolating cubics and letting S_i and S_{i+1} represent the second derivatives at the points (x_i, y_i) and (x_{i+1}, y_{i+1}) simplifies the mathematical procedure.

$$\begin{aligned} S_i &= 6a_i(x_i - x_i) + 2b_i \\ &= 2b_i \end{aligned} \quad (3.13)$$

$$\begin{aligned} S_{i+1} &= 6a_i(x_{i+1} - x_i) + 2b_i \\ &= 6a_i h_i + 2b_i \end{aligned} \quad (3.14)$$

From Equations (3.13) and (3.14),

$$b_i = \frac{S_i}{2} ; \quad (3.15)$$

$$a_i = \frac{S_{i+1} - S_i}{6h_i} . \quad (3.16)$$

Substituting the relations for a_i , b_i , and d_i from Equations (3.16), (3.15), and (3.8) into Equation (3.9) and then solving for c_i :

$$y_{i+1} = \left(\frac{S_{i+1} - S_i}{6h_i} \right) h_i^3 + \frac{S_i}{2} h_i^2 + c_i h_i + y_i ; \quad (3.17)$$

$$c_i = \frac{y_{i+1} - y_i}{h_i} - \frac{2h_i S_i + h_i S_{i+1}}{6} . \quad (3.18)$$

Invoking the equality of slopes condition for two cubics that join at (x_i, y_i) , Equation (3.11) becomes

$$y'_i = 3a_i(x_i - x_i)^2 + 2b_i(x_i - x_i) + c_i = c_i . \quad (3.19)$$

In the previous interval from x_{i-1} to x_i , the slope at (x_i, y_i) becomes

$$\begin{aligned} y'_i &= 3a_{i-1}(x_i - x_{i-1})^2 + 2b_{i-1}(x_i - x_{i-1}) + c_{i-1} \\ &= 3a_{i-1}h_{i-1}^2 + 2b_{i-1}h_{i-1} + c_{i-1} . \end{aligned} \quad (3.20)$$

Equating Equations (3.19) and (3.20) and substituting for a , b , c , and d in terms of S and y yields

$$\begin{aligned} y'_i &= \frac{y_{i+1} - y_i}{h_i} - \frac{2h_i S_i + h_i S_{i+1}}{6} \\ &= 3 \left(\frac{S_i - S_{i-1}}{6h_{i-1}} \right) h_{i-1}^2 + 2 \left(\frac{S_{i-1}}{2} \right) h_{i-1} + \frac{y_i - y_{i-1}}{h_{i-1}} \\ &\quad - \frac{2h_{i-1} S_{i-1} + h_{i-1} S_i}{6} \end{aligned} \quad (3.21)$$

Simplifying Equation (3.21) produces

$$h_{i-1} S_{i-1} + (2h_{i-1} + 2h_i) S_i + h_i S_{i+1} = 6 \left(\frac{y_{i+1} - y_i}{h_i} - \frac{y_i - y_{i-1}}{h_{i-1}} \right) . \quad (3.22)$$

Equation (3.22) applies at each cubic location beginning in the second cubic interval and ending in the next to last cubic interval and gives $n - 2$ equations relating the n values of S_i .

Specifying the end conditions for the whole curve provides the two equations that involve S_1 and S_n . Three choices exist for end conditions where the specification of which end condition is somewhat arbitrary. The first end condition in Equation (3.23) assumes that end cubics approach linearity at their extremes.

$$S_1 = S_n = 0 \quad (3.23)$$

The second end condition in Equation (3.24) assumes that end cubics approach parabolas at their extremities.

$$(S_1 = S_2), (S_n = S_{n-1}) \quad (3.24)$$

The third end condition in Equations (3.25) and (3.26) treats S_1 as a linear extrapolation from S_2 and S_3 and treats S_n as a linear extrapolation from S_{n-1} and S_{n-2} . At the left end

$$\frac{S_2 - S_1}{h_1} = \frac{S_3 - S_2}{h_2}, \quad S_1 = \frac{(h_1 + h_2)S_2 - h_1S_3}{h_2}. \quad (3.25)$$

At the right end

$$\frac{S_n - S_{n-1}}{h_{n-1}} = \frac{S_{n-1} - S_{n-2}}{h_{n-2}}, \quad S_n = \frac{(h_{n-2} + h_{n-1})S_{n-1} - h_{n-1}S_{n-2}}{h_{n-2}}. \quad (3.26)$$

The first condition, often called a *natural spline*, sometimes flattens the curve too much at the ends. The third end condition sometimes gives too much curvature to the ends. The best curve fit is given when one knows the slope of the function at the endpoints.

Writing the equations for S_2, S_3, \dots, S_{n-1} from Equation (3.22) in matrix form produces Equation (3.27). In Equation (3.27), $n - 2$ equations exist with n unknowns in the S vector. The selection of end conditions eliminates two unknowns, S_1 and S_n , thereby reducing the S vector to $n - 2$ unknowns. The vector S may now be solved. After finding values for S in each interval, values in the i th interval for a_i, b_i, c_i , and d_i are found using

Equations (3.16), (3.15), (3.18), and (3.8) respectively.

$$\begin{aligned}
 & \begin{bmatrix} h_1 & 2(h_1 + h_2) & h_2 & & \\ & h_2 & 2(h_2 + h_3) & h_3 & \\ & & & \ddots & \\ & & & & h_{n-2} & 2(h_{n-2} + h_{n-1}) & h_{n-1} \end{bmatrix} \begin{bmatrix} S_1 \\ S_2 \\ S_3 \\ \vdots \\ S_{n-1} \\ S_n \end{bmatrix} \\
 &= 6 \begin{bmatrix} \frac{y_3 - y_2}{h_2} - \frac{y_2 - y_1}{h_1} \\ \frac{y_4 - y_3}{h_3} - \frac{y_3 - y_2}{h_2} \\ \vdots \\ \frac{y_n - y_{n-1}}{h_{n-1}} - \frac{y_{n-1} - y_{n-2}}{h_{n-2}} \end{bmatrix} \quad (3.27)
 \end{aligned}$$

3.3.4 Model Adequacy. In fitting empirical models, model adequacy checks require an analysis of the residuals occurring from the comparison of measured and modeled data. The major plots that graphically represent the fit of the empirical model include the normal probability plot of residuals, the plot of residuals versus fitted values, and the plot of residuals versus individual variable parameters [14]. Residuals account for the difference between modeled values and true, expected values.

3.3.4.1 Normal Probability Plot of Residuals. A normal probability plot of residuals is just a graph of the cumulative distribution of the residuals on normal probability paper, that is, graph paper with the ordinate scaled so that the cumulative normal distribution plots as a straight line [14]. To construct a normal probability plot, arrange the residuals in increasing order and plot the k th probability of these ordered residuals versus the cumulative probability point [14]. If the underlying error distribution is normally distributed and the empirical model closely fits the system response data, the normal probability plot will resemble a straight line similar to the plot of Figure 3.2 [14].

3.3.4.2 Plot of Residuals versus Fitted Values. A plot of residuals versus fitted values plots the empirically modeled values versus their residual values on a standard

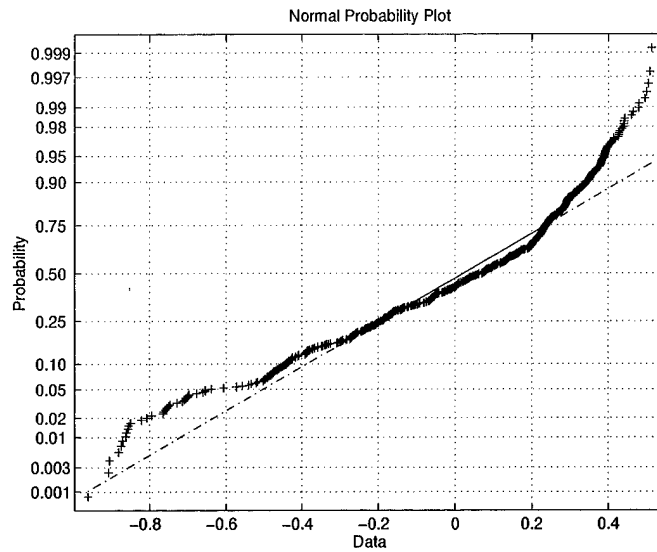


Figure 3.2 Normal Probability Plot of Least Squares System Response Model

xy graph. For an empirical model containing normally distributed random systematic error, residual versus fitted value plots should be structure-less thereby indicating that the empirical model does not follow any specific prediction trend [14]. For example, Figure 3.3 represents a typical residual versus fitted value plot.

3.3.4.3 Plot of Residuals versus Individual Variable Parameters. A plot of residuals versus individual input variables plots the individual variable levels versus empirical model residuals thereby graphically indicating the variability of the measured system response as a function of the individual input variable [14]. The amount of variation in model residuals relating to specific variable levels indicates the impact that each variable level has on the prediction accuracy of the empirical model. Figure 3.4 represents a typical residual versus variable parameter plot where the variable level near 3.45 introduces less variation in the empirical model accuracy than the levels near 2.85 and 3.75.

3.4 Analysis of Variance

The third task in the design methodology development, the analysis of variable effects on the measured system response, uses an Analysis of Variance (ANOVA) test. ANOVA tests apply to both full factorial designed experiments and central composite designed

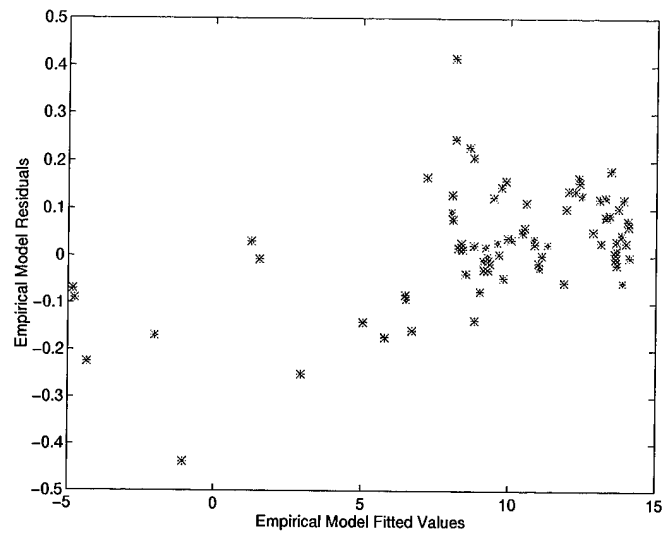


Figure 3.3 Plot of Residuals Versus Fitted Values

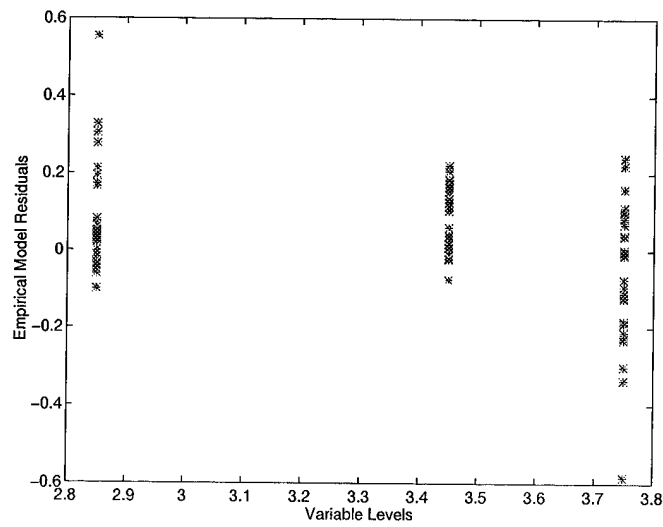


Figure 3.4 Plot of Residuals Versus Individual Variable Parameter

Variable One	Variable Two			
	1	2	...	b
1	y_{111}, y_{112} ..., y_{11n}	y_{121}, y_{122} ..., y_{12n}	...	y_{1b1}, y_{1b2} ..., y_{1bn}
2	y_{211}, y_{212} ..., y_{21n}	y_{221}, y_{222} ..., y_{22n}	...	y_{2b1}, y_{2b2} ..., y_{2bn}
\vdots	\vdots	\vdots	\vdots	\vdots
a	y_{a11}, y_{a12} ..., y_{a1n}	y_{a21}, y_{a22} ..., y_{a2n}	...	y_{ab1}, y_{ab2} ..., y_{abn}

Table 3.3 General Two Variable Full Factorial Design

experiments with any number of experiment input variables and levels with the single requirement that at least two replicates, repeated measurements, are taken at each measurement location. This section closely follows Montgomery's development of the two-factor ANOVA test that describes a two-factor full factorial designed experiment [14]. Using a sum of squares approach and a Chi Square, χ^2 , distribution test statistic, the F statistic, ANOVA tests analyze the effects introduced by experiment variables and the effects introduced by variable interactions on the measured system response.

Using the general case of the two-factor full factorial designed experiment with a total levels of variable A , b total levels of variable B , and n replicates, the measured system response, y_{ijk} , for the i th level of A , the j th level of B , and the k th replicate appears in the general form of Table 3.3. Equation (3.28) describes the measured system response.

$$y_{ijk} = \mu + \tau_i + \beta_j + (\tau\beta)_{ij} + \epsilon_{ijk} \quad (3.28)$$

where:

- μ denotes the overall mean effect,
- τ_i denotes the effect of the i th level of variable A ,
- β_j denotes the effect of the j th level of variable B ,
- $(\tau\beta)_{ij}$ denotes the effect of interaction between τ_i and β_j ,
- ϵ_{ijk} denotes a random error component.

3.4.1 Test Hypotheses. In the two-factor ANOVA test, row, column, and interaction effects are of equal interest. Two hypotheses for row effects state that either the effects for all row levels equal zero, or at least one row effect does not equal zero.

$$H_0 : \tau_1 = \tau_2 = \cdots = \tau_a = 0 \quad (3.29)$$

$$H_1 : \text{at least one } \tau_i \neq 0$$

The two hypotheses for column effects state that either the effects for all column levels equal zero, or at least one column effect does not equal zero.

$$H_0 : \beta_1 = \beta_2 = \cdots = \beta_b = 0 \quad (3.30)$$

$$H_1 : \text{at least one } \beta_i \neq 0$$

Concerning variable interaction, two hypotheses state that either the effects for all row column interaction levels equal zero, or at least one row column interaction effect does not equal zero.

$$H_0 : (\tau\beta)_{ij} = 0 \text{ for all } i, j \quad (3.31)$$

$$H_1 : \text{at least one } (\tau\beta)_{ij} \neq 0$$

The hypotheses seek to determine whether experiment variables influence the system response or should be excluded from the entire experiment.

3.4.2 Statistical Analysis. The statistical analysis used in ANOVA tests begins with a sum of squares approach based on Equation (3.32)

$$SS_T = SS_A + SS_B + SS_{AB} + SS_E \quad (3.32)$$

where:

- SS_T denotes the total sum of squares,
- SS_A denotes the sum of squares pertaining to variable A ,

- SS_B denotes the sum of squares pertaining to variable B ,
- SS_{AB} denotes the sum of squares pertaining to variable interactions,
- SS_E denotes the sum of squares pertaining to random error.

In the case of variables A and B with n replicates and the system response y_{ijk} , some initial equations must be defined before continuing.

$$\begin{aligned}
 y_{i..} &= \sum_{j=1}^b \sum_{k=1}^n y_{ijk} & \bar{y}_{i..} &= \frac{y_{i..}}{bn} & i &= 1, 2, \dots, a \\
 y_{.j.} &= \sum_{i=1}^a \sum_{k=1}^n y_{ijk} & \bar{y}_{.j.} &= \frac{y_{.j.}}{an} & j &= 1, 2, \dots, b \\
 y_{ij.} &= \sum_{k=1}^n y_{ijk} & \bar{y}_{ij.} &= \frac{y_{ij.}}{n} & i &= 1, 2, \dots, a; j = 1, 2, \dots, b \\
 y_{...} &= \sum_{i=1}^a \sum_{j=1}^b \sum_{k=1}^n y_{ijk} & \bar{y}_{...} &= \frac{y_{...}}{abn}
 \end{aligned} \tag{3.33}$$

The *dot* notation used above indicates that the operation is performed for all levels of the variable place holder that the *dot* resides in. Formulas for the sum of squares in Equation (3.32) are listed below.

$$SS_T = \sum_{i=1}^a \sum_{j=1}^b \sum_{k=1}^n y_{ijk}^2 - \frac{y_{...}^2}{abn} \tag{3.34}$$

$$SS_A = \sum_{i=1}^a \frac{y_{i..}^2}{bn} - \frac{y_{...}^2}{abn} \tag{3.35}$$

$$SS_B = \sum_{j=1}^b \frac{y_{.j.}^2}{an} - \frac{y_{...}^2}{abn} \tag{3.36}$$

For convenience, SS_{AB} is obtained in two stages.

$$SS_{Subtotals} = \sum_{i=1}^a \sum_{j=1}^b \frac{y_{ij.}^2}{n} - \frac{y_{...}^2}{abn} \tag{3.37}$$

$$SS_{AB} = SS_{Subtotals} - SS_A - SS_B \tag{3.38}$$

$$SS_E = SS_T - SS_{AB} - SS_A - SS_B \tag{3.39}$$

Effect	Symbol	Degrees of freedom
<i>A</i>	DOF_A	$a - 1$
<i>B</i>	DOF_B	$b - 1$
<i>AB</i> interaction	DOF_{AB}	$(a - 1)(b - 1)$
Error	DOF_E	$ab(n - 1)$
Total	DOF_T	$abn - 1$

Table 3.4 Degrees of Freedom

Table 3.4 lists the degrees of freedom associated with each sum of squares. Recalling that variable *A* has *a* levels, variable *B* has *b* levels, and the experiment has *n* replicates, degrees of freedom indicate the total number of variable levels left that the variable may take on without remaining in the same position. In the case of variable interaction *AB*, simultaneously changing the levels of both *A* and *B* limits the possible number of available variable combinations to $(a - 1)(b - 1)$, thus describing the number of degrees of freedom. In terms of the systematic error effect, since there are *n* replicates for each variable combination the system response has $(n - 1)$ degrees of freedom for each variable level combination. As a result for the entire set of variable combinations, the systematic error has $ab(n - 1)$ degrees of freedom. In terms of the total number of degrees of freedom, the two-factor full factorial designed experiment has *abn* total measured system responses leaving $abn - 1$ degrees of freedom.

Each sum of squares divided by its degrees of freedom is a mean square. The mean squares applicable to the ANOVA test pertain to *A*, *B*, *AB*, and error.

$$MS_A = \frac{SS_A}{DOF_A} \quad (3.40)$$

$$MS_B = \frac{SS_B}{DOF_B} \quad (3.41)$$

$$MS_{AB} = \frac{SS_{AB}}{DOF_{AB}} \quad (3.42)$$

$$MS_E = \frac{SS_E}{DOF_E} \quad (3.43)$$

Table 3.5 displays the resulting ANOVA table and corresponding *F* statistics. The *F* statistic determines whether to reject or accept the null hypotheses mentioned in Section 3.4.1.

Source of Variation	Sum of Squares	Degrees of Freedom	Mean Square	F_0
A treatments	SS_A	DOF_A	MS_A	$F_0 = \frac{MS_A}{MS_E}$
B treatments	SS_B	DOF_B	MS_B	$F_0 = \frac{MS_B}{MS_E}$
Interactions	SS_{AB}	DOF_{AB}	MS_{AB}	$F_0 = \frac{MS_{AB}}{MS_E}$
Error	SS_E	DOF_E	MS_E	
Total	SS_T	DOF_T		

Table 3.5 ANOVA Table for the Two-Factor Factorial Experiment

Variable	Variable B				$y_{i..}$
	A	15	70	125	
1	130 155 74 180	34 40 80 75	20 70 82 58	998	
2	150 188 159 126	136 122 106 115	25 70 58 45	1300	
3	138 110 168 160	174 120 150 139	96 104 82 60	1501	
$y_{.j.}$	1738	1291	770	$3799 = y_{...}$	

Table 3.6 Experiment Data for Example ANOVA Test

To determine acceptance or rejection, the F statistic uses a confidence interval measure, α , that indicates a percentile region in which the hypothesis under test is true. In the case of row effects due to A , if $F_0 < F_{\alpha, DOF_A, DOF_E}$, then accept H_0 , and reject H_1 . Otherwise, reject H_0 , and accept H_1 . In the case of column effects due to B , if $F_0 < F_{\alpha, DOF_B, DOF_E}$, then accept H_0 , and reject H_1 . Otherwise, reject H_0 , and accept H_1 . In the case of variable interaction due to AB , if $F_0 < F_{\alpha, DOF_{AB}, DOF_E}$, then accept H_0 , and reject H_1 . Otherwise, reject H_0 , and accept H_1 . Several statistical texts such as Montgomery and Box and Draper include values for the F statistic in tabular form for confidence intervals ranging from one percent to 25 percent [5, 14].

3.4.3 Example Analysis of Variance Test. Using the ANOVA method just described, Montgomery provides an example two-factor ANOVA test with four replicates by analyzing the data of Table 3.6 [14]. The sum of squares are computed as follows:

$$SS_T = (130)^2 + (155)^2 + (74)^2 + \cdots + (60)^2 - \frac{(3799)^2}{36} = 77646.97 \quad (3.44)$$

Source of Variation	Sum of Squares	Degrees of Freedom	Mean Square	F_0	$\alpha = 0.05$ F statistic
<i>A</i> treatments	10683.72	2	5341.86	7.91	3.35
<i>B</i> treatments	39118.72	2	19558.36	28.97	3.35
Interactions	9613.78	4	2403.44	3.56	2.73
Error	18230.75	27	675.21		
Total	77646.97	35			

Table 3.7 Example ANOVA Results

$$SS_A = \frac{(998)^2 + (1300)^2 + (1501)^2}{(3)(4)} - \frac{(3799)^2}{36} = 10683.72 \quad (3.45)$$

$$SS_B = \frac{(1738)^2 + (1291)^2 + (770)^2}{(3)(4)} - \frac{(3799)^2}{36} = 39118.72 \quad (3.46)$$

$$\begin{aligned}
SS_{AB} &= \frac{(130 + 155 + 74 + 180)^2}{4} + \frac{(34 + 40 + 80 + 75)^2}{4} + \frac{(20 + 70 + 82 + 58)^2}{4} \\
&\quad + \frac{(150 + 188 + 159 + 126)^2}{4} + \frac{(136 + 122 + 106 + 115)^2}{4} + \frac{(25 + 70 + 58 + 45)^2}{4} \\
&\quad + \frac{(138 + 110 + 168 + 160)^2}{4} + \frac{(174 + 120 + 150 + 139)^2}{4} + \frac{(96 + 104 + 82 + 60)^2}{4} \\
&\quad - \frac{(3799)^2}{36} - 10683.72 - 39118.72 \\
&= 9613.78
\end{aligned} \quad (3.47)$$

$$SS_E = 77646.97 - 10683.72 - 39118.72 - 9613.78 = 18230.75 \quad (3.48)$$

The analysis of variance is shown in Table 3.7. Using a five percent confidence interval, the independent variable F statistic becomes

$$F_{0.05,2,27} = 3.35, \quad (3.49)$$

and the variable interaction F statistic becomes

$$F_{0.05,4,27} = 2.73. \quad (3.50)$$

Since the calculated independent variable F_0 statistics exceed Equation (3.49) and the calculated variable interaction F_0 statistic exceeds Equation (3.50), the effects of the in-

dependent variables and their interactions are significant within a 95 percent confidence interval. As a result, null hypotheses are considered false, and the alternative hypotheses are accepted. Each variable and their interactions are significant to the example experiment.

3.5 Optimization Procedures

After gathering, modeling, and analyzing the system response data, the next step in this design methodology implements an optimization procedure to locate an optimum system configuration for a desired system response. This section discusses two methods of optimization. The first method, referred to here as the quadratic optimization method, uses a technique reserved for least squares modeling and is limited to second order empirical models. The second method uses the *Simplex* optimization method that implements a gradient search approach and applies to empirical models of any order.

3.5.1 Quadratic Optimization Method. Based on least squares system modeling, the quadratic optimization method consists of two phases: a linear phase and a quadratic phase [14]. Using system models of the forms:

$$\hat{y} = \beta_0 + \sum_{i=1}^k \beta_i x_i + \epsilon \quad (3.51)$$

and

$$\hat{y} = \beta_0 + \sum_{i=1}^k \beta_i x_i + \sum_{i=1}^k \beta_{ii} x_i^2 + \underbrace{\sum_i \sum_j \beta_{ij} x_i x_j}_{i < j} + \epsilon \quad (3.52)$$

for the linear and quadratic phase respectively, the quadratic optimization method attempts to optimize system response surfaces similar to Figure 3.5.

3.5.1.1 Sequential Procedure. The quadratic optimization method sequentially locates vicinities of system optimum responses and applies more elaborate system models to continue searching for the optimum location [14]. Using the linear equation to locate an approximate optimum vicinity, the quadratic optimization method applies a

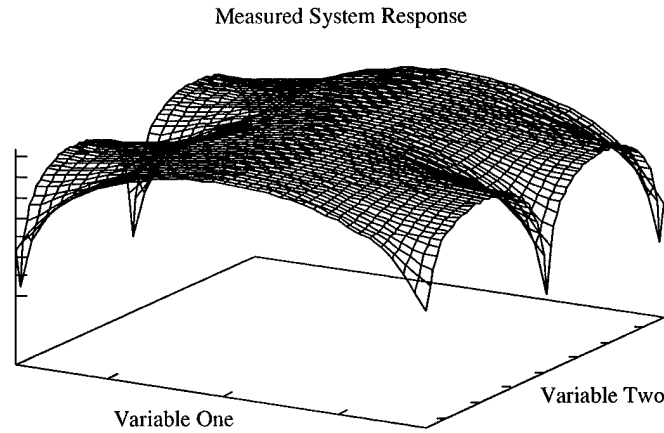


Figure 3.5 System Graphical Surface Response

second-order model in the vicinity and continues the search. Upon locating an optimum vicinity, the quadratic optimization method recalculates Equation (3.52) over a smaller variable region and proceeds with the optimum search. Unfortunately, for each new second-order model, the quadratic optimization method requires new measured system response data in each new optimum vicinity.

3.5.1.2 Second-Order Model Analysis. Replacing Equation (3.52) with a simpler matrix linear algebra equation of the form

$$\hat{y} = \beta_0 + \bar{x}'\bar{b} + \bar{x}'\bar{\beta}\bar{x} + \epsilon \quad (3.53)$$

where

$$\bar{x}' = [x_1, x_2, x_3, \dots, x_k], \quad (3.54)$$

$$\bar{x} = \begin{bmatrix} x_1 \\ x_2 \\ x_3 \\ \vdots \\ x_k \end{bmatrix}, \quad (3.55)$$

$$\bar{b} = \begin{bmatrix} \beta_1 \\ \beta_2 \\ \beta_3 \\ \vdots \\ \beta_k \end{bmatrix}, \quad (3.56)$$

and

$$\bar{\beta} = \begin{bmatrix} \beta_{11} & \frac{\beta_{12}}{2} & \dots & \frac{\beta_{1k}}{2} \\ & \beta_{22} & \dots & \frac{\beta_{2k}}{2} \\ & & \ddots & \vdots \\ \text{symmetrical} & & & \beta_{kk} \end{bmatrix} \quad (3.57)$$

allows for the straightforward location of optimum vicinities. Optimum system responses may be either maximum or minimum system responses. In the case of a desired maximum system response, derivatives with respect to input variables taken in the vicinity of a maximum system response quickly indicate its location.

$$\frac{d\hat{y}}{d\bar{x}} = \bar{b} + 2\bar{\beta}\bar{x} = 0 \quad (3.58)$$

$$\begin{bmatrix} \frac{d\hat{y}}{dx_1} \\ \frac{d\hat{y}}{dx_2} \\ \frac{d\hat{y}}{dx_3} \\ \vdots \\ \frac{d\hat{y}}{dx_k} \end{bmatrix} = \begin{bmatrix} \beta_1 \\ \beta_2 \\ \beta_3 \\ \vdots \\ \beta_k \end{bmatrix} + 2 \begin{bmatrix} \beta_{11}x_1 & \frac{\beta_{12}}{2}x_2 & \frac{\beta_{13}}{2}x_3 & \dots & \frac{\beta_{1k}}{2}x_k \\ \frac{\beta_{12}}{2}x_1 & \beta_{22}x_2 & \frac{\beta_{23}}{2}x_3 & \dots & \frac{\beta_{2k}}{2}x_k \\ \frac{\beta_{13}}{2}x_1 & \frac{\beta_{23}}{2}x_2 & \beta_{33}x_3 & \dots & \frac{\beta_{3k}}{2}x_k \\ \vdots & \vdots & \vdots & \ddots & \vdots \\ \frac{\beta_{1k}}{2}x_1 & \dots & & & \beta_{kk}x_k \end{bmatrix} = 0 \quad (3.59)$$

Linear algebraic techniques quickly determine optimum values for \bar{x} and \hat{y} .

$$\bar{x}_{opt} = -\frac{1}{2}(\bar{\beta}^{-1})\bar{b} \quad (3.60)$$

$$\hat{y}_{opt} = \beta_0 + \frac{1}{2}\bar{x}'_{opt}\bar{b} \quad (3.61)$$

The accuracy of the quadratic optimization method depends on the accuracy of the second-order system model and the second-order model's ability to characterize the true system response.

3.5.2 *Simplex Method.* The simplex optimization method is a systematic procedure of trials which arrives at the optimal solution through the following iterative steps [16]:

1. Determine a basic feasible solution.
2. Replace the first basic feasible solution by another which improves the function f toward the optimal solution.
3. Continue the process until $f_{optimal}$ is obtained, which will be indicated by a computational limiting criteria, or until the computations indicate that $f_{optimal}$ approaches infinity.

In general, the function under consideration contains n variables and is described by

$$f = c_1x_1 + c_2x_2 + \cdots + c_nx_n \quad (3.62)$$

with m constraint equations

$$\begin{cases} a_{11}x_1 + a_{12}x_2 + \cdots + a_{1n}x_n \leq b_1 , \\ a_{21}x_1 + a_{22}x_2 + \cdots + a_{2n}x_n \leq b_2 , \\ \vdots \\ a_{m1}x_1 + a_{m2}x_2 + \cdots + a_{mn}x_n \leq b_m , \end{cases} \quad m < n \quad (3.63)$$

with the restriction that $x_j \geq 0$ for all j [16]. In Equation (3.63), x_j represents the j th design variable, a_{ij} represents design variable coefficients, and b_i represents the i th design limitation. For convenience, the constraint equations are multiplied by -1 whenever necessary so that all $b_i \geq 0$. Furthermore, all inequalities are changed to equalities by the algebraic addition of new variables with unit coefficients; that is,

$$a_{i1}x_1 + a_{i2}x_2 + \cdots + a_{in}x_n \pm x_{n+i} = b_i \quad (i = 1, \dots, m) . \quad (3.64)$$

The new variables, called slack variables, do not contribute to the value of the object function; that is, their coefficients c_j are taken to be zero. For example, in the case of four

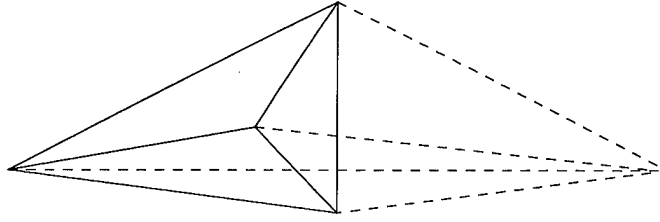


Figure 3.6 Expansion of Simplex Constraint Equations Towards an Optimal Solution

design variables with three constraint equations, $n = 4$ and $m = 3$,

$$f = \sum_{j=1}^{n+m} c_j x_j = c_1 x_1 + c_2 x_2 + c_3 x_3 + c_4 x_4 + c_5 x_5 + c_6 x_6 + c_7 x_7 \quad (3.65)$$

with $c_5 = c_6 = c_7 = 0$.

From the m constraint equations, the system represents m hyperplanes where typically an improved feasible solution is a corner in the corresponding hyperpolyhedron [8]. To locate a further improved feasible solution, the constraint equations are adjusted to shift the resulting hyperpolyhedron in the direction of a further optimal solution. For example, in Figure 3.6 the corner of the original hyperpolyhedron corresponding to the largest functional value is moved through the opposite hyperpolyhedron face to a point with a lower functional value. Once again, a feasible solution corresponding to an improved optimal solution generally resides in a corner of the newly formed hyperpolyhedron. The process continues until limiting criteria are satisfied and the final optimal solution is determined.

3.6 Closing Comments

RSM is a learning and iterative process. The normal application of RSM requires numerous repetitions of the entire procedure for accurate, reliable results. From the first RSM task, constant brainstorming of new input variables and consideration of new experimental designs must occur throughout the process to guarantee all possible relative factors have been considered. From the second RSM task, empirical modeling provides a means of predicting system responses in a specific region of interest without using cumbersome mechanistic models where the adequacy of the empirical model is easily determined using simple graphical techniques. From the third RSM task, analysis of variable effects on

the desired system response using ANOVA tests helps determine both strong and weak variable effects thereby identifying both necessary system variables and variables of lesser importance. From the final RSM task, optimization of the system under study using an empirical model and either the quadratic optimization method or the simplex optimization method provides a fast means of computing an optimal system solution compared to tedious mechanistic model testing. The final comment, RSM is not intended to provide increased insight into system operations, but rather, RSM simply describes system performance as it relates to various input variables.

IV. Optimized Design Methodology Development

Using the properties of dielectric overlays and the methods of Response Surface Methodology with designed experiments as outlined in Chapters II and III, this chapter develops an optimized design methodology for the cavity-backed microstrip antenna of Figure 4.1 by implementing a full factorial designed experiment, cubic spline empirical modeling, Analysis of Variance (ANOVA) tests, and simplex method optimization. The design methodology seeks an optimized antenna design with minimum average antenna gain above the antenna's bore sight. Section 4.1 develops the full factorial designed experiment, and Section 4.2 compares the adequacies of the cubic spline empirical model to those of a second order least squares empirical model. Section 4.3 performs the ANOVA tests indicating variable effects introduced on the measured system response, and Section 4.4 locates an optimized antenna design through the use of the simplex optimization method. Finally, Section 4.5 studies empirical modeling of antenna input impedance and studies average antenna gain empirical modeling close to a metallic cavity ground plane.

4.1 Experiment Development

From Chapter III, the first Response Surface Methodology (RSM) task designs a series of experiments that yields reliable system response measurements in a design region of interest. The task of measuring reliable system responses requires answers to the five questions of Section 3.2. This section provides solutions to each question as it relates to Figure 4.1 and develops the needed parameters for the creation of a four-variable, five-level, full factorial designed experiment.

4.1.1 Input Variables. The first question of Section 3.2 addresses the issue of designed experiment input variables. The antenna design of Figure 4.1 provides several possibilities of experimental variable selections upon which to build a designed experiment. A feasible number of system response measurements, empirical system modeling, and time constraints limit the number of designed experiment variables to four variables which include:

1. Antenna operating frequency,

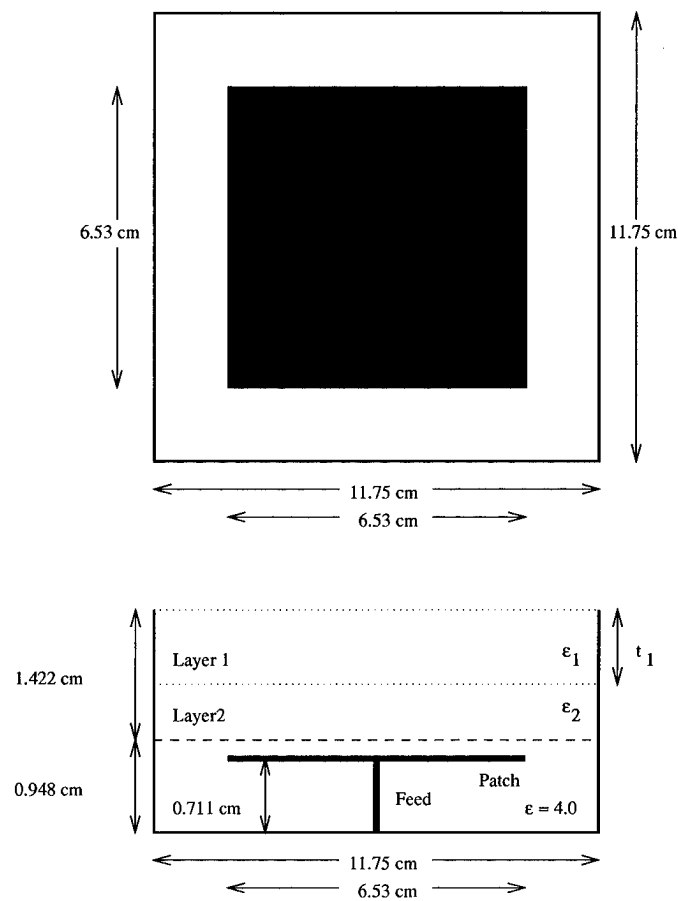


Figure 4.1 Antenna Configuration

Cavity Dimensions:	
Length	11.75 cm
Width	11.75 cm
Height	2.37 cm
Patch Dimensions:	
Length	6.53 cm
Width	6.53 cm
Patch Location	Centered 0.711 cm Above Cavity Bottom
Feed Pin Location	0.653 cm Off Center
Substrate Relative Permittivity	4.0
Substrate Thickness	0.948 cm

Table 4.1 Constant Antenna Design Parameters

2. First dielectric superstrate layer relative permittivity,
3. Second dielectric superstrate layer relative permittivity,
4. First dielectric superstrate layer thickness.

Table 4.1 lists the remaining antenna design parameters and their respective constant design values.

4.1.2 Variable Screening Procedure. The second question of Section 3.2 addresses the importance of each individual variable parameter used in the designed experiment. Based on information provided in Chapter II and system knowledge, the four chosen experiment variables strongly influence all possible antenna responses of Figure 4.1. Therefore, the antenna operating frequency, the first dielectric superstrate layer relative permittivity, the second dielectric superstrate layer relative permittivity, and the first dielectric superstrate layer thickness are excellent choices of designed experiment variables.

4.1.3 Variable Levels. The third question of Section 3.2 addresses the number of levels of each designed experiment variable. The number of levels for each variable directly impacts the ability of the designed experiment to capture the measured system response under all possible variable conditions. Unfortunately, a large number of variable levels requires a greater number of system response measurements and results in increased time expenditures. Therefore, for an adequate coverage of the antenna response space within a

feasible time limit, this design methodology limits the variable level number to five levels for each variable.

4.1.3.1 Antenna Operating Frequency. The first designed experiment variable, antenna operating frequency, necessitated two initial antenna experiments for an adequate selection of frequency levels. Using a Hybrid Finite Element Method (HFEM) electromagnetic analysis code and the antenna configuration of Figure 4.1, the first experiment set both dielectric superstrate layer relative permittivity values equal to 1.0 and performed gain and input impedance calculations in the frequency range of 1.0 GHz to 1.4 GHz. Following the same procedure as the first experiment, the second experiment set both dielectric superstrate relative permittivities to 8.0 and repeated the gain and impedance calculations in the frequency range from 0.9 GHz to 1.4 GHz. Converting the antenna input impedance measurements from the two preliminary experiments to antenna input admittances and plotting the admittances using Smith charts normalized to the admittance corresponding to 50 ohms, Figure 4.2 plots admittances from the first frequency experiment, and Figure 4.3 plots admittances from the second experiment according to their respective frequency values. Interpolating from both experiments, the antenna input admittance approaches the normalized 1.0 mho circle in the frequency range bounded by 1.2 and 1.3 GHz. As a result, using 1.3 GHz as an upper frequency limit led to the frequency level selections consisting of 0.9, 1.0, 1.1, 1.2, and 1.3 GHz.

4.1.3.2 First and Second Dielectric Superstrate Layer Permittivities. Level selections of the second and third designed experiment variables, the first and second dielectric superstrate layer relative permittivities from Figure 4.1, came about from practical antenna design experience. Common dielectric materials with relative permittivity values in the range of 1.0 to 8.0 are readily available or at least manufacturable. Therefore, the accessibility of common dielectric materials led to the selections of 1.0, 2.0, 4.0, 6.0, and 8.0 for dielectric relative permittivity values used in the designed experiment.

4.1.3.3 First Dielectric Superstrate Layer Thickness. Using an HFEM antenna analysis code and the spatial partitioning property of HFEM codes within cavity

50 Ohm Characteristic Impedance, Frequency (1.0 GHz to 1.4 GHz)

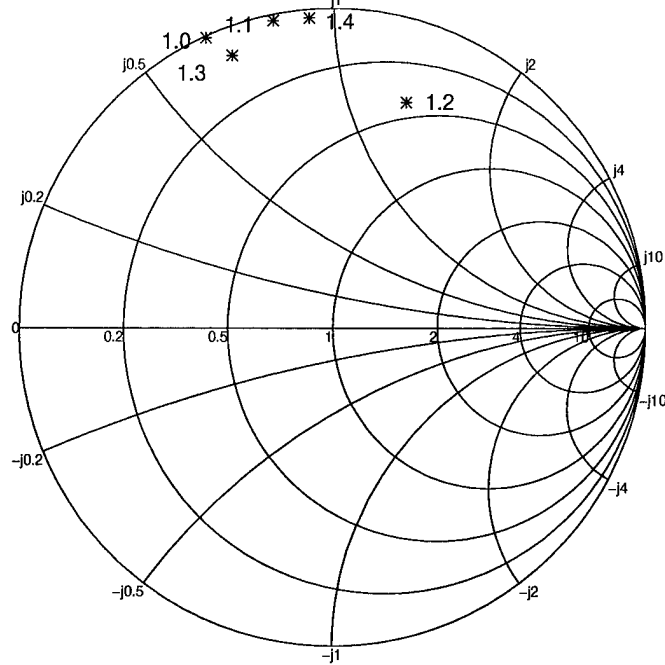


Figure 4.2 Smith Chart Analysis of Input Admittance Values With First and Second Superstrate Dielectric Relative Permittivities Equal to 1.0 ($\epsilon_{r1} = \epsilon_{r2} = 1.0$)

50 Ohm Characteristic Impedance, Frequency (0.9 GHz to 1.4 GHz)

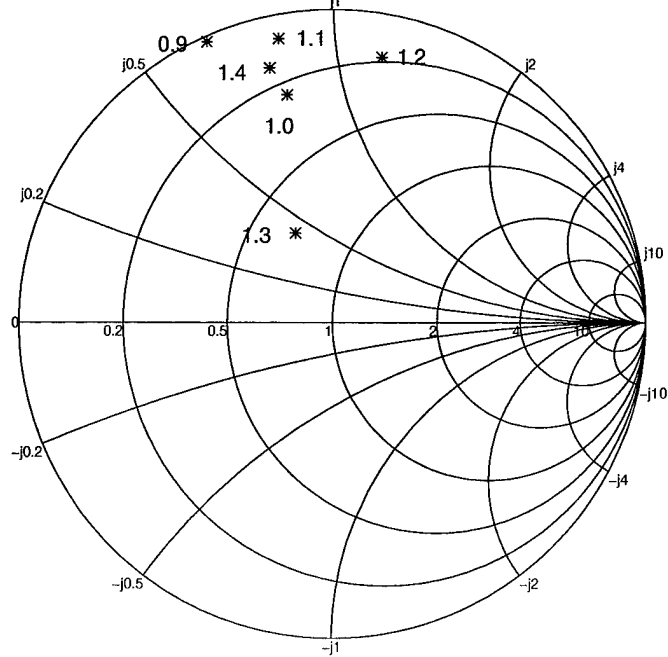


Figure 4.3 Smith Chart Analysis of Input Admittance Values With First and Second Superstrate Dielectric Relative Permittivities Equal to 8.0 ($\epsilon_{r1} = \epsilon_{r2} = 8.0$)

Frequency (GHz)	0.9, 1.0, 1.1 1.2, and 1.3
First Layer Relative Permittivity	1, 2, 4, 6, and 8
Second Layer Relative Permittivity	1, 2, 4, 6, and 8
First Layer Thickness (cm)	0.237, 0.474, 0.711, 0.948, and 1.185

Table 4.2 Variable Antenna Design Parameters

dimensions, the level selections for the fourth designed experiment variable, the first dielectric superstrate layer thickness, was limited to HFEM nodal dimensions. The first dielectric superstrate layer thickness levels include 0.237, 0.474, 0.711, 0.948, and 1.185 centimeters. Worth noting, due to constant cavity dimensions and a constant substrate depth, variations in the first superstrate thickness directly impact the thickness of the second superstrate layer causing the second superstrate layer to compensate for the remaining cavity space. Table 4.2 lists the designed experiment variables and their corresponding variable levels.

4.1.4 System Response. In this development of an optimized design methodology for the antenna in Figure 4.1, the desired system response is the average antenna gain over the angular region described in Equations (4.1) and (4.2).

$$0^\circ \leq \theta \leq 20^\circ \quad (4.1)$$

$$0^\circ \leq \phi \leq 360^\circ \quad (4.2)$$

Using gain calculations in five degree increments, Equation (4.3) defines average antenna gain.

$$averagegain = 20 \log \left(\frac{10^{\left(\frac{gain_{0^\circ}}{20}\right)} + 10^{\left(\frac{gain_{5^\circ}}{20}\right)} + \dots + 10^{\left(\frac{gain_{20^\circ}}{20}\right)}}{5} \right) \quad (4.3)$$

4.1.5 Experimental Design. The fourth question of Section 3.2 addresses the type of experimental design used to gather measured system response data. The electromagnetic properties of the antenna design in Figure 4.1 and antenna radiation pattern lobing

Test	Layer 1 (cm)	ϵ_{r1}	ϵ_{r2}	Freq (GHz)	Gain (dB)
1	0.237	1	1	0.9	y_1
2	0.237	1	1	1.0	y_2
3	0.237	1	1	1.1	y_3
4	0.237	1	1	1.2	y_4
5	0.237	1	1	1.3	y_5
6	0.237	1	2	0.9	y_6
\vdots	\vdots	\vdots	\vdots	\vdots	\vdots
625	1.185	8	8	1.3	y_{625}

Table 4.3 Full Factorial Design

necessitate a full factorial designed experiment. The full factorial experiment measures the average antenna gain response at each variable level combination. Since five variable levels for each of the four variables were selected, the full factorial experiment determines the average antenna gain at 625 (5^4) total experimental locations. Table 4.3 lists the full factorial experiment used in this experiment.

4.1.6 Hybrid Finite Element Method Measurements. The fifth question of Section 3.2 addresses the means of measuring the system response. In this optimized design methodology development, an HFEM electromagnetic analysis code directly suited for rectangular cavity aperture antennas is used that uses brick segments to facilitate field solutions in the cavity region and integral equations to solve for field quantities in the unbounded external region.

4.2 Average Antenna Gain Empirical Modeling

From Chapter III, the second RSM task determines an empirical model that accurately describes the measured system response, the average antenna gain. Several possible empirical models exist of which cubic splines and least squares represent two common techniques. Section 4.2.1 addresses the application of cubic spline empirical modeling to this multi-dimensional space problem, and Section 4.2.2 provides a second order least squares empirical model applicable to the optimization technique discussed in Section 3.5.1.

Section 4.2.3 compares the effectiveness of the cubic spline empirical model with the effectiveness of the least squares empirical model.

4.2.1 Cubic Splines Empirical Modeling. The application of cubic splines in a multi-dimensional space requires an extension of the cubic spline derivation of Section 3.3.3. Utilizing a small portion of the Wilson [20] cubic spline algorithm that extends the theory of Section 3.3.3 to multi-dimensional space, the cubic spline empirical modeling algorithm performs the following sequential steps:

1. Use the initial 625 (5^4) test configurations of the full factorial designed experiment and their corresponding gain values and creates cubic splines in the direction of the first input variable, the antenna operating frequency, at all possible level combinations of the remaining three input variables.
2. Set the antenna operating frequency variable to its desired input value.
3. Determine average antenna gain values in terms of the remaining three input variables and their corresponding five levels at the desired antenna operating frequency for a total of 125 (5^3) new average antenna gain values.
4. Use the resulting 125 possible test configurations and their corresponding gain values and creates cubic splines in the direction of the second input variable, the first dielectric superstrate layer permittivity, at all possible level combinations of the remaining two input variables.
5. Set the first dielectric superstrate layer permittivity value to its desired input value.
6. Determine average antenna gain values in terms of the remaining two input variables and their corresponding five levels at the desired input values of both the antenna operating frequency and the first dielectric superstrate layer permittivity for a total of 25 (5^2) calculations.
7. Use the resulting 25 possible test configurations and their corresponding gain values and creates cubic splines in the direction of the third input variable, the second dielectric superstrate layer permittivity, at all possible levels of the remaining input variable.

8. Set the second dielectric superstrate layer permittivity value to its desired input value.
9. Determine average antenna gain values in terms of the remaining input variable, the first dielectric superstrate layer thickness, and its corresponding five levels at the desired input values of antenna operating frequency, first dielectric superstrate layer permittivity, and second dielectric superstrate layer permittivity for a total of five calculations.
10. Use the resulting five possible test configurations and their corresponding gain values and creates cubic splines in the direction of the final input variable, first dielectric superstrate layer thickness.
11. Set the first dielectric superstrate layer thickness to its desired input level and calculates the final average antenna gain value that now represents the desired levels of all four input variables.

The multi-dimensional cubic spline empirical model provides a computationally efficient model which can be optimized using the simplex optimization method.

4.2.2 Least Squares Empirical Modeling. Using the average antenna gain measurements obtained from the full factorial designed experiment of Section 4.1.5 and a least squares software routine from *Matlab*, Equation (4.4) defines a second-order quadratic equation describing the antenna of Figure 4.1 for the variable ranges of Table 4.2.

$$\begin{aligned}
 y_{gain} = & -11.2938(freq)^2 + 0.0018(\epsilon_{r2})^2 \\
 & + 0.0004(\epsilon_{r1})^2 - 0.0050(thick_1)^2 \\
 & - 0.4264(freq)(\epsilon_{r2}) - 0.3090(freq)(\epsilon_{r1}) \\
 & + 0.0479(freq)(thick_1) - 0.0067(\epsilon_{r2})(\epsilon_{r1}) \\
 & + 0.0105(\epsilon_{r2})(thick_1) - 0.0105(\epsilon_{r1})(thick_1) \\
 & + 27.6203(freq) + 0.4040(\epsilon_{r2}) + 0.3682(\epsilon_{r1}) \\
 & - 0.0189(thick_1) - 14.6896
 \end{aligned} \tag{4.4}$$

Frequency (GHz)	0.95, 1.15, 1.25
First Layer Permittivity	1.5, 5, 7
Second Layer Permittivity	1.5, 5, 7,
First Layer Thickness (cm)	0.237, 0.711, 1.185

Table 4.4 Model Adequacy Test Variable Levels

Test	Layer 1 (cm)	ϵ_{r1}	ϵ_{r2}	Freq (GHz)	Gain (dB)
1	0.237	1.5	1.5	0.95	y_1
2	0.237	1.5	1.5	1.15	y_2
3	0.237	1.5	1.5	1.25	y_3
4	0.237	1.5	5	0.95	y_4
\vdots	\vdots	\vdots	\vdots	\vdots	\vdots
81	1.185	7	7	1.25	y_{81}

Table 4.5 Model Adequacy Test Cases

4.2.3 Average Antenna Gain Model Adequacy. Using a set of 81 test cases from Table 4.4 and Table 4.5, the techniques of Section 3.3.4 pictorially describe the empirical modeling adequacies of the cubic spline and least squares models.

4.2.3.1 Normal Probability Plot of Residuals. Using the normal probability plot technique of Section 3.3.4.1, Figure 4.4 indicates that the cubic spline empirical model accuracy far exceeds that of the least squares empirical model. In Figure 4.4, since the cumulative probabilities of the cubic spline model residuals approximate a straight line better than the cumulative probabilities of the least squares model residuals, the normally distributed systematic error in the cubic spline model is less than the systematic error in the least squares model. Furthermore, from the cubic spline empirical model, the average antenna gain residuals vary over a net range of 1.2 dB, while residuals from the least squares empirical model vary over a net range of approximately 4.5 dB, a significantly larger gain region than the cubic spline model. Table 4.6 lists the residual mean and the residual standard deviation for both empirical models.

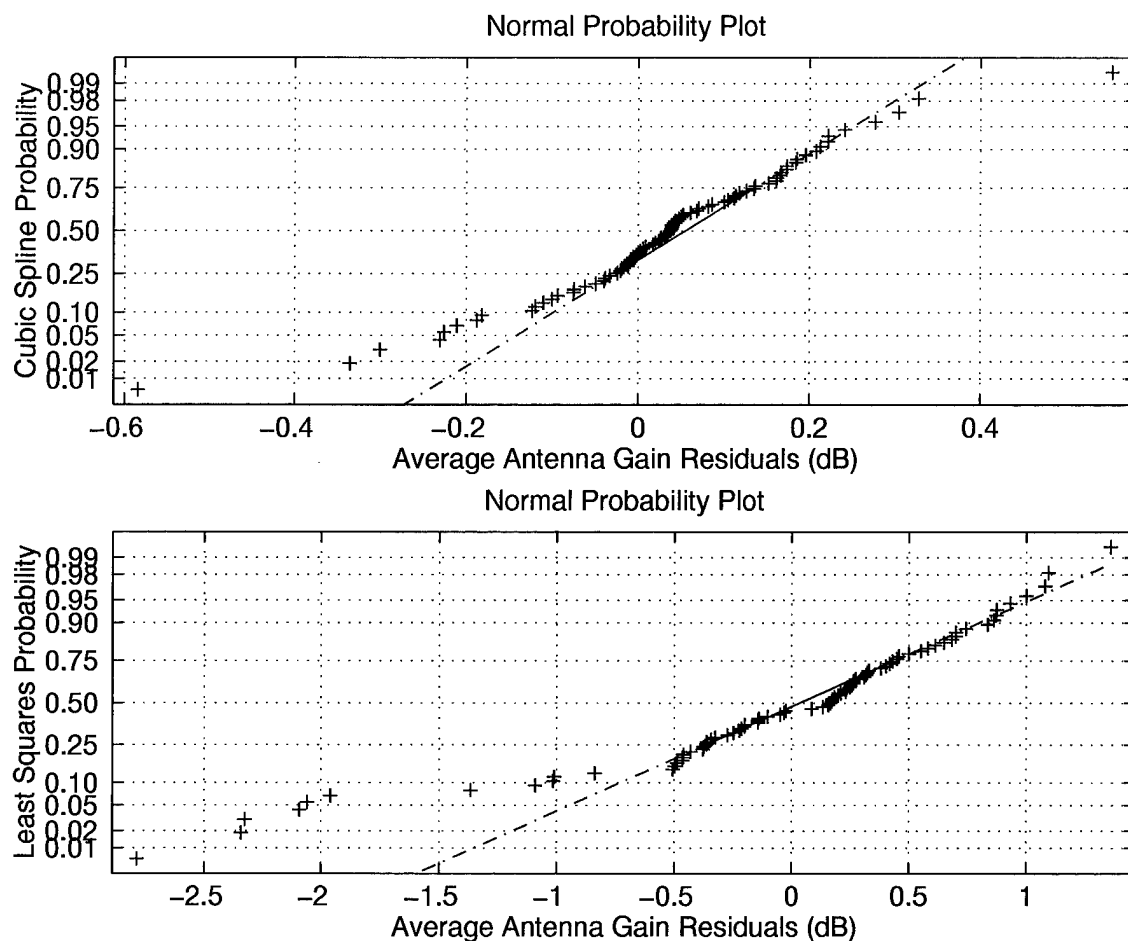


Figure 4.4 Normal Probability Plots of Cubic Spline and Least Squares System Response Models

Cubic Spline:	
Residual Mean	0.0357 dB
Residual Standard Deviation	0.1592 dB
Least Squares:	
Residual Mean	-0.0579 dB
Residual Standard Deviation	0.8240 dB

Table 4.6 Mean and Standard Deviation Values of Cubic Spline and Least Squares Residuals

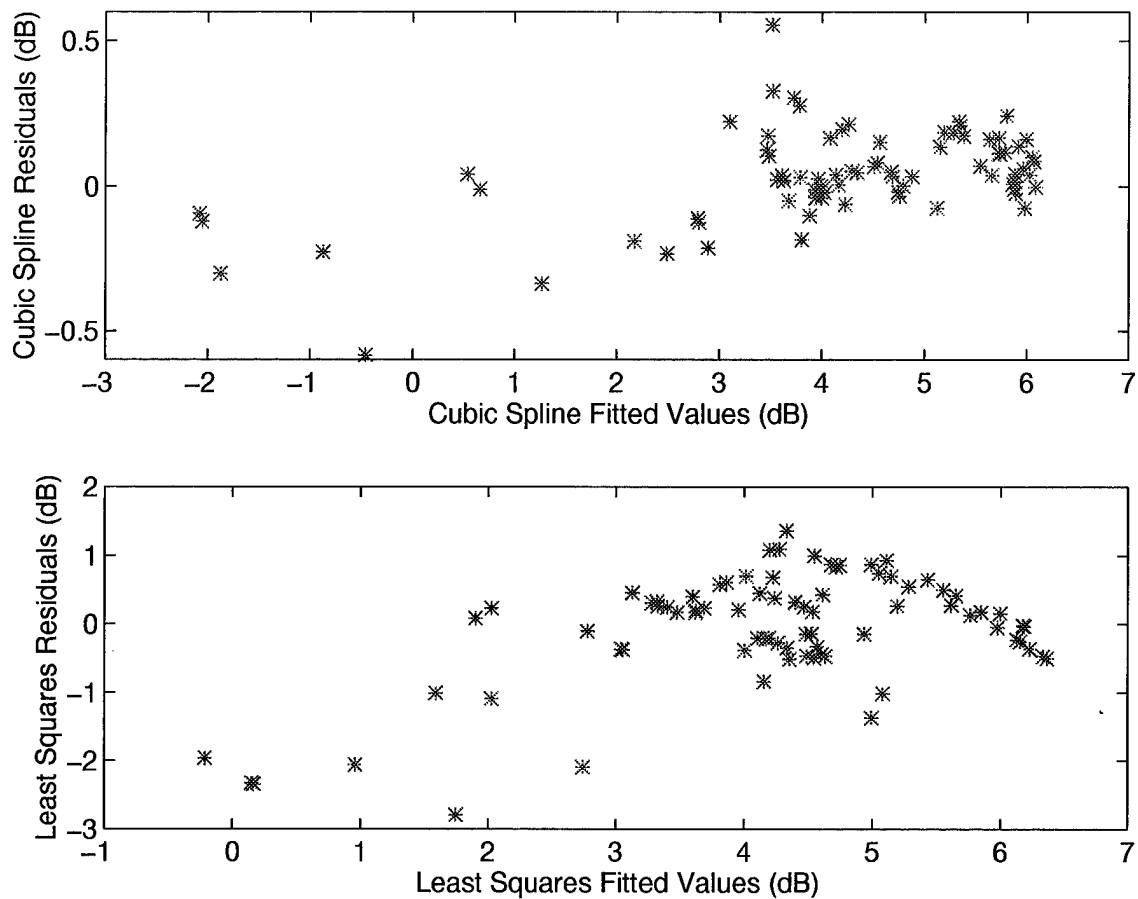


Figure 4.5 Cubic Spline and Least Squares Residuals Versus Fitted Values

4.2.3.2 Residuals Versus Fitted Value Plots. Using the graphical techniques of Section 3.3.4.2, the plots of empirical model residuals versus the empirical model predicted average antenna gain values in Figure 4.5 indicate that the cubic spline model residuals vary much less than those from the least squares model. As indicated in the normal probability plots in Figure 4.4, the residual versus fitted value plots indicate that the cubic spline model residuals vary over a net range of 1.2 dB, and the least squares model residuals vary over a net range of 4.5 dB. Since both plots in Figure 4.5 are structure-less, both empirical models indicate a normal random distribution of model residuals.

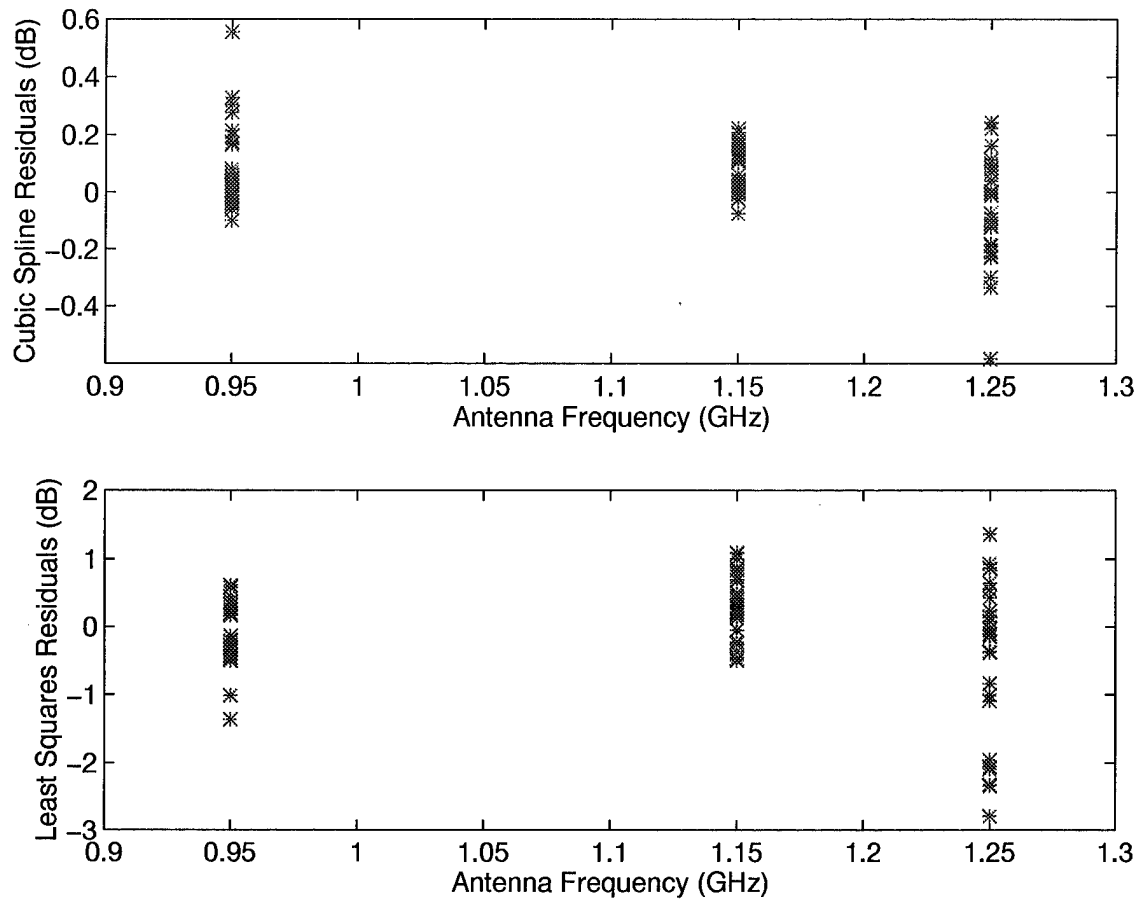


Figure 4.6 Cubic Spline and Least Squares Residuals Versus Frequency Values

4.2.3.3 Residuals Versus Variable Parameter Plots. Using the graphical technique of Section 3.3.4.3, the plots of residuals versus input variable parameters in Figures 4.6, 4.7, 4.8, and 4.9 again indicate that the cubic spline empirical model outperforms the least squares empirical model. As before, residuals from the cubic spline empirical model vary over an approximate net range of 1.2 dB, and residuals from the least squares empirical model vary over an approximate net range of 4.5 dB.

From the model adequacy plots, cubic spline empirical modeling far exceeds the least squares performance and will be implemented throughout the remainder of this experiment.

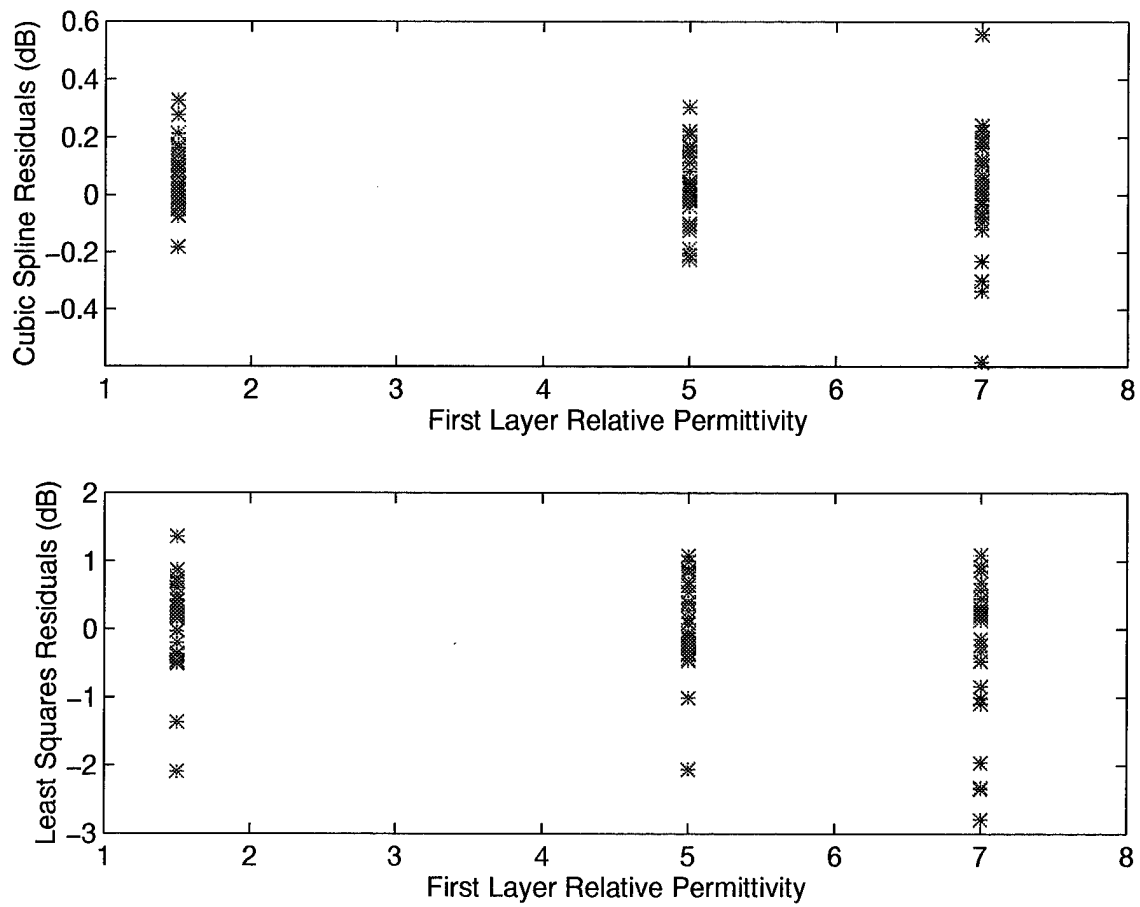


Figure 4.7 Cubic Spline and Least Squares Residuals Versus First Layer Relative Permittivity Values

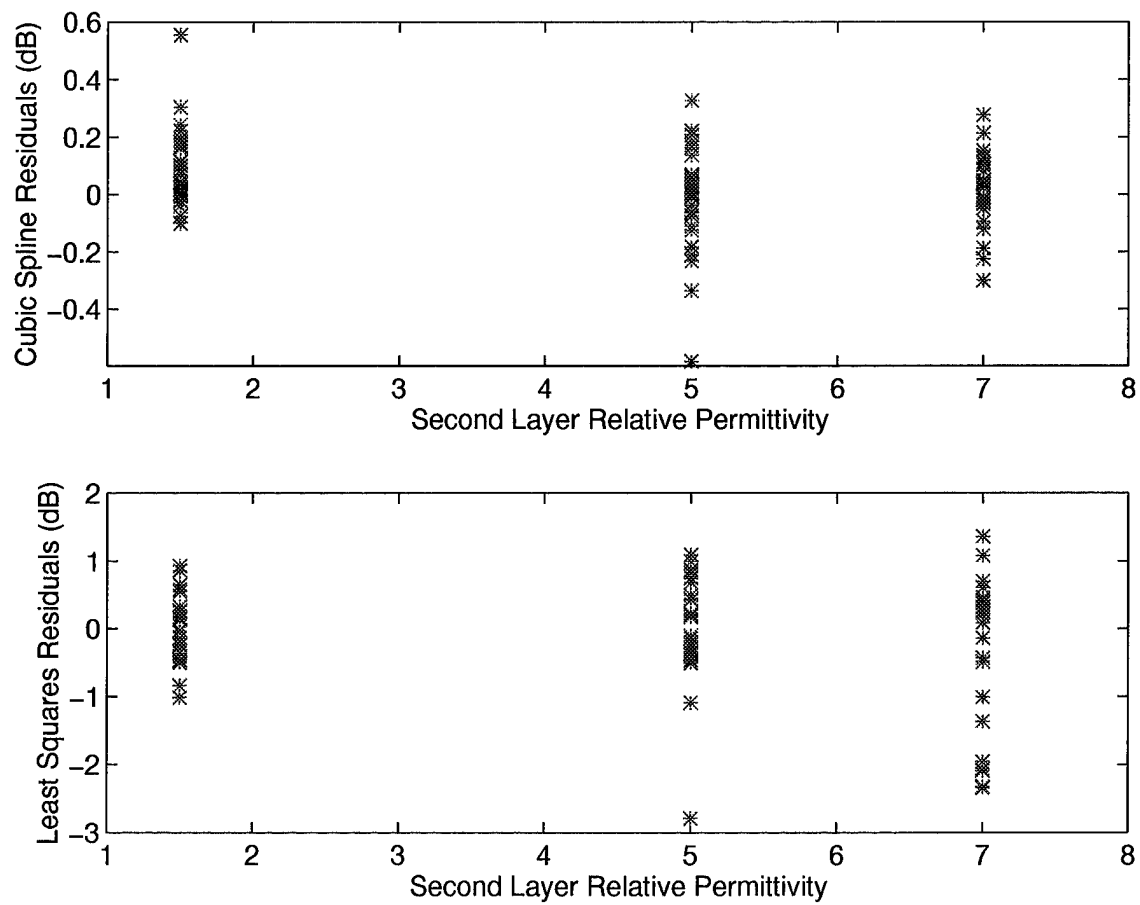


Figure 4.8 Cubic Spline and Least Squares Residuals Versus Second Layer Relative Permittivity Values

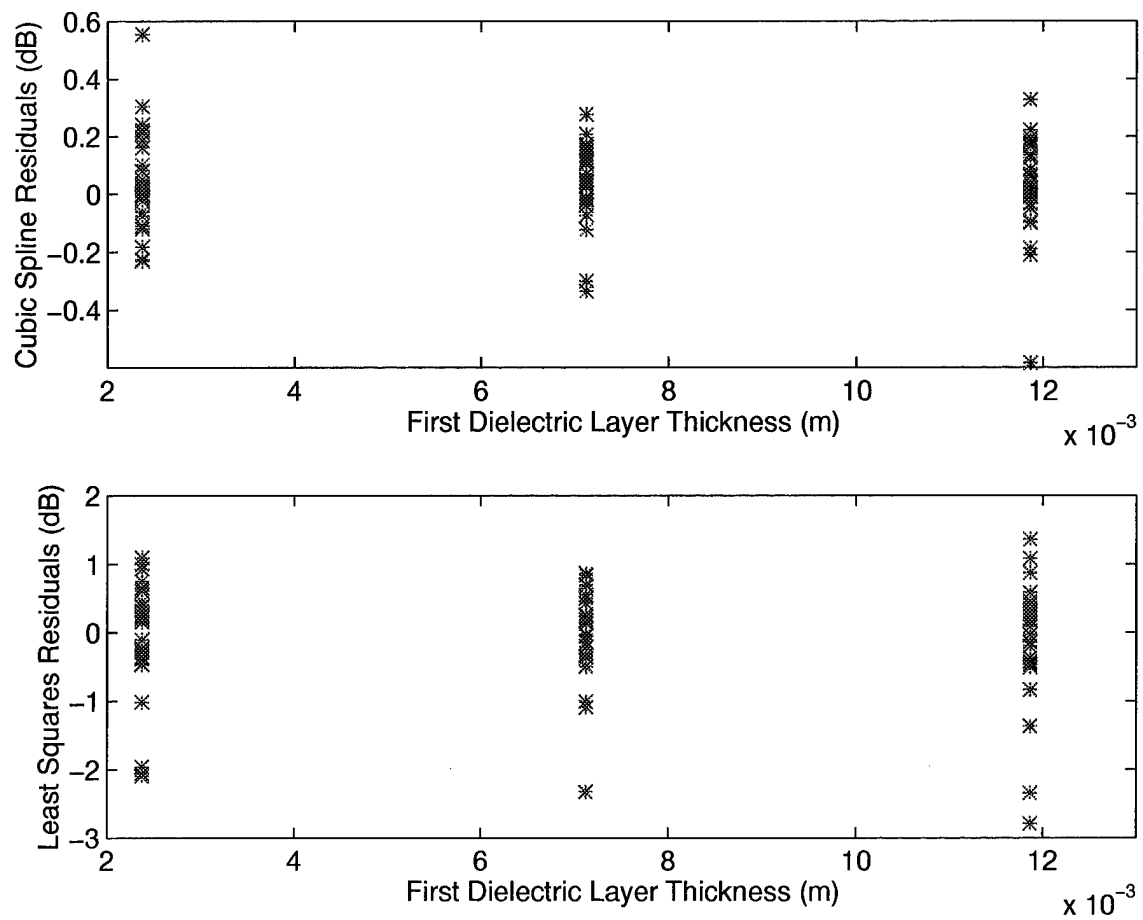


Figure 4.9 Cubic Spline and Least Squares Residuals Versus First Layer Thickness Values

4.3 Analysis of Variance

From Chapter III, the third RSM task analyzes the measured system response in relation to the effects introduced by the designed experiment input variables and their interactions. Section 4.3.1 implements the ANOVA techniques of Section 3.4 to analyze the effects introduced by the antenna operating frequency on the average antenna gain by using average antenna gain predictions from the cubic spline empirical model. After completing the cubic spline based ANOVA test for frequency effects, Section 4.3.1 then validates the frequency test by reaccomplishing the frequency ANOVA test using average antenna gain values from the HFEM code and compares findings. The purpose of repeating the frequency ANOVA test using HFEM results is to demonstrate the reliability of the cubic spline empirical model for ANOVA testing thereby minimizing the computational effort and time expenditures brought on by using HFEM results. After proving the effectiveness of cubic spline empirical modeling for ANOVA tests, Section 4.3.2 accomplishes an ANOVA test studying the effects of all four input variables as well as their interactions using the cubic spline empirical model.

4.3.1 Frequency Effects ANOVA Test. Applying the technique of Section 3.4, this section demonstrates the usefulness of empirical modeling on ANOVA testing by comparing results from a cubic spline empirical model based frequency ANOVA test to results from a HFEM based frequency ANOVA test. Using the test hypotheses of Section 3.4.1, the frequency effects ANOVA test attempts to prove one of two possible hypotheses true. The null hypothesis, H_0 , specifies that none of the frequency levels used in the ANOVA test effect the average antenna gain, while the alternate hypothesis, H_1 , specifies that at least one of the frequency levels effect the antenna gain. Using identical normal randomly distributed sets of ten replicates for each frequency level for the variable values given in Table 4.7, Tables 4.8 and 4.9 summarize the results of the two frequency ANOVA tests. In each case, the calculated F_0 statistic exceeds the required F statistic with the one percent confidence level and proves the null hypotheses false. These frequency ANOVA tests results demonstrate that the cubic spline empirical model adequately predicts ANOVA results and

Frequency (GHz)	0.95, 1.05, 1.15, and 1.25
First Layer Relative Permittivity	4
Second Layer Relative Permittivity	4
First Layer Thickness (cm)	0.711
Replicates Per Frequency Level	10

Table 4.7 Frequency ANOVA Test Variable Levels

Factor	Sum of Squares	Degrees of Freedom	Mean Square	F_0	$\alpha = 0.01$ F Statistic
Frequency	23.79	3	7.93	14.96	4.31
Error	18.94	36	0.53		
Total	42.73	39			

Table 4.8 Cubic Spline Empirical Model Frequency ANOVA Test Results

is well suited to perform a full ANOVA test consisting of the four variables used in the full factorial designed experiment and their possible interactions.

4.3.2 Full Effects ANOVA Test. Since Section 4.3.1 proved the usefulness of the cubic spline empirical model for ANOVA testing, this section uses the cubic spline gain predictions to extend the ANOVA test in Section 4.3.1 to include all four variable parameters used in the full factorial designed experiment. The full ANOVA test includes interactions among the variables and studies each factor's effect on the average antenna gain. Using 100 normal randomly distributed replicates of the variable combinations listed in Table 4.10, the ANOVA test proves that each variable used in the full factorial design strongly influences the average antenna gain for the antenna design of Figure 4.1 in the angular region described by Equations (4.1) and (4.2).

Factor	Sum of Squares	Degrees of Freedom	Mean Square	F_0	$\alpha = 0.01$ F Statistic
Frequency	24.89	3	8.30	14.07	4.31
Error	21.19	36	0.59		
Total	46.08	39			

Table 4.9 HFEM Frequency ANOVA Test Results

Frequency (GHz)	0.95, 1.05, 1.15, and 1.25
First Layer Relative Permittivity	1.5, 3, 5, and 7
Second Layer Relative Permittivity	1.5, 3, 5, and 7
First Layer Thickness (cm)	0.356, 0.593, 0.830, and 1.067
Replicates Per Combination	100

Table 4.10 Full ANOVA Test Variable Levels

4.3.2.1 Full ANOVA Test Hypotheses. Extending the test hypotheses of Section 3.4.1 to four variables, the null hypothesis, H_0 , for each variable parameter predicts that none of the variable levels effect the average antenna gain, while the alternate hypothesis, H_1 , of each variable predicts that at least one variable level effects the average antenna gain. In terms of variable interaction, for each variable interaction combination the null hypothesis predicts that none of the variable levels included in the interaction combination effect the average antenna gain, while the alternate hypothesis predicts that at least one variable level included in the interaction combination effects the measured average antenna gain. In other words, the ANOVA test determines the sensitivity of the antenna gain to changes in the antenna operating frequency, the first and second dielectric superstrate relative permittivities, and the first dielectric superstrate thickness as well as their interactions.

4.3.2.2 Full ANOVA Statistical Analysis. Applying the statistical techniques of Section 3.4.2 to the four experimental variables, Table 4.11 summarizes the results of the full ANOVA test. In each case, the calculated F_0 statistic exceeds the required F statistic with the confidence level of 1 percent and proves the null hypotheses false. Each variable factor and variable interaction factor significantly affects the average antenna gain. From Table 4.11, frequency has the greatest influence on the average antenna gain for the cavity-backed antenna of Figure 4.1. Since cavities resonate at specific frequencies according to their dimensions in frequency wavelengths, the frequency effects for the full ANOVA test follow engineering expectations. The relative permittivity of the second superstrate layer has the second largest influence on the average antenna gain of

Factor Number	Factor	Sum of Squares	Degrees of Freedom	Mean Square	F_0	$\alpha = 0.01$ F Statistic
1	<i>freq</i>	8018.94	3	2672.98	4135.62	3.8
2	ϵ_{r1}	1892.91	3	630.97	976.23	3.8
3	ϵ_{r2}	4317.31	3	1439.10	2226.58	3.8
4	<i>thick</i> ₁	50.78	3	16.93	26.19	3.8
5	<i>freq</i> ϵ_{r1}	5147.94	9	571.99	884.99	2.4
6	<i>freq</i> ϵ_{r2}	10821.47	9	1202.39	1860.33	2.4
7	<i>freqthick</i> ₁	121.56	9	13.51	20.90	2.4
8	$\epsilon_{r1}\epsilon_{r2}$	1277.47	9	141.94	219.61	2.4
9	ϵ_{r1} <i>thick</i> ₁	320.75	9	35.64	55.14	2.4
10	ϵ_{r2} <i>thick</i> ₁	566.41	9	62.93	97.37	2.4
11	<i>freq</i> $\epsilon_{r1}\epsilon_{r2}$	1286.12	27	47.63	73.70	1.75
12	<i>freq</i> ϵ_{r1} <i>thick</i> ₁	871.59	27	32.28	49.95	1.75
13	<i>freq</i> ϵ_{r2} <i>thick</i> ₁	900.25	27	33.34	51.59	1.75
14	$\epsilon_{r1}\epsilon_{r2}$ <i>thick</i> ₁	153.44	27	5.68	8.79	1.75
15	<i>freq</i> $\epsilon_{r1}\epsilon_{r2}$ <i>thick</i> ₁	308.41	81	3.81	5.89	1.4
	Error	14981.94	23180	0.65		
	Total	51037.28	23435			

Table 4.11 Full ANOVA Test Results

this particular antenna configuration. It stands to reason due to its close proximity to the antenna radiating aperture that the second dielectric superstrate layer's relative permittivity has a stronger influence than the first dielectric superstrate. In fact, the variable interaction created by the interaction between antenna operating frequency and the second dielectric superstrate relative permittivity has the third largest influence on the average antenna gain. In terms of manufacturing tolerances and variable sensitivities, this full ANOVA test indicates that tolerances relating to frequency and the relative permittivity of the second dielectric superstrate are the most critical and require tight manufacturing control. The remaining factors studied in this full ANOVA test are easily ranked according to their impact on the average antenna gain where each factor strongly influences the average antenna gain.

4.4 Optimization Procedures

From Chapter III, the fourth RSM task searches for the optimal levels of the input variables that produce the desired optimized system response. In this experiment, the

Frequency	1.3 GHz
First Layer Relative Permittivity	6.0
Second Layer Relative Permittivity	8.0
First Layer Thickness	0.474 cm
Average Gain (HFEM)	-5.779 dB

Table 4.12 Initial Optimized Location Guess

Frequency	1.3 GHz
First Layer Relative Permittivity	6.696
Second Layer Relative Permittivity	8.0
First Layer Thickness	0.512 cm
Elapsed Optimization Time	≈ 1 min
Simplex Iterations	180
Average Gain (Empirical Model)	-5.890 dB
Average Gain (HFEM)	-6.206 dB
Input Impedance (HFEM)	$48.080 + j42.937$
Gain Accuracy	3.8 percent
Gain Improvement Over Initial Guess	4.8 percent
HFEM Optimization Validation Period	2 hrs, 59 mins

Table 4.13 Optimized Antenna Design

desired response is a minimum average antenna gain over the angular region described by Equations (4.1) and (4.2). Using the simplex optimization method of Section 3.5.2, the cubic spline average antenna gain empirical model, the initial optimized design guess given in Table 4.12, and the optimization flow chart of Figure 4.10, the resulting optimized antenna design is listed in Table 4.13. In terms of field quantities, the average antenna gain of the optimized design compares within 3.8 percent of the validated HFEM optimized design configuration solution with a net average antenna gain reduction of 4.8 percent over the initial guess design. The resulting antenna radiation pattern of Figure 4.11 indicates a null located above the antenna bore sight in the desired angular region thus demonstrating that this is a feasible optimized design methodology.

Figures 4.12, 4.13, 4.14, 4.15, 4.16, and 4.17 represent the average antenna gain response of the optimized antenna design as variable pairs approach their optimized values. For example, in Figure 4.12 as the first layer relative permittivity approaches 6.696, the permittivity optimized value, and as the antenna operating frequency approaches 1.3 GHz,

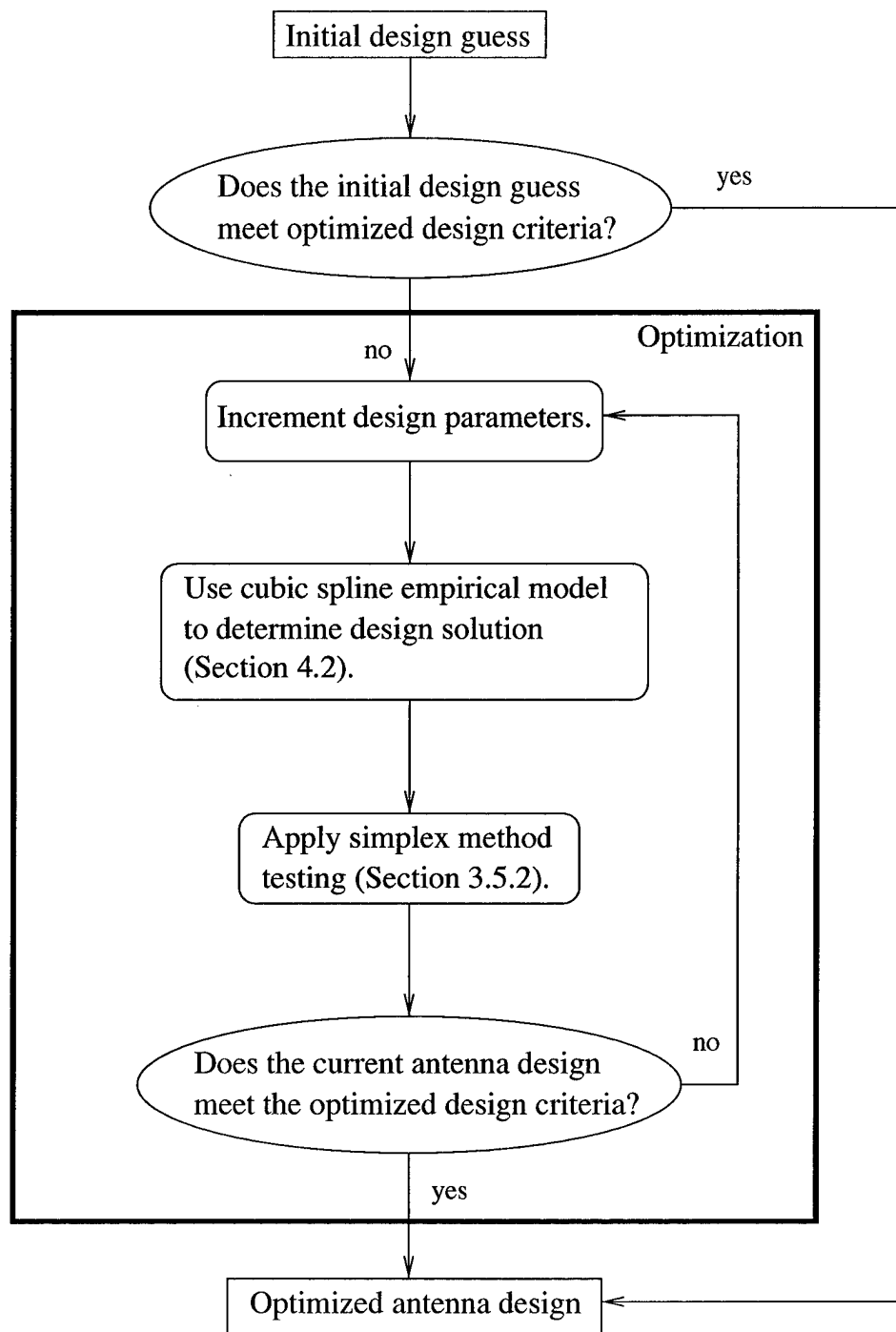


Figure 4.10 Optimization Process Flow Chart

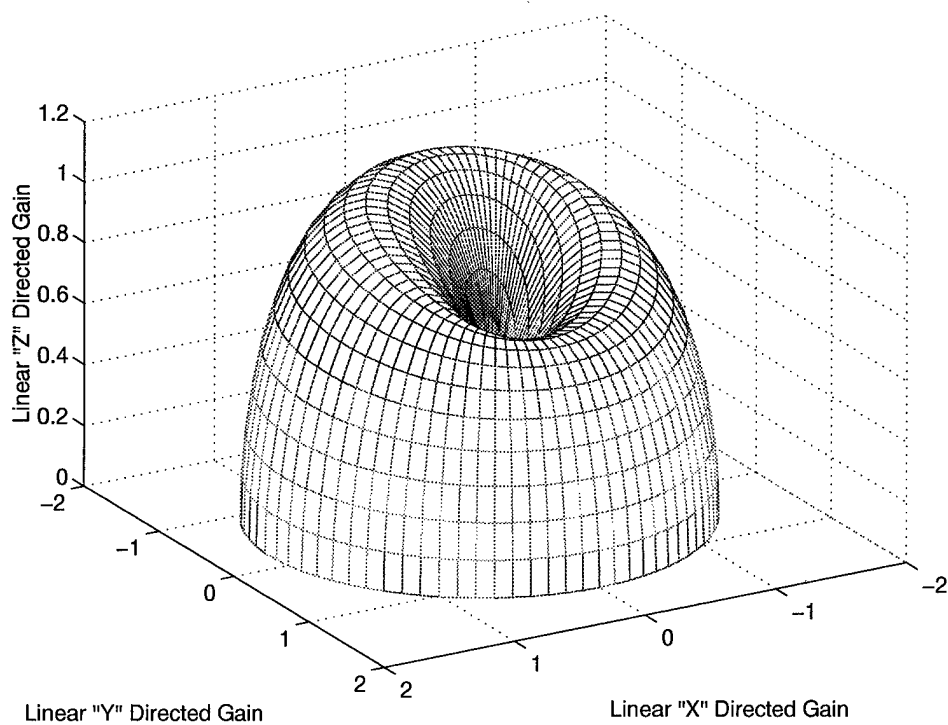


Figure 4.11 Optimized Antenna Pattern

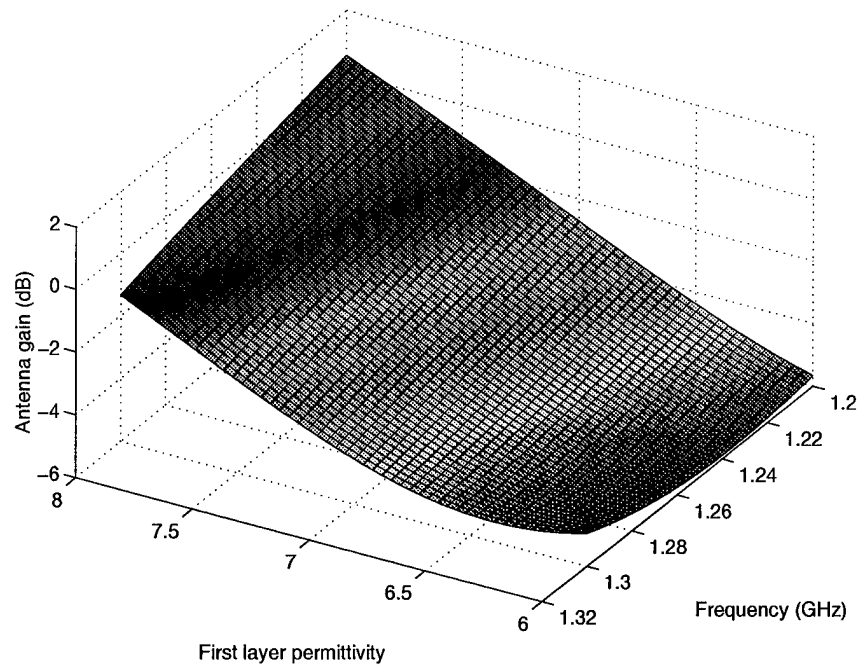


Figure 4.12 First Layer Relative Permittivity and Frequency Effects Near the Optimized Location

the frequency optimized value, the average antenna gain approaches a minimum value near -6.0 dB.

Besides the location of an optimized antenna design, Table 4.13 yields some interesting points. Using the validated cubic spline empirical model to locate an optimized antenna design for the antenna configuration of Figure 4.1, each simplex method iteration took approximately 0.33 seconds to complete. When validating the optimized design using an HFEM code, the single antenna design configuration took approximately three hours to calculate. Assuming each simplex iteration would take as long, it would have taken 23 days for the HFEM code to come up with the optimized design that the RSM method found in only one minute. This is the power of RSM and designed experiments. The design methodology used in this experiment is accurate and a tremendous time saving tool.

4.5 Additional System Response Modeling Possibilities

In addition to the average antenna gain system response in the angular region described by Equations (4.1) and (4.2), other possible desired system responses exist for the

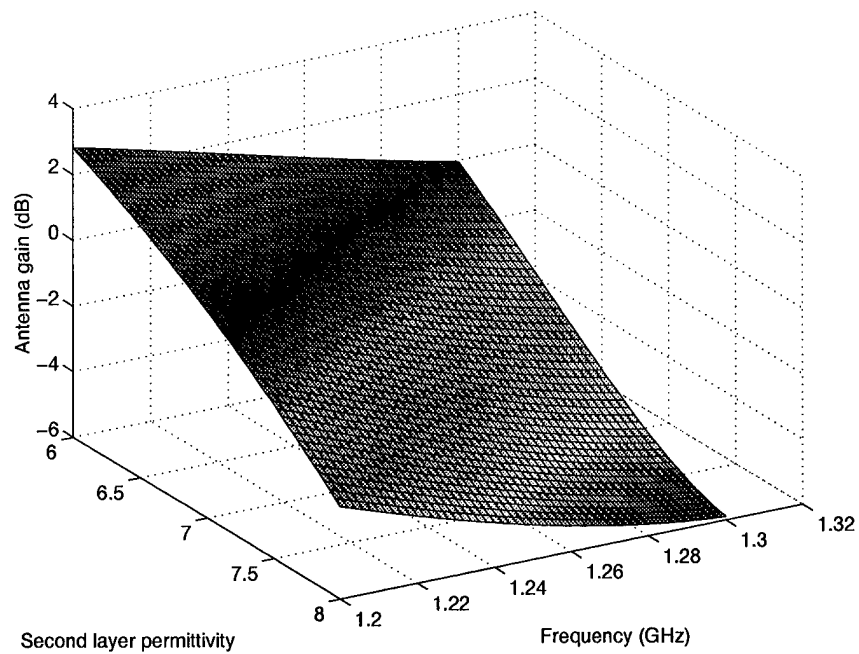


Figure 4.13 Second Layer Relative Permittivity and Frequency Effects Near the Optimized Location

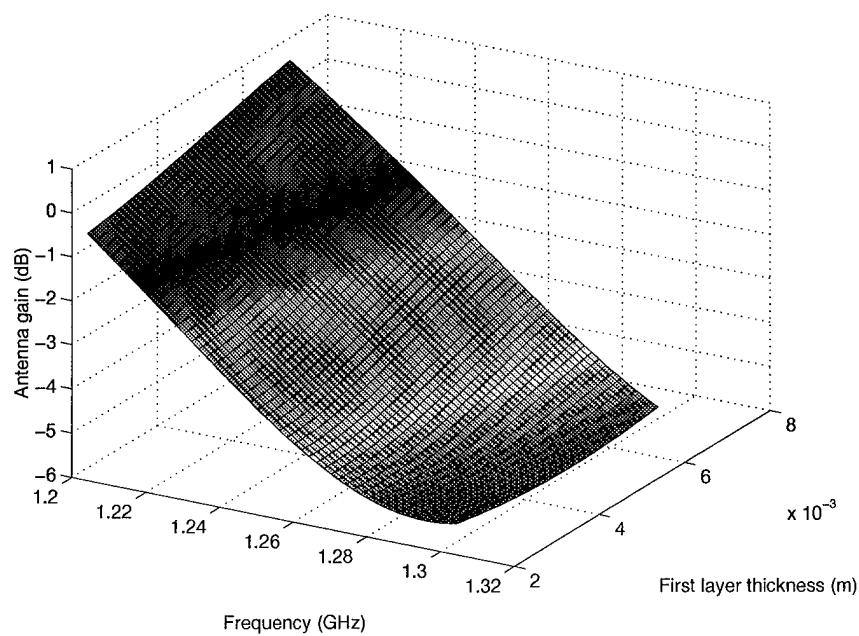


Figure 4.14 First Layer Thickness and Frequency Effects Near the Optimized Location

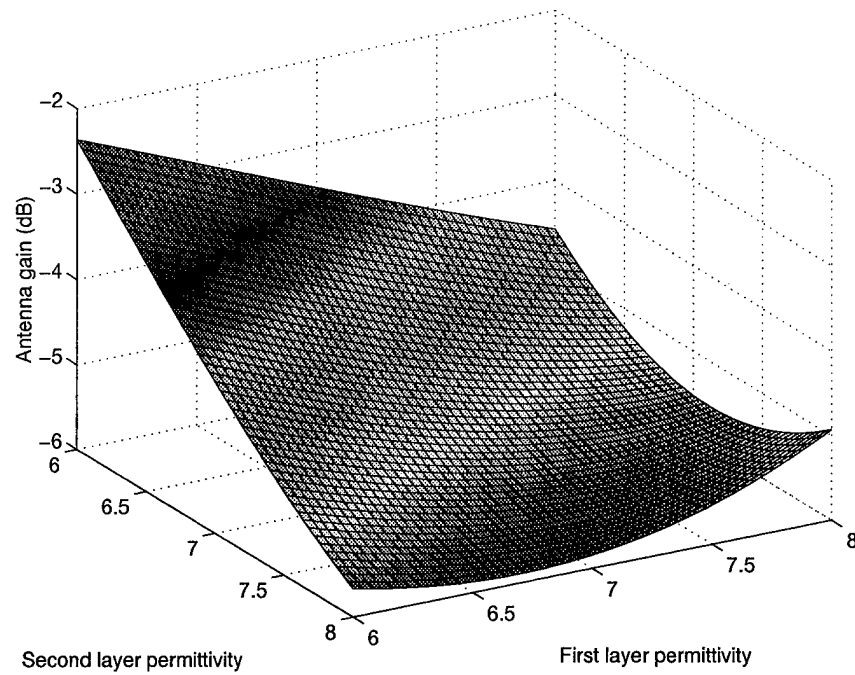


Figure 4.15 First and Second Layer Relative Permittivity Effects Near the Optimized Location

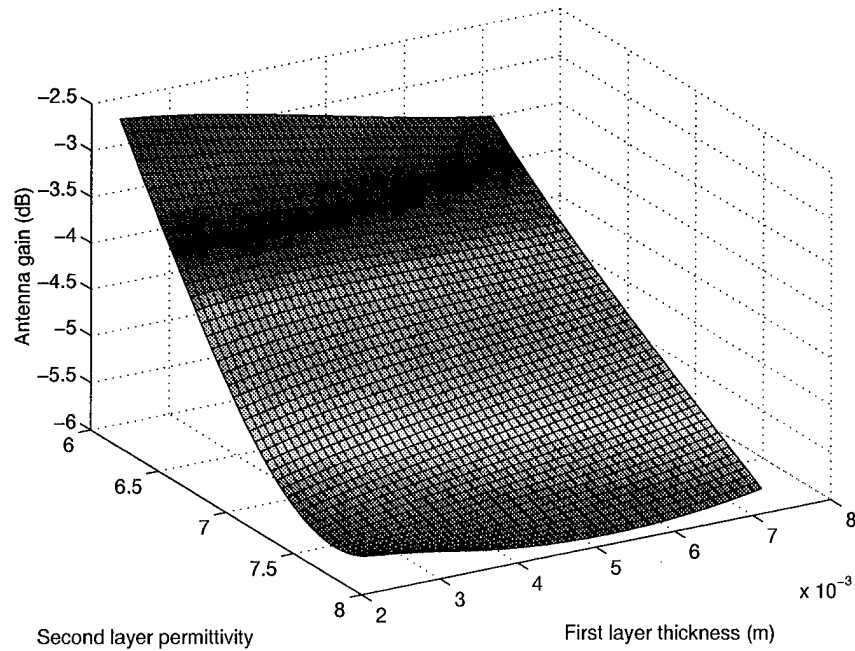


Figure 4.16 First Layer Thickness and Second Layer Relative Permittivity Effects Near the Optimized Location

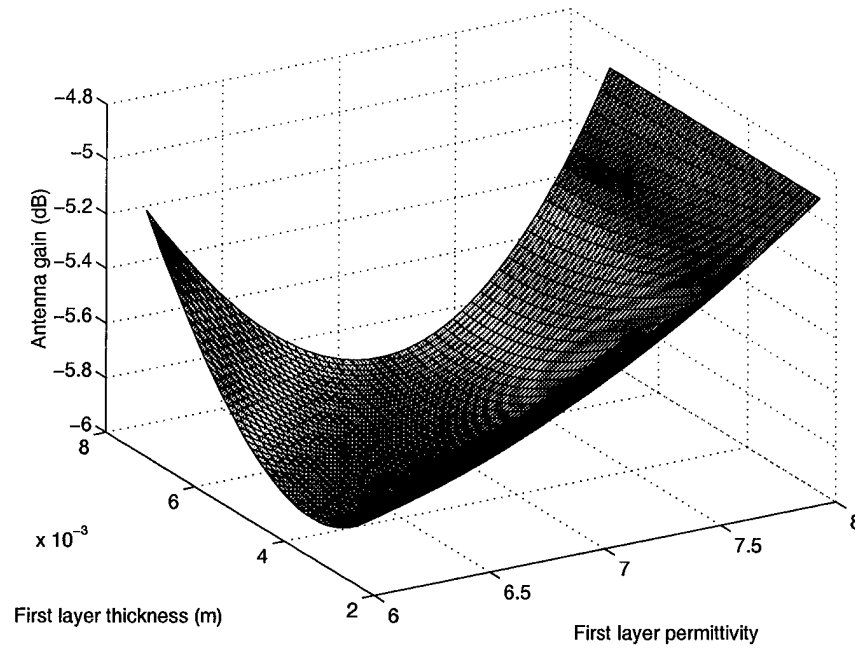


Figure 4.17 First Layer Relative Permittivity and Thickness Effects Near the Optimized Location

antenna design of Figure 4.1 such as antenna input impedance or average antenna gain near the cavity ground plane. Using the full factorial designed experiment of Section 4.1.5 and the model adequacy tests in Section 4.2.3, Section 4.5.1 analyzes the ability of the cubic spline empirical modeling technique to adequately describe the performance of antenna input impedance within the input variable ranges of Table 4.2. Likewise, Section 4.5.2 analyzes the ability of the cubic spline empirical modeling technique to adequately describe the average antenna gain in the angular region described by Equations (4.5) and (4.6) within the input variable ranges of Table 4.2.

$$70^\circ \leq \theta \leq 85^\circ \quad (4.5)$$

$$0^\circ \leq \phi \leq 360^\circ \quad (4.6)$$

4.5.1 Input Impedance Modeling. At first glance, the impedance modeling adequacy plots of Figures 4.18, 4.19, 4.20, 4.21, 4.22, and 4.23 indicate that the cubic spline

Real Impedance Residual Mean	-0.0941 ohms
Real Impedance Residual Standard Deviation	4.4942 ohms
Imaginary Impedance Residual Mean	0.9459 ohms
Imaginary Impedance Residual Standard Deviation	6.6533 ohms

Table 4.14 Real and Imaginary Impedance Residual Means and Standard Deviations

empirical model poorly characterizes the antenna's input impedance performance. In fact, from the normal probability plots both the real and imaginary impedance residuals vary over a large range of impedances. Likewise, from the residuals versus fitted value plots and the residuals versus individual variable plots both the real and imaginary impedance residuals vary over an excessively large impedance range. Furthermore, Table 4.14 lists the mean impedance residuals along with corresponding residual standard deviations for both the real and imaginary impedance components indicating the poor modeling performance of the cubic spline empirical model. Despite the high modeling variability, one encouraging prospect remains. The impedance empirical models predict impedance trends, and if employed correctly in a weighted or combined optimization procedure, the impedance empirical models may provide a useful optimization tool. Chapter V employs a combined optimization procedure composed of both average antenna gain and antenna impedance empirical models.

4.5.2 Average Antenna Gain Modeling Near the Cavity Ground Plane. In a similar situation, the modeling adequacy plots of Figures 4.24, 4.25, 4.26, 4.27, 4.28, and 4.29 give little indication that the four variable cubic spline empirical model accurately describes the average antenna gain near the cavity ground plane. Using Equations (4.5) and (4.6), the average antenna gain near the antenna ground plane is described by

$$averagegain = 20 \log \left(\frac{10^{\left(\frac{gain_{70^\circ}}{20}\right)} + 10^{\left(\frac{gain_{75^\circ}}{20}\right)} + 10^{\left(\frac{gain_{80^\circ}}{20}\right)} + 10^{\left(\frac{gain_{85^\circ}}{20}\right)}}{4} \right). \quad (4.7)$$

The antenna gain normal probability plot of Figure 4.24 shows that the average antenna gain residuals vary over a total range of approximately 8.2 dB which is repeated in the residuals versus fitted values plot and the residuals versus individual variable plots. Table 4.15

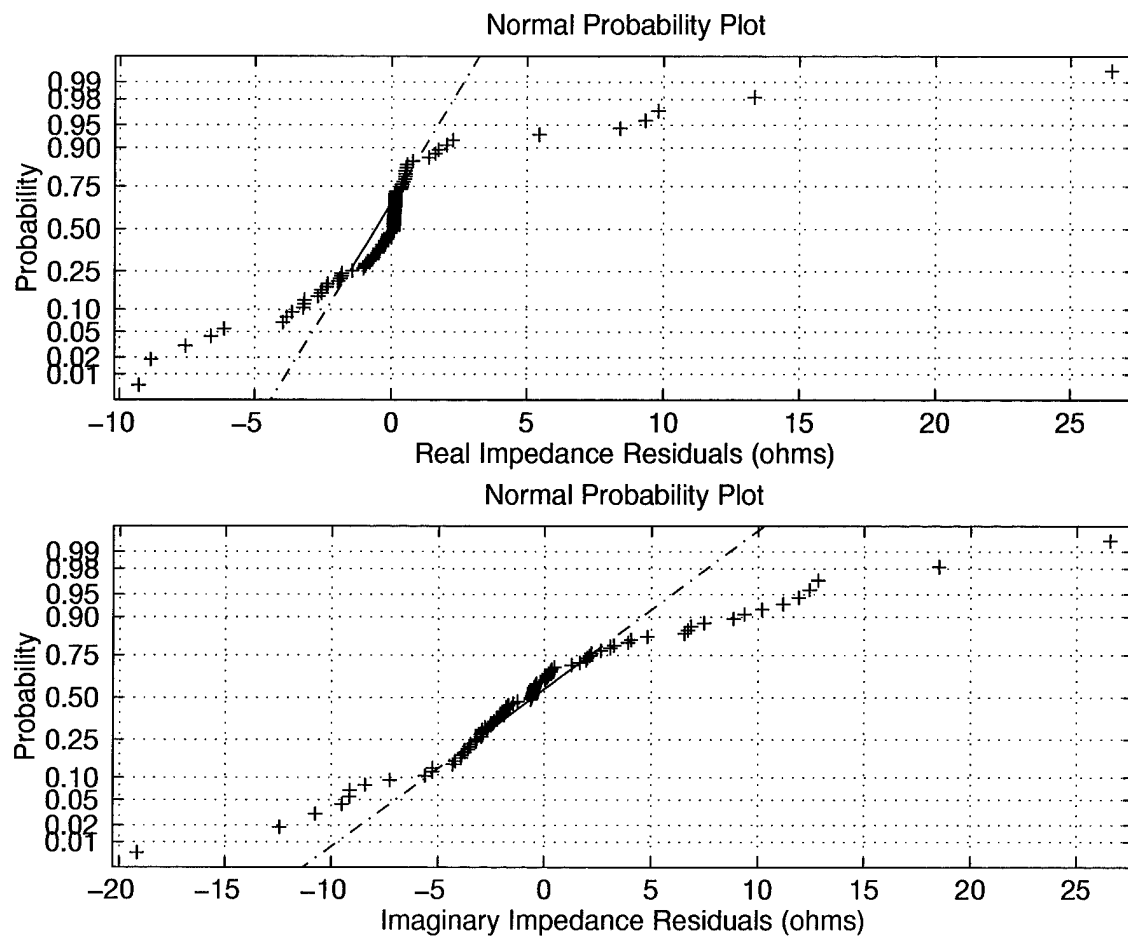


Figure 4.18 Normal Probability Plots of Cubic Spline Input Impedance Residuals

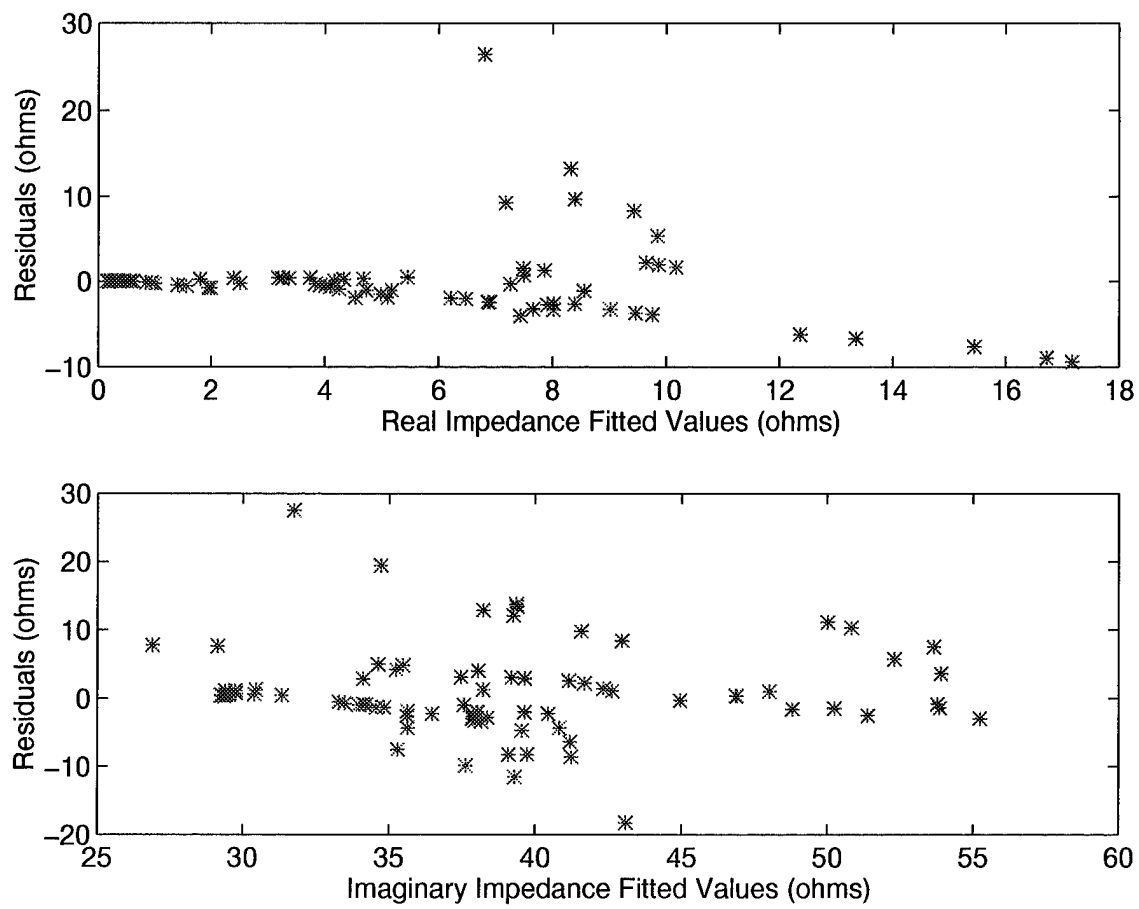


Figure 4.19 Cubic Spline Impedance Residuals Versus Fitted Values

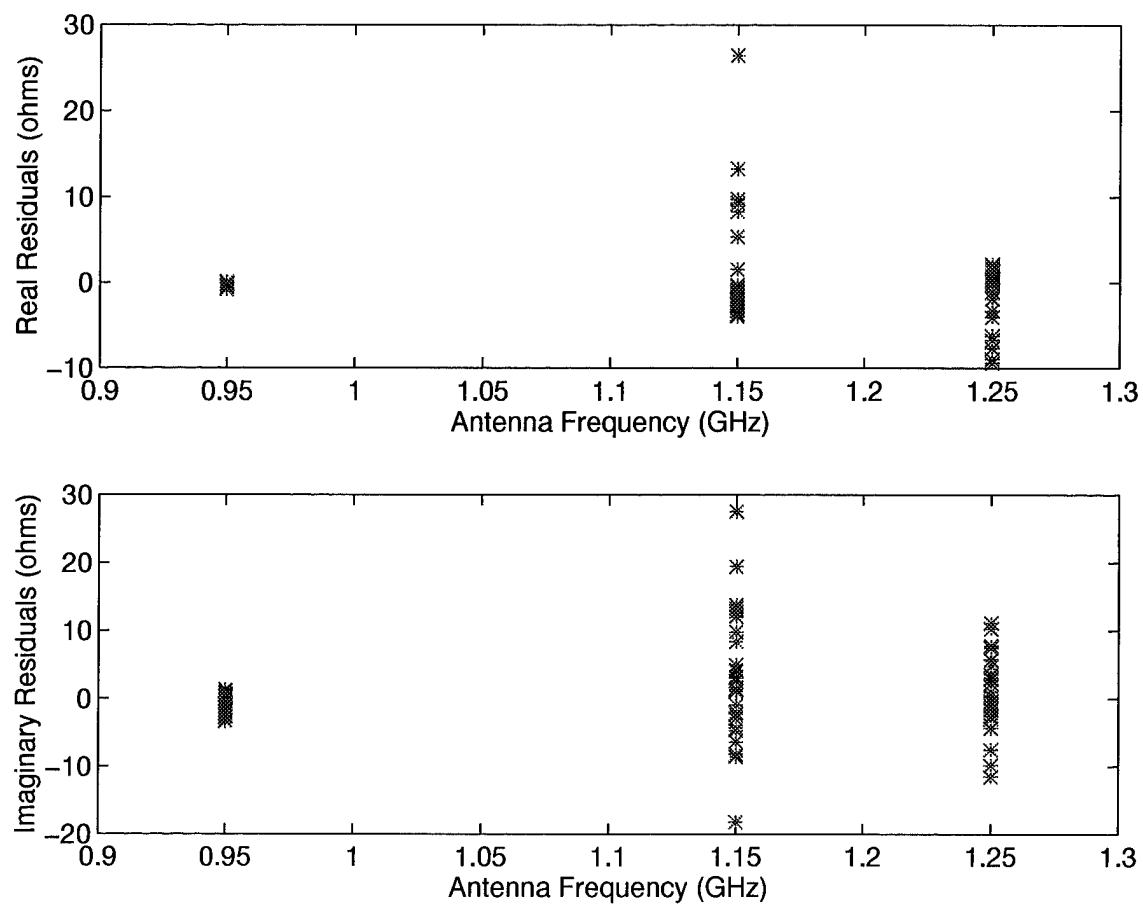


Figure 4.20 Cubic Spline Impedance Residuals Versus Frequency Values

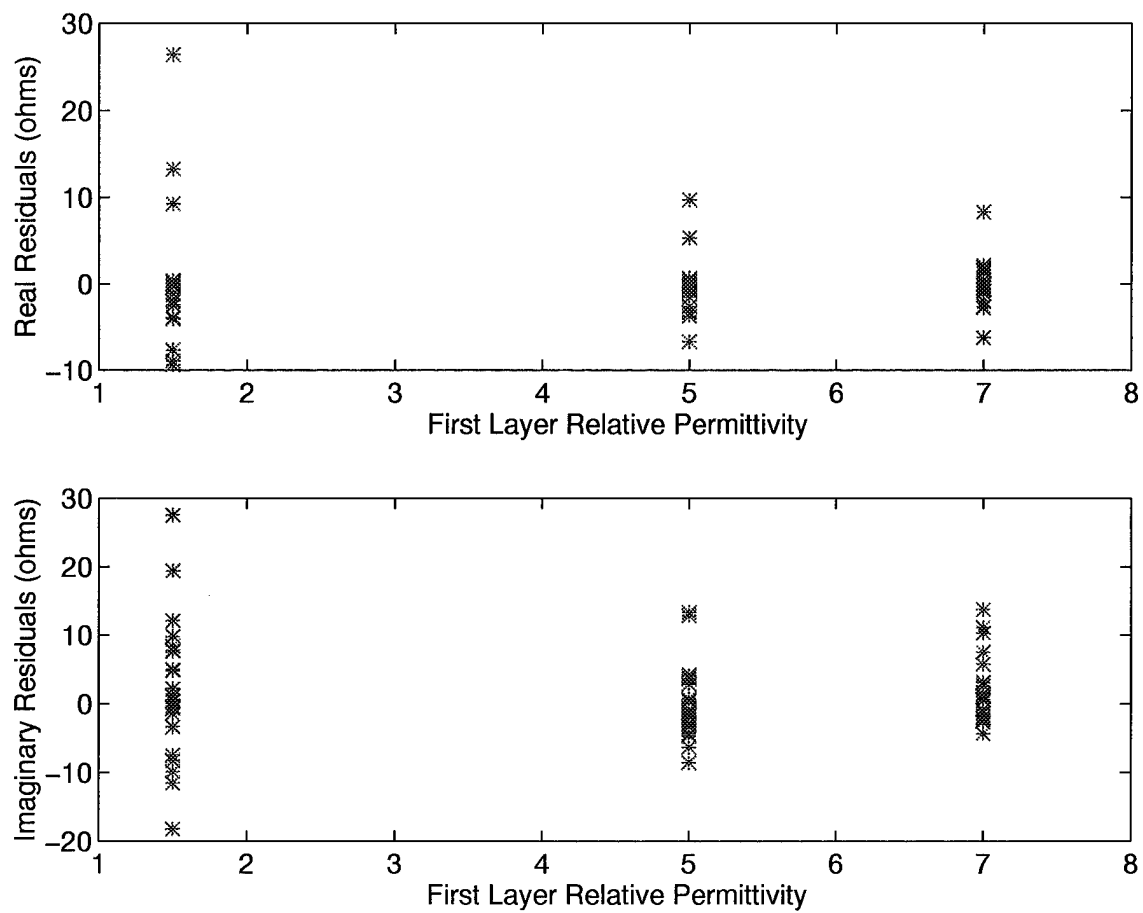


Figure 4.21 Cubic Spline Impedance Residuals Versus First Layer Relative Permittivity Values

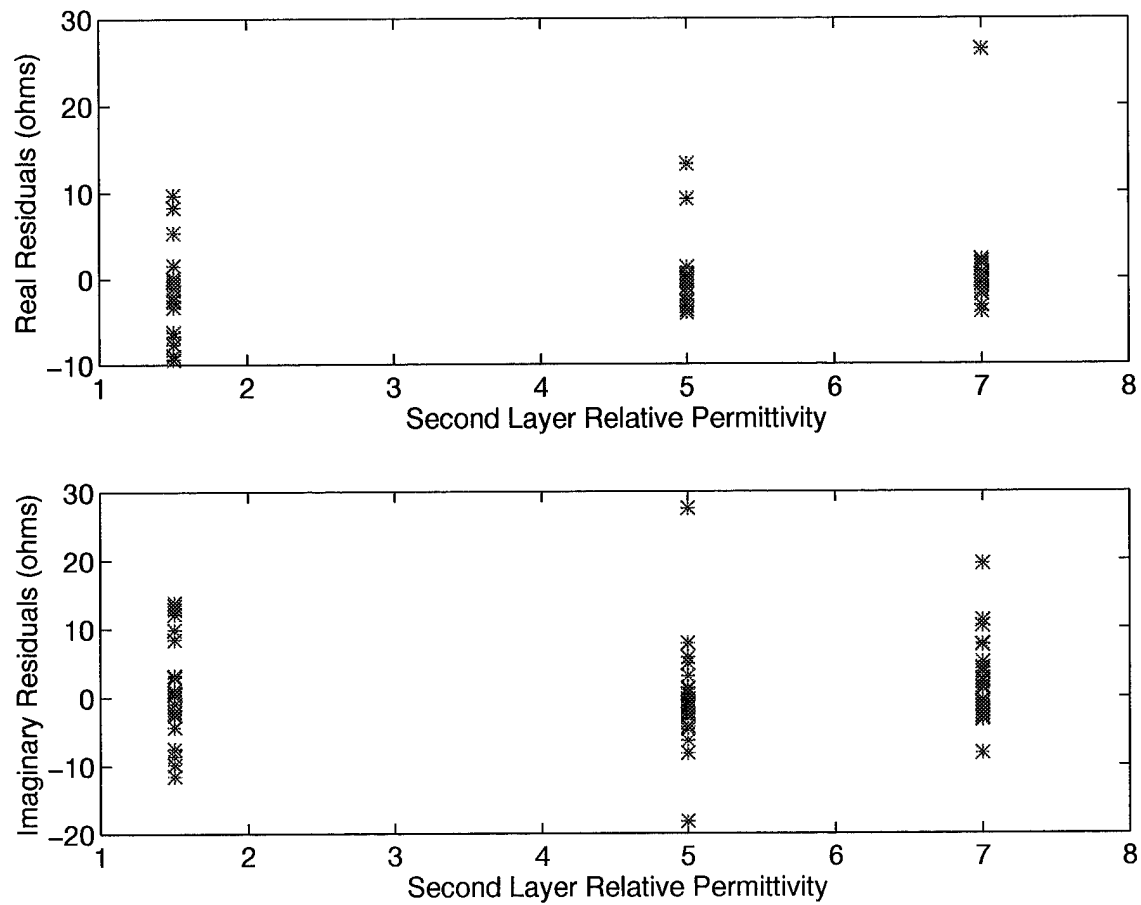


Figure 4.22 Cubic Spline Impedance Residuals Versus Second Layer Relative Permittivity Values

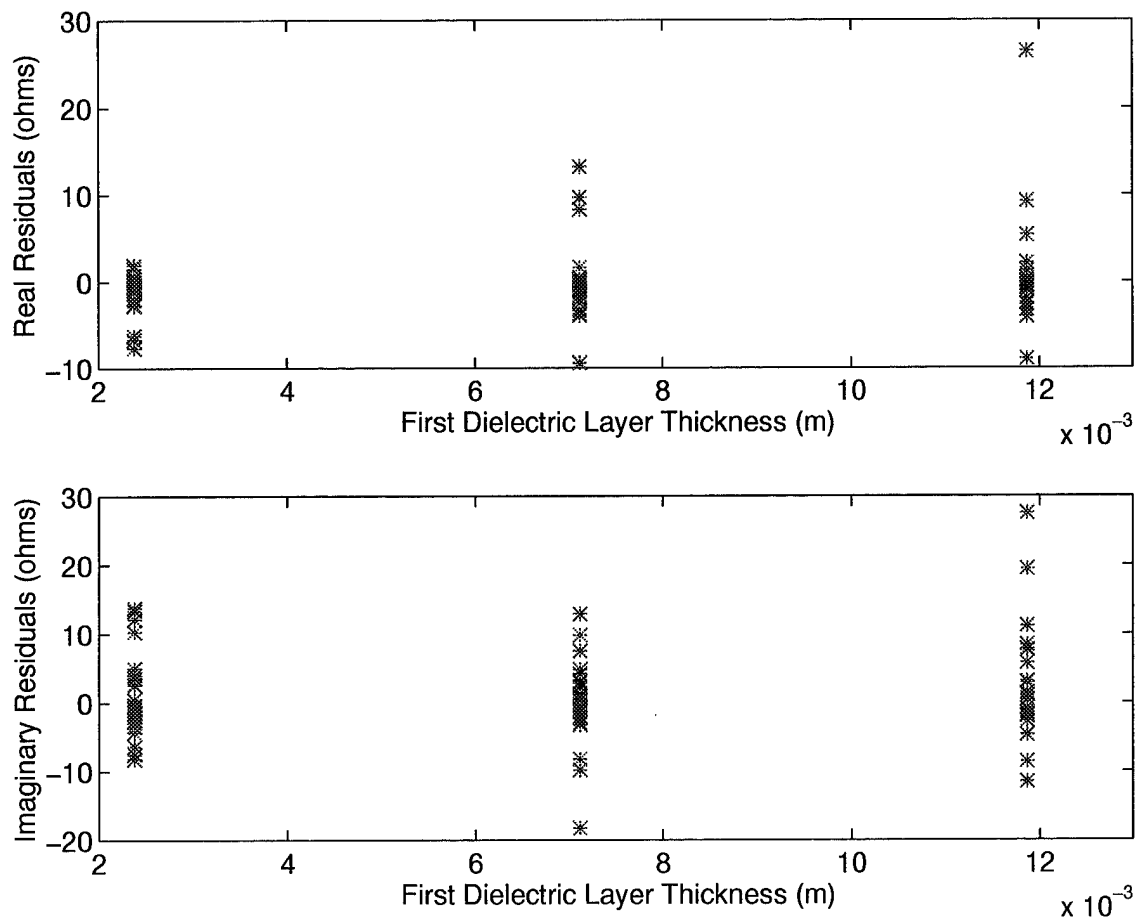


Figure 4.23 Cubic Spline Impedance Residuals Versus First Layer Thickness Values

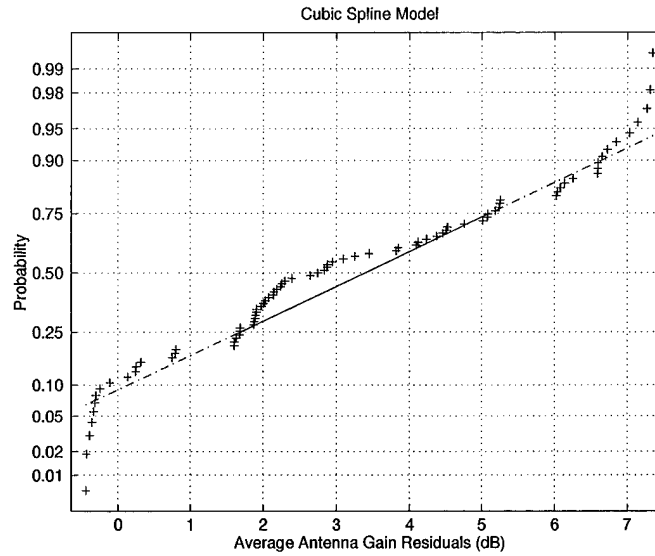


Figure 4.24 Cubic Spline Normal Probability Plot of Residuals Near Ground Plane

Residual Mean	0.0357 dB
Residual Standard Deviation	0.1592 dB

Table 4.15 Average Antenna Gain Cubic Spline Model Residual Mean And Residual Standard Deviation Values Near Ground Plane

lists the residual mean and residual standard deviation values of the average antenna gain empirical model near the cavity ground plane.

Empirical modeling near the antenna ground plane requires smaller variable steps in the full factorial designed experiment to adequately predict average antenna gain. Lobing effects due to antenna pattern side lobes and metallic cavity interaction make empirical modeling more strenuous. In addition, using a narrower angular region such as

$$85^{\circ} \leq \theta \leq 90^{\circ} \quad (4.8)$$

$$0^{\circ} \leq \phi \leq 360^{\circ} \quad (4.9)$$

with average antenna gain measurements performed at one degree increments could possibly provide a better opportunity to accurately characterize the antenna performance near the ground plane.

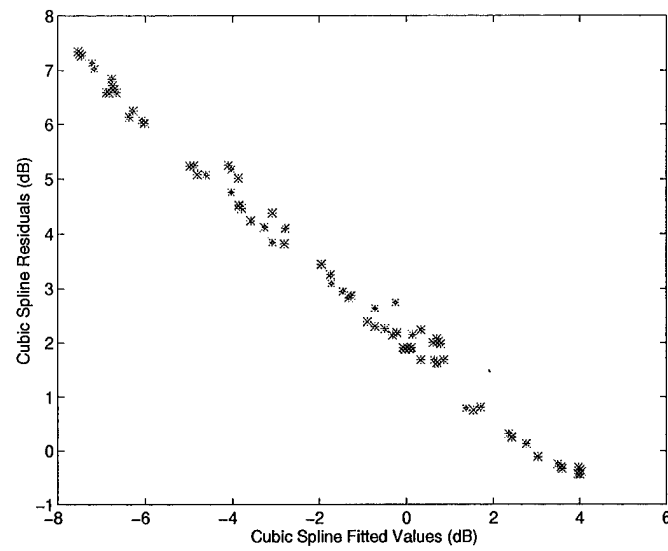


Figure 4.25 Cubic Splines Residuals Near Ground Plane Versus Fitted Values

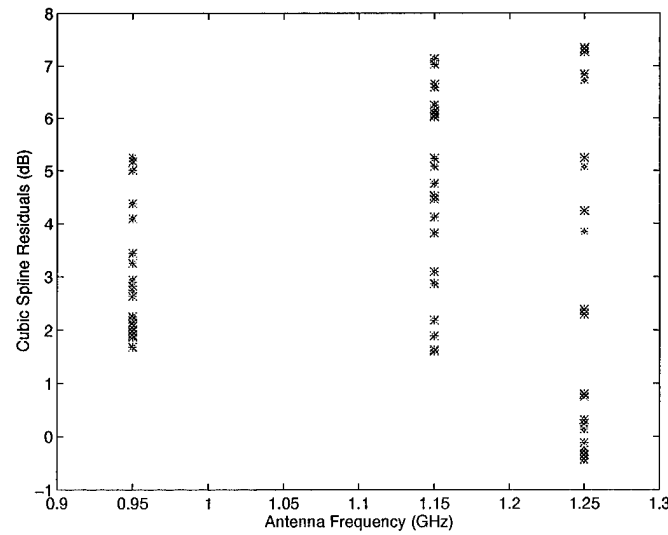


Figure 4.26 Cubic Splines Residuals Near Ground Plane Versus Frequency Values

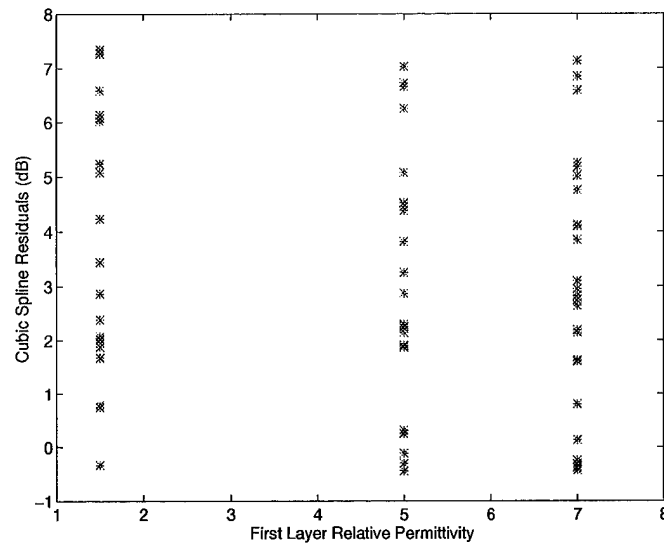


Figure 4.27 Cubic Spline Residuals Near Ground Plane Versus First Layer Relative Permittivity Values

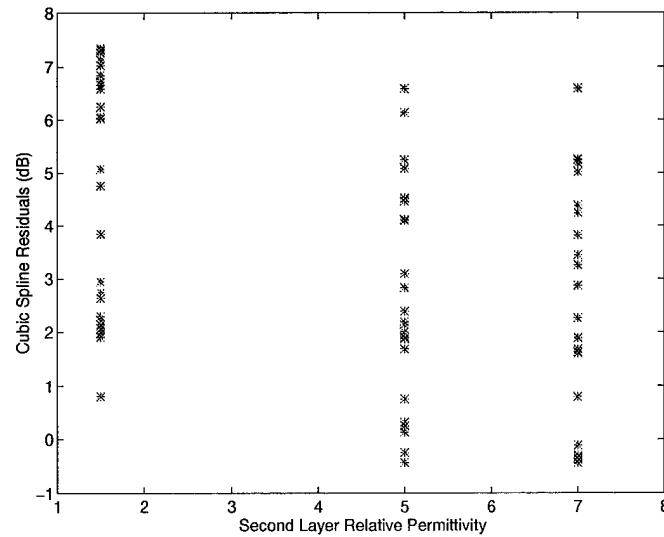


Figure 4.28 Cubic Spline Residuals Near Ground Plane Versus Second Layer Relative Permittivity Values

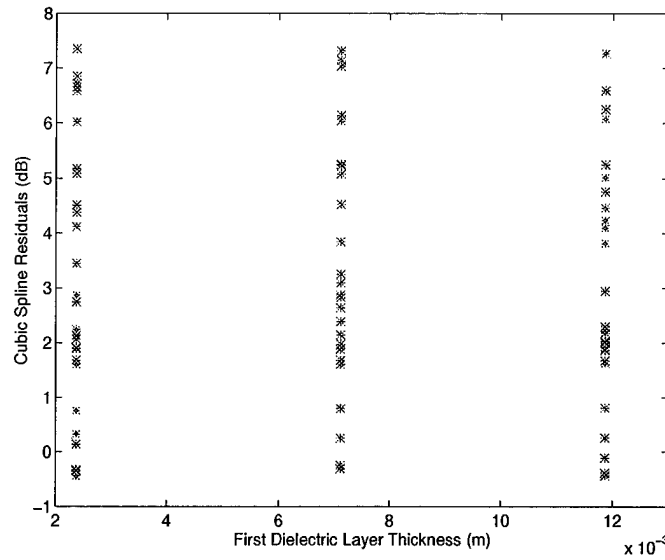


Figure 4.29 Cubic Spline Residuals Near Ground Plane Versus First Layer Thickness Values

4.6 Closing Comments

Developed here, an RSM based optimized antenna design methodology composed of a full factorial designed experiment, a cubic spline empirical model, empirical model ANOVA tests, and the simplex optimization method successfully determined an optimized antenna design for the microstrip antenna configuration of Figure 4.1 for average antenna gain in the angular regions in Equations (4.1) and (4.2). Validated by HFEM code comparisons the optimized design methodology showed its strength in the time savings observed while performing the optimization procedure. In addition, using the cubic spline empirical model to perform ANOVA testing for the full variable case quickly demonstrated the antenna design sensitivity to variable changes and indicated the design areas requiring close manufacturing control. The next step towards completely establishing this optimized design methodology for this antenna configuration is its application to a realizable antenna with accessible dielectric values followed by antenna range validation.

V. Optimized Design Methodology Implementation

This chapter implements the optimized design methodology developed in Chapter IV and uses a more accessible dielectric substrate with a relative permittivity value of 4.5. Changing the substrate's dielectric constant requires the scaling of Figure 4.1 which allows for minor design variable adjustments. This implementation of the design methodology uses a full factorial designed experiment, cubic spline empirical modeling, and simplex optimization as in Chapter IV, but it applies a combined optimization function that requires minimum average antenna gain and 50 Ohm input impedance. The optimization results produce a realizable antenna design that corresponds well with Hybrid Finite Element Method (HFEM) results and with antenna range measurements.

5.1 Experiment Development

Since changing the substrate relative permittivity of Figure 4.1, scaling using Equation (5.1) produced the antenna of Figure 5.1 with dimensions listed in Table 5.1.

$$ScaleFactor = \frac{\sqrt{\epsilon_{old}}}{\sqrt{\epsilon_{new}}} \quad (5.1)$$

In Equation (5.1) ϵ_{old} represents the substrate permittivity of Figure 4.1, and ϵ_{new} represents the substrate permittivity of Figure 5.1. The new antenna configuration and the intention of optimizing the antenna design well within the variable ranges rather than at variable limits led to adjustments of the input variable levels used in the design methodology development of Chapter IV.

5.1.1 Design Methodology Input Variable Levels. As in Chapter IV, the design methodology input variables include:

1. Antenna operating frequency,
2. First dielectric superstrate layer relative permittivity,
3. Second dielectric superstrate layer relative permittivity,
4. First dielectric superstrate layer thickness.

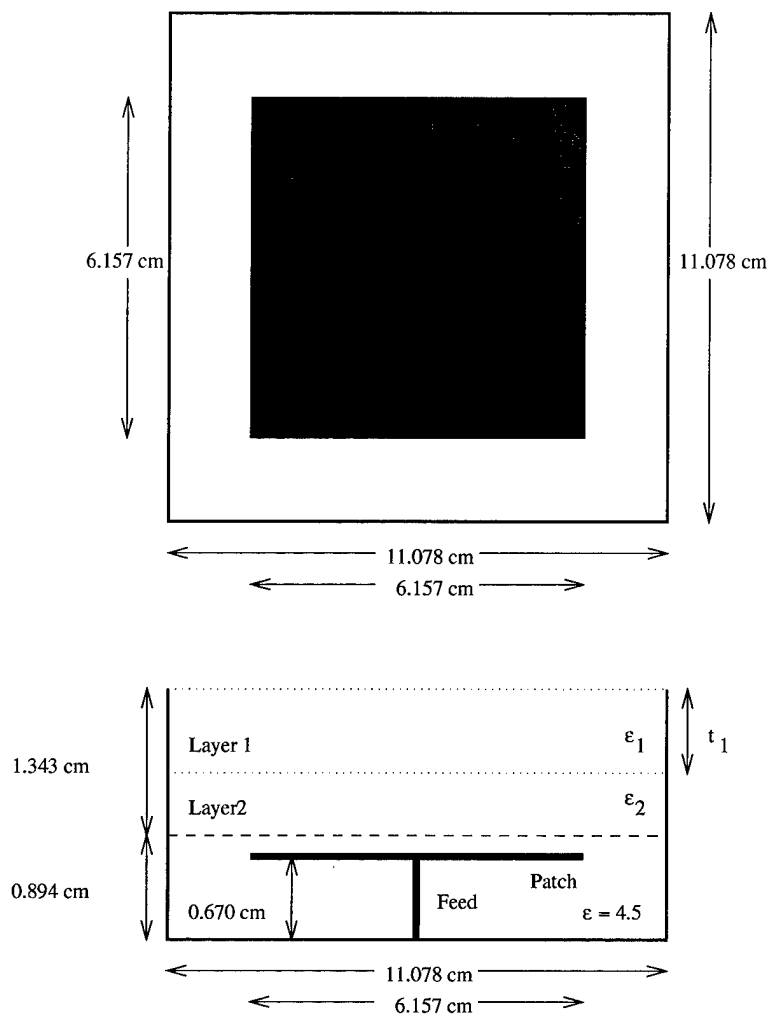


Figure 5.1 Scaled Antenna Design

Scale Factor	0.94281
Cavity Dimensions:	
Length	11.078 cm
Width	11.078 cm
Height	2.237 cm
Patch Dimensions:	
Length	6.157 cm
Width	6.157 cm
Patch Location	Centered 0.670 cm Above Cavity Bottom
Feed Pin Location	0.615 cm Off Center
Substrate Permittivity	4.5
Substrate Thickness	0.894 cm

Table 5.1 Scaled Constant Antenna Design Parameters

5.1.1.1 Antenna Operating Frequency. As in Section 4.1.3.1, two preliminary HFEM tests that determine antenna input impedances for the scaled antenna configuration of Figure 5.1 located the frequency range of interest. Using first and second dielectric layer relative permittivities of 1.0 each and a characteristic impedance of 50 ohms, Figure 5.2 shows the antenna input admittance response using frequencies from 1.1 to 1.3 GHz. Likewise, using first and second dielectric layer relative permittivities of 10.0 and a characteristic impedance of 50 ohms, Figure 5.3 shows the antenna admittance response using frequencies from 1.2 to 1.4 GHz. Since the optimized antenna design found in Section 4.4 converged to the upper frequency limit used in Chapter IV, new frequency levels are needed. From Figures 5.2 and 5.3, the new frequency levels include 1.2, 1.25, 1.3, 1.35, and 1.4 GHz. Using Equation (5.2),

$$f = \frac{C}{2L}, \quad (5.2)$$

where C is the speed of light and L is the antenna cavity width, the new frequency level range covers the unfilled antenna cavity half wavelength resonant frequency, 1.353 GHz.

5.1.1.2 First and Second Dielectric Superstrate Layer Permittivities. As in Section 4.1.3.2, using practical antenna design experience and desiring easily accessible dielectric materials led to the selection of new first and second dielectric superstrate layer relative permittivities. In addition since the optimized antenna design of Section 4.4 converged to an upper limit for the second dielectric layer relative permittivity, the new relative permittivity values include 2.0, 4.0, 6.0, 8.0, and 10.0.

5.1.1.3 First Dielectric Superstrate Layer Thickness. As in Section 4.1.3.3, the partitioning property of the HFEM code used in the full factorial designed experiment limits the levels for the first dielectric superstrate layer to include 0.2237, 0.4474, 0.6711, 0.8948, and 1.1185 centimeters. Table 5.2 lists the new designed experiment variables and their corresponding variable levels.

5.1.2 Measured Responses. The measured responses from the full factorial designed experiment include both the average antenna gain from Equation (4.3) over the

50 Ohm Characteristic Impedance, Frequency (1.10 GHz to 1.30 GHz)

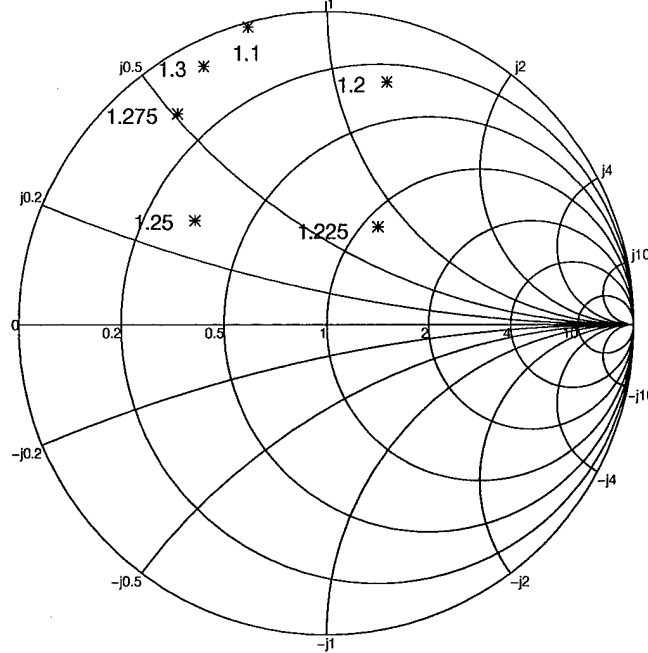


Figure 5.2 Scaled Antenna Smith Chart Analysis of Input Impedance Values With First and Second Superstrate Dielectric Relative Permittivities Equal to 1.0 ($\epsilon_{r1} = \epsilon_{r2} = 1.0$)

Frequency (GHz)	1.20, 1.25, 1.30 1.35, and 1.40
First Layer Relative Permittivity	2, 4, 6, 8, and 10
Second Layer Relative Permittivity	2, 4, 6, 8, and 10
First Layer Thickness (cm)	0.2237, 0.4474, 0.6711, 0.8948, and 1.1185

Table 5.2 Scaled Variable Antenna Design Parameters

50 Ohm Characteristic Impedance, Frequency (1.20 GHz to 1.40 GHz)

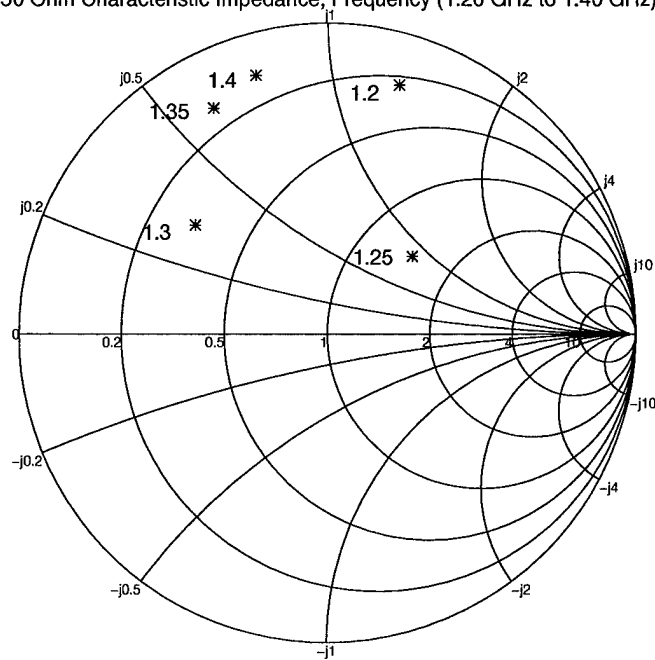


Figure 5.3 Scaled Antenna Smith Chart Analysis of Input Impedance Values With First and Second Superstrate Dielectric Relative Permittivities Equal to 10.0 ($\epsilon_{r1} = \epsilon_{r2} = 10.0$)

Test	Layer 1 (cm)	ϵ_{r1}	ϵ_{r2}	Freq (GHz)	Gain (dB)
1	0.2237	2	2	1.20	y_1
2	0.2237	2	2	1.25	y_2
3	0.2237	2	2	1.30	y_3
4	0.2237	2	2	1.35	y_4
5	0.2237	2	2	1.40	y_5
6	0.2237	2	4	1.20	y_6
\vdots	\vdots	\vdots	\vdots	\vdots	\vdots
625	1.2185	10	10	1.40	y_{625}

Table 5.3 Scaled Antenna Full Factorial Design

Frequency (GHz)	1.26, 1.32, 1.38
First Layer Relative Permittivity	3, 7, 9
Second Layer Relative Permittivity	3, 7, 9,
First Layer Thickness (cm)	0.2237, 0.6711, 1.1185

Table 5.4 Scaled Antenna Model Adequacy Test Variable Levels

angular region described by Equations (4.1) and (4.2) and the antenna input impedance. Later, the simplex optimization method combines the average antenna gain and the antenna input impedance to form a combined optimization function to locate an antenna design with minimum average gain and an input impedance of 50 ohms.

5.1.3 Experimental Design. Using a similar full factorial designed experiment as Section 4.1.5 with new input variable levels, Table 5.3 lists the new four-variable, five-level designed experiment. This full factorial experiment includes 625 (5^4) system response measurements for both the average antenna gain and the antenna input impedance.

5.2 Average Antenna Gain and Input Impedance Modeling

Using the cubic spline multi-dimensional empirical modeling algorithm introduced in Section 4.2.1, the variable levels of Table 5.4, and the cases listed in Table 5.5, Section 5.2.1 and Section 5.2.2 demonstrate empirical modeling adequacies for average antenna gain and the antenna input impedance respectively.

Test	Layer 1 (cm)	ϵ_{r1}	ϵ_{r2}	Freq (GHz)	Gain (dB)
1	0.2237	3	3	1.26	y_1
2	0.2237	3	3	1.32	y_2
3	0.2237	3	3	1.38	y_3
4	0.2237	3	7	1.26	y_4
\vdots	\vdots	\vdots	\vdots	\vdots	\vdots
81	1.1185	9	9	1.38	y_{81}

Table 5.5 Scaled Antenna Model Adequacy Test Cases

5.2.1 Average Antenna Gain Model Adequacy. Following the example of Section 4.2.3, this section applies the empirical model adequacy tests of Section 3.3.4 to verify the accuracy of the average antenna gain cubic spline empirical model for the new scaled antenna. From Figure 5.4, the empirical model varies over a net range of approximately 2.2 dB, 1.0 dB greater than the cubic spline empirical model used in Section 4.2.3. The residuals in the normal probability plot of Figure 5.4 form less of a straight line than the residuals of Figure 4.4 and indicate less of a good model fit. Fortunately, the residual mean and the residual standard deviation values listed in Table 5.6 for the new average antenna gain empirical model closely correspond to those of Table 4.6. Recall that the new scaled antenna employs higher dielectric permittivities than the previous antenna configuration. Therefore, the increased variability of the empirical model most likely originates from the larger superstrate and substrate permittivities. Figure 5.5 indicates somewhat of a normal random distribution of model residual error with very close average gain predictions between -2.0 dB and 2.0 dB. Figures 5.6, 5.7, 5.8, and 5.9 show the effects of variable levels on the average antenna gain. From Figure 5.6, the test case frequencies, 1.32 and 1.38 GHz, strongly affected the average gain since both reside near the unfilled cavity half wavelength resonant frequency, 1.353 GHz. Furthermore, from Figure 5.7 high relative permittivity values from the first dielectric layer caused increased model residual values, while lower relative permittivity values from the second dielectric layer seen in Figure 5.8 caused increased model residual values. Worth noting here, the thickness of the second dielectric superstrate layer directly depends on the thickness of the first dielectric superstrate layer. From Figure 5.1, when the first superstrate layer thickness equals 0.6711 cm, the second superstrate layer thickness also equals 0.6711 cm. Figure 5.9 indicates that

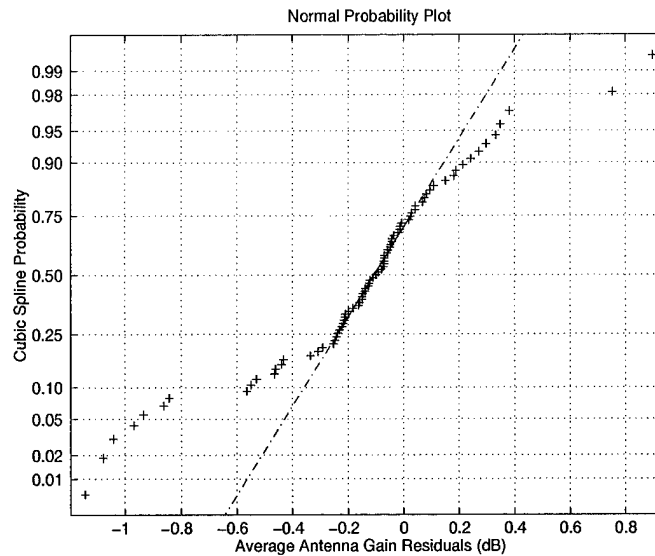


Figure 5.4 Average Antenna Gain Empirical Model Normal Probability Plots of Residuals

Residual Mean	-0.1431 dB
Residual Standard Deviation	0.3567 dB

Table 5.6 Average Antenna Gain Empirical Model Residual Mean And Residual Standard Deviation Values

when the first superstrate layer thickness equals 0.6711 cm, the empirical model remains accurate with low model residuals. Despite the increased variability of the average antenna gain empirical model, the model still successfully predicts antenna gain trends and still provides a useful gain prediction tool.

5.2.2 Antenna Input Impedance Model Adequacy. As in Section 5.2.1, this section employs the empirical model adequacy tests of Section 3.3.4 to verify the accuracy of the antenna input impedance cubic spline empirical model for both real and imaginary impedances. From Figure 5.10, neither the real nor the imaginary impedance empirical models precisely predict antenna input impedance. Worth noting, the real and imaginary impedance residual means and residual standard deviations listed in Table 5.7 closely match those listed in Table 4.14 for the previous configuration but still remain large. Figures 5.11, 5.12, 5.13, 5.14, and 5.15 indicate the wide variability of the antenna input impedance models and show no sign of strong antenna impedance influences do to a single

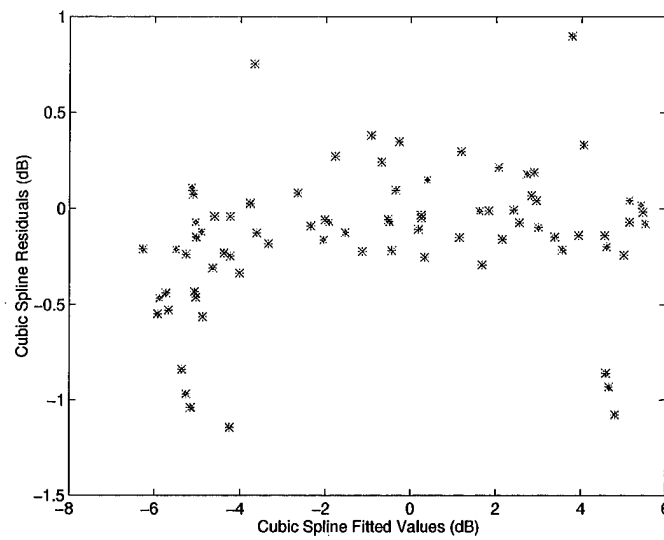


Figure 5.5 Average Antenna Gain Empirical Model Residuals Versus Fitted Values

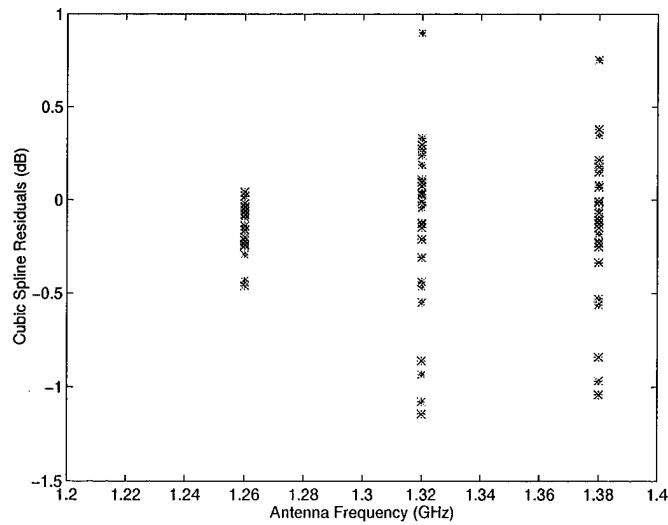


Figure 5.6 Average Antenna Gain Empirical Model Residuals Versus Frequency Values

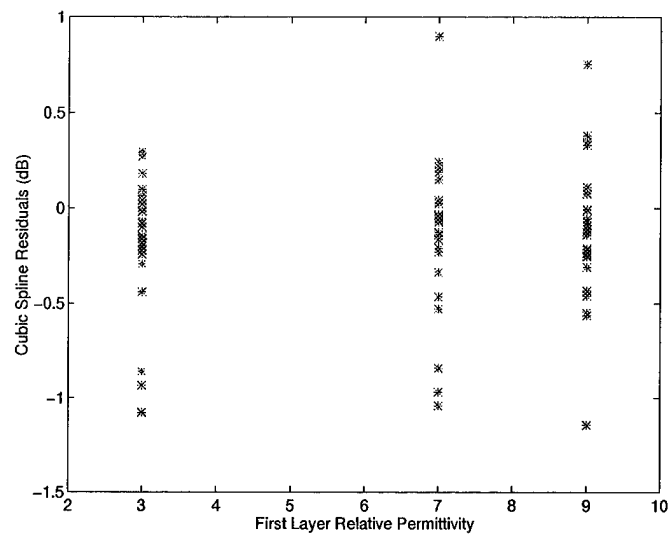


Figure 5.7 Average Antenna Gain Empirical Model Residuals Versus First Layer Relative Permittivity Values

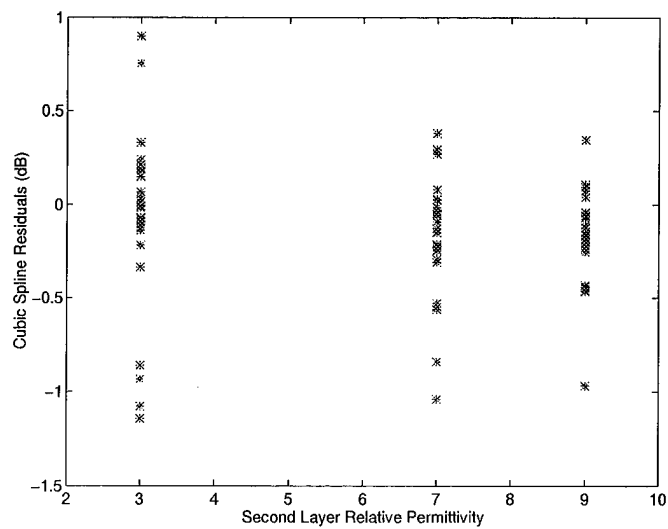


Figure 5.8 Average Antenna Gain Empirical Model Residuals Versus Second Layer Relative Permittivity Values

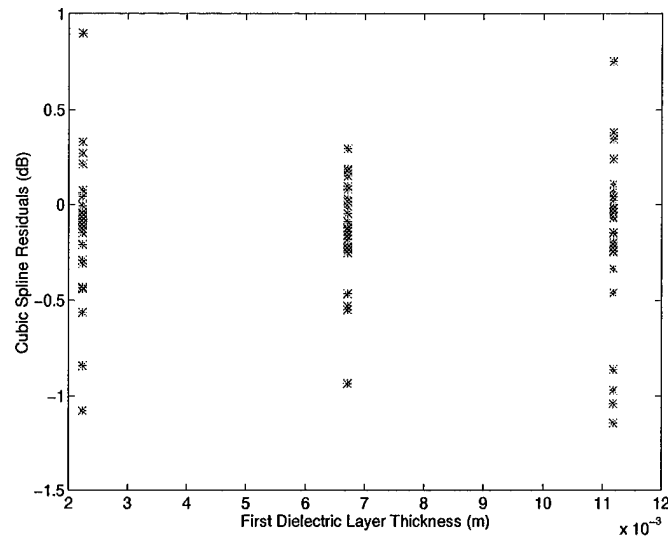


Figure 5.9 Average Antenna Gain Empirical Model Residuals Versus First Layer Thickness Values

Mean Real Impedance Residual	1.3091 ohms
Real Impedance Residual Standard Deviation	4.1565 ohms
Mean Imaginary Impedance Residual	1.5775 ohms
Imaginary Impedance Residual Standard Deviation	6.5177 ohms

Table 5.7 Real and Imaginary Antenna Input Impedance Empirical Model Mean Residual and Residual Standard Deviations Values

variable or variable level. Fortunately, like the average antenna gain empirical model of Section 5.2.1 the impedance empirical models still predict impedance trends and provide a useful tool for antenna design optimization.

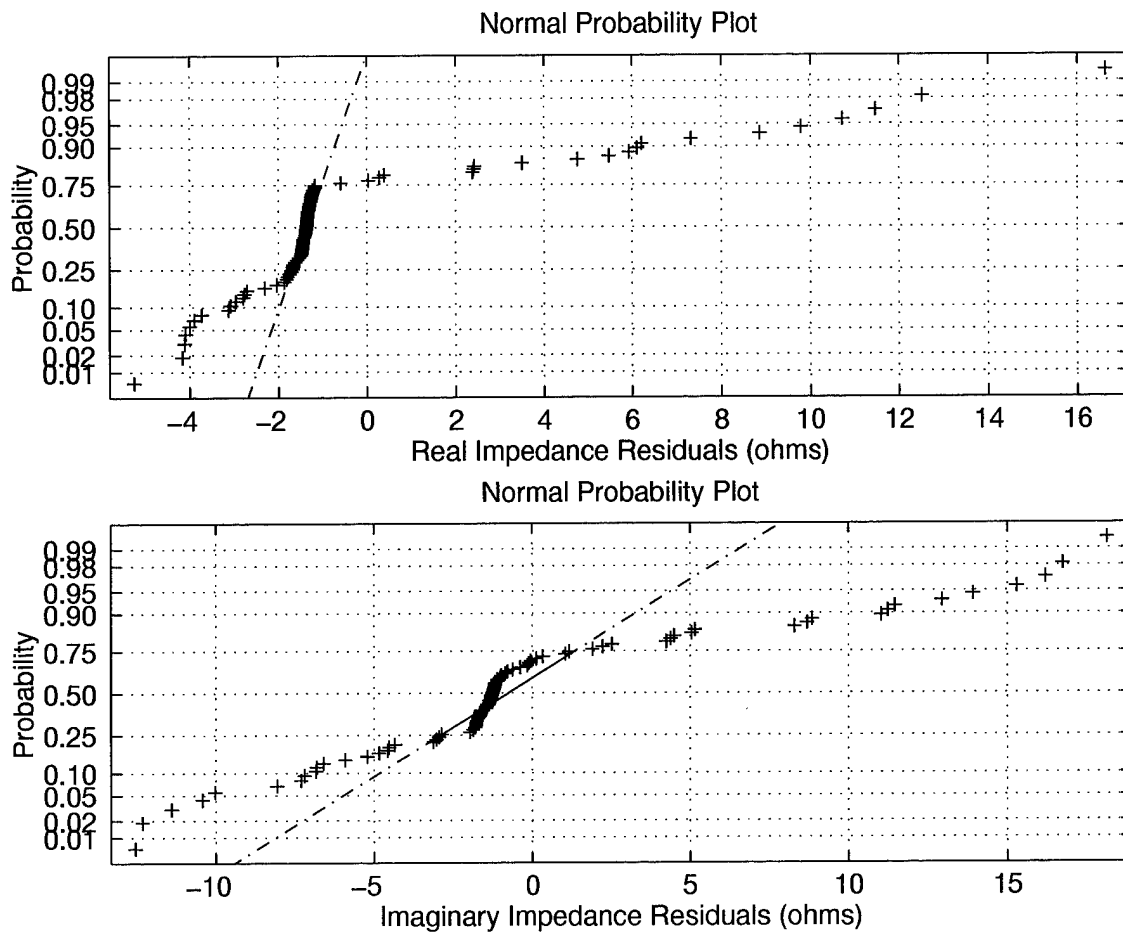


Figure 5.10 Antenna Input Impedance Empirical Model Normal Probability Plots of Residuals

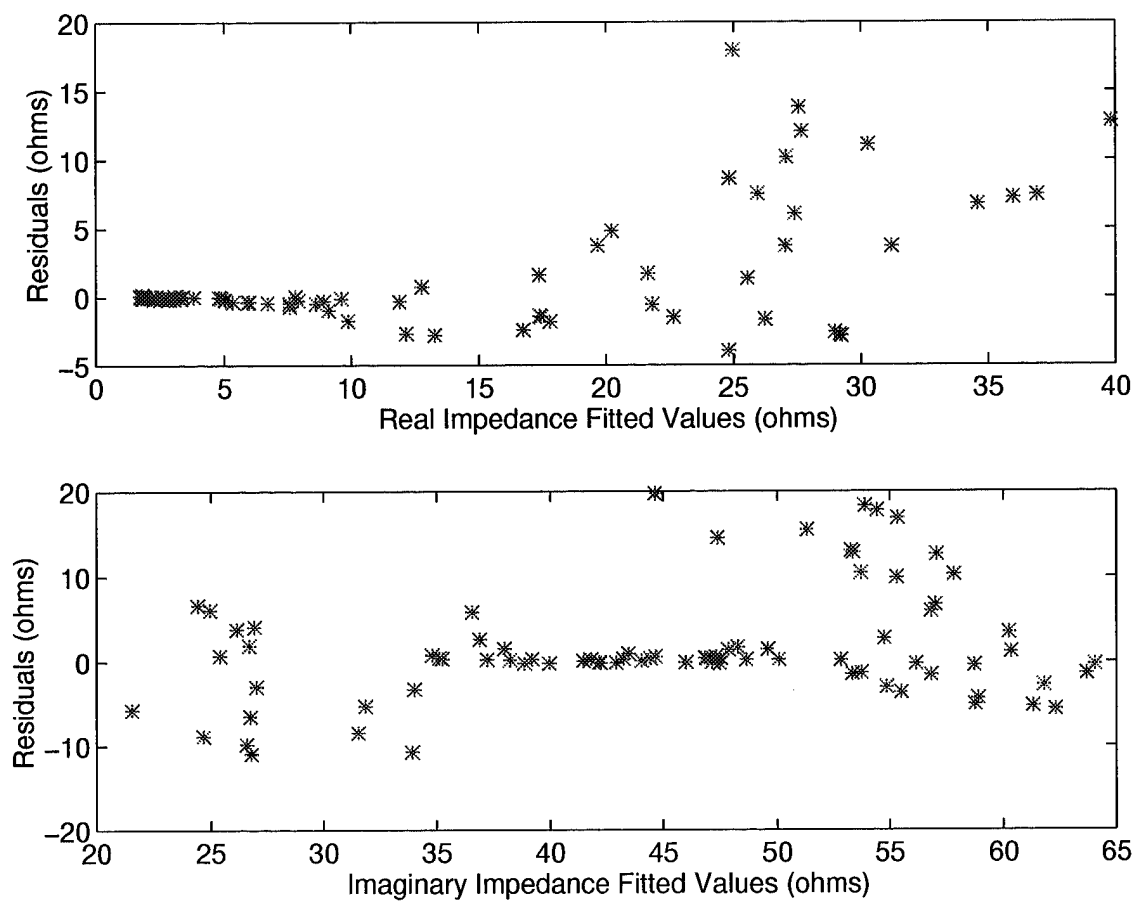


Figure 5.11 Antenna Input Impedance Empirical Model Residuals Versus Fitted Values

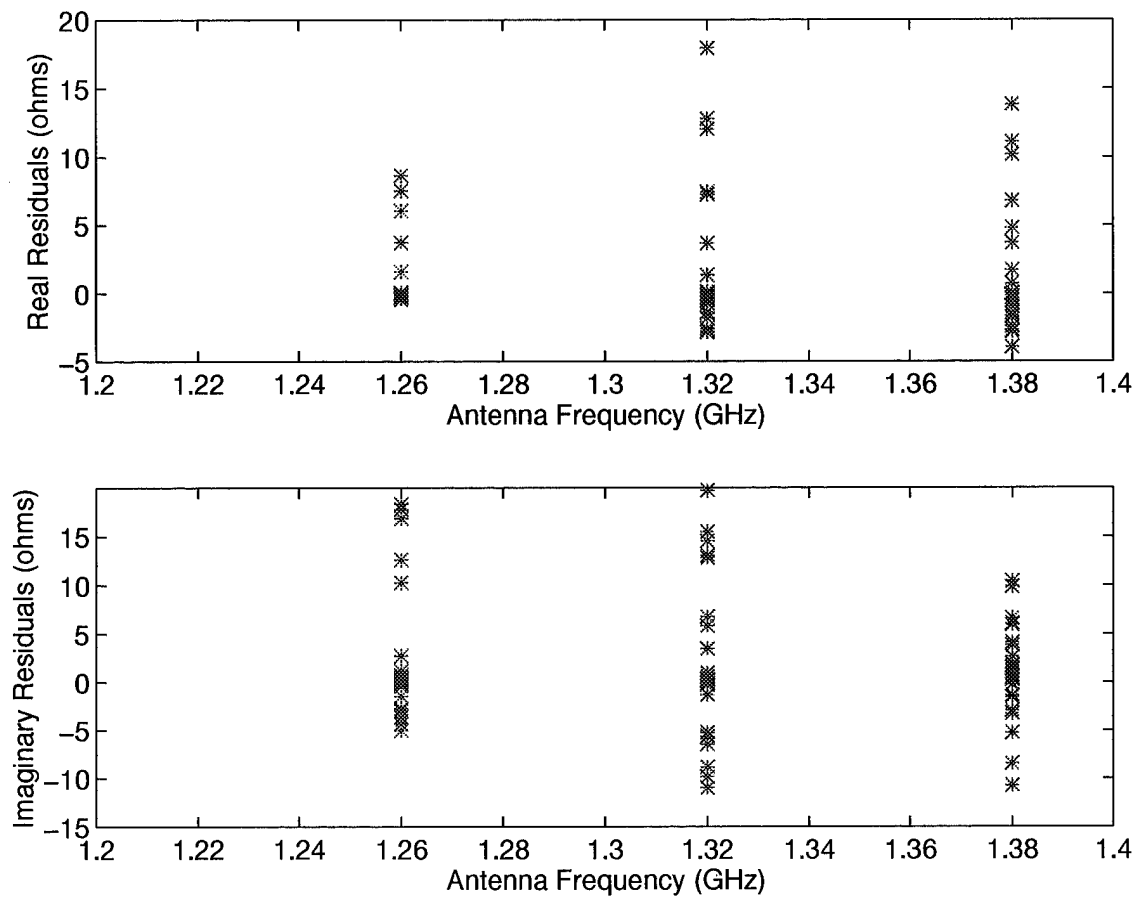


Figure 5.12 Antenna Input Impedance Empirical Model Residuals Versus Frequency Values

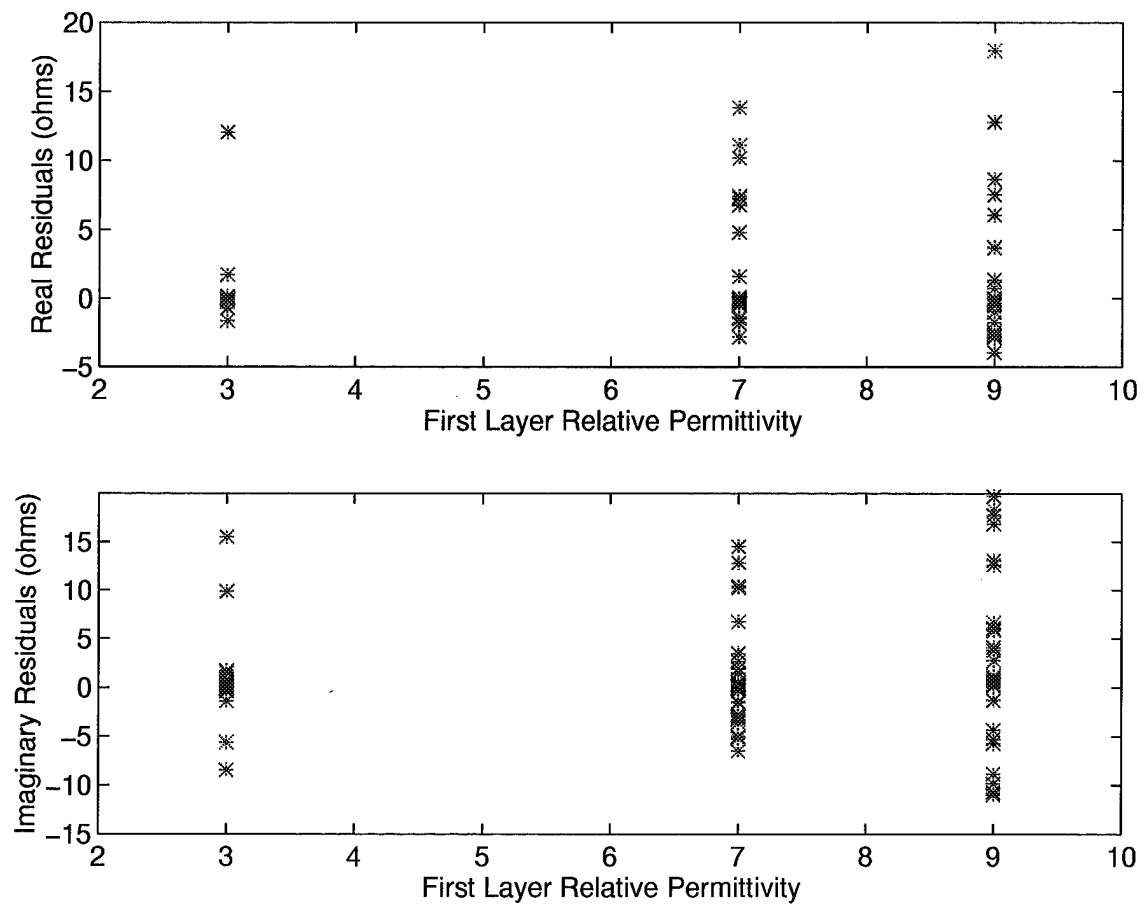


Figure 5.13 Antenna Input Impedance Empirical Model Residuals Versus First Layer Relative Permittivity Values

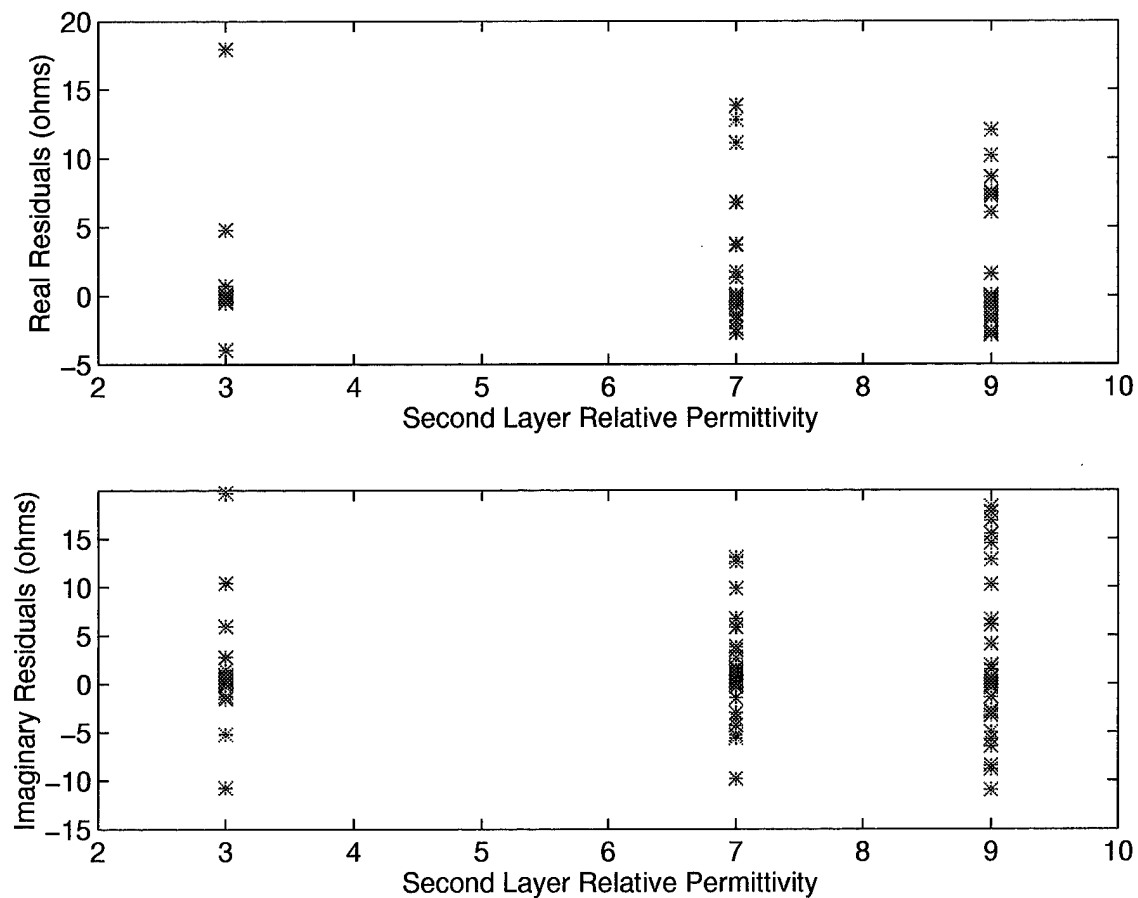


Figure 5.14 Antenna Input Impedance Empirical Model Residuals Versus Second Layer Relative Permittivity Values

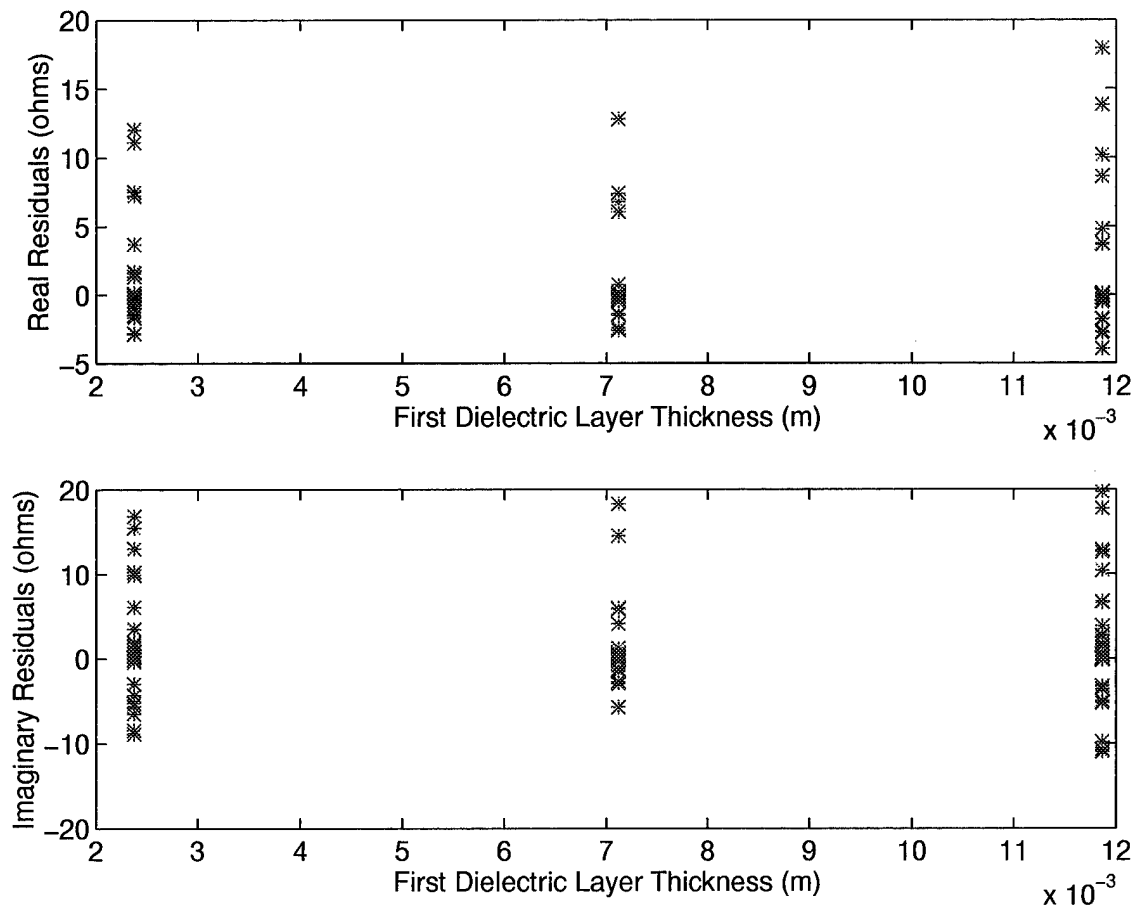


Figure 5.15 Antenna Input Impedance Empirical Model Residuals Versus First Layer Thickness Values

Frequency	1.30 GHz
First Layer Relative Permittivity	6.0
Second Layer Relative Permittivity	10.0
First Layer Thickness	0.4474 cm
Average Gain (HFEM)	-4.7748 dB
Input Impedance (HFEM)	$19.5875 + j67.6017$ ohms
Optimized Solution	25.638

Table 5.8 Optimization Starting Point

5.3 Average Antenna Gain and Antenna Input Impedance Optimization

Since the goal of this chapter is the design of a realizable antenna for the configuration in Figure 5.1, the optimization requirements include:

1. Minimum average antenna gain in the angular region described in Equations (4.1) and (4.2).
2. Input impedance of 50 ohms.

Using the simplex optimization method as in Section 4.4, the empirical models of Sections 5.2.1 and 5.2.2, and the combined optimization function of Equation (5.3),

$$solution = averagegain + abs(50 - real(impedance)) \quad (5.3)$$

the optimization procedure searches through antenna radiation patterns like those of Figures 5.16 and 5.17 to satisfy the optimization requirements. Using the optimization starting point of Table 5.8 with its radiation pattern shown in Figure 5.18, the simplex optimization method converged to the optimized antenna design location listed in Table 5.9 with huge improvements over the starting point design. Figure 5.19 provides the optimized design radiation pattern, while Figures 5.20, 5.21, 5.22, 5.23, 5.24, and 5.25 show the combined optimization response as variable pairs approach their optimized values.

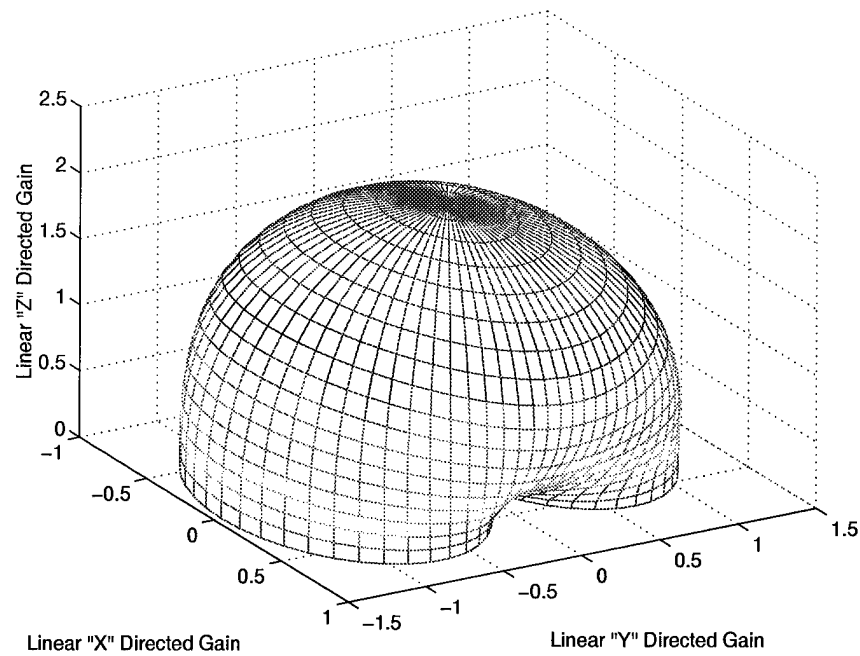


Figure 5.16 Antenna Radiation Pattern (Frequency = 1.2 GHz, First Superstrate Dielectric Layer Permittivity = Second Superstrate Dielectric Layer Relative Permittivity = 2.0)

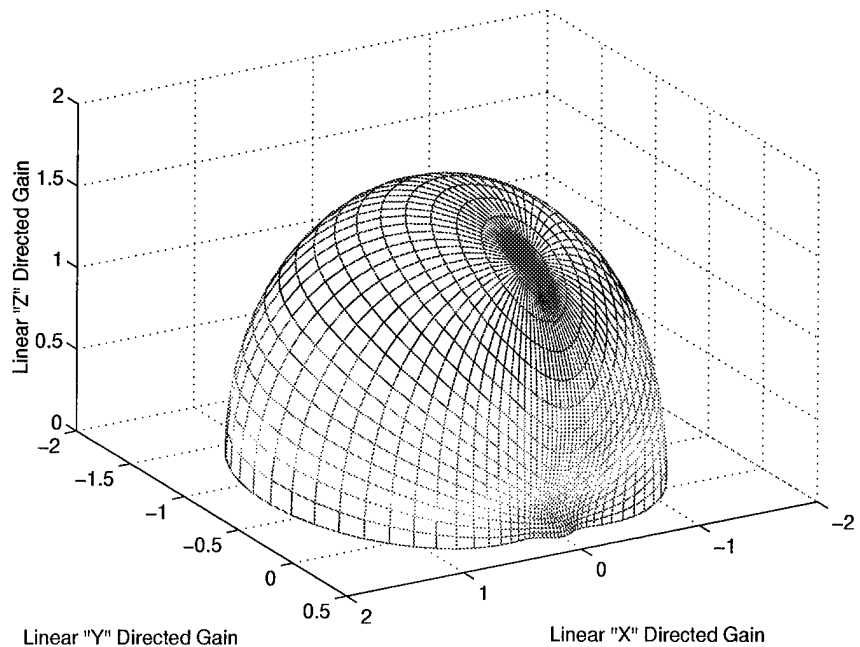


Figure 5.17 Antenna Radiation Pattern (Frequency = 1.4 GHz, First Superstrate Dielectric Layer Permittivity = Second Superstrate Dielectric Layer Relative Permittivity = 10.0)

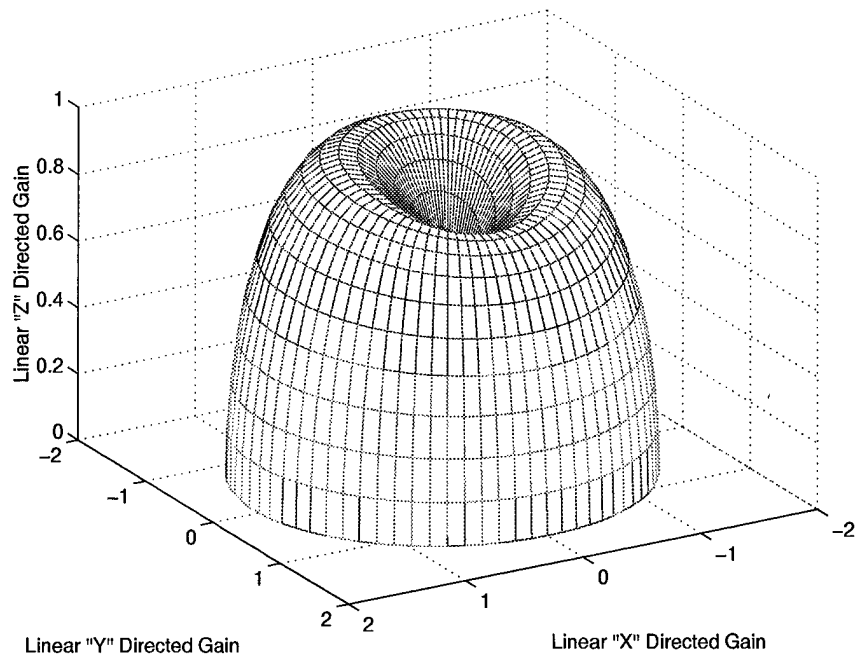


Figure 5.18 Optimization Starting Radiation Pattern

Frequency	1.353 GHz
First Layer Relative Permittivity	6.010
Second Layer Relative Permittivity	9.966
First Layer Thickness	0.673 cm
Elapsed Optimization Time	≈ 2 mins
Average Gain (Empirical Model)	-6.501 dB
Input Impedance (Empirical Model)	$50.00 + j38.086$ ohms
Average Gain (HFEM)	-6.794 dB
Input Impedance (HFEM)	$48.611 + j36.232$ ohms
Gain Accuracy	4.3 percent
Impedance Accuracy	3.7 percent (magnitude)
Weighted Optimization Value	-6.501 (Empirical values)
Weighted Optimization Value	-5.405 (HFEM values)

Table 5.9 Optimized Antenna Design

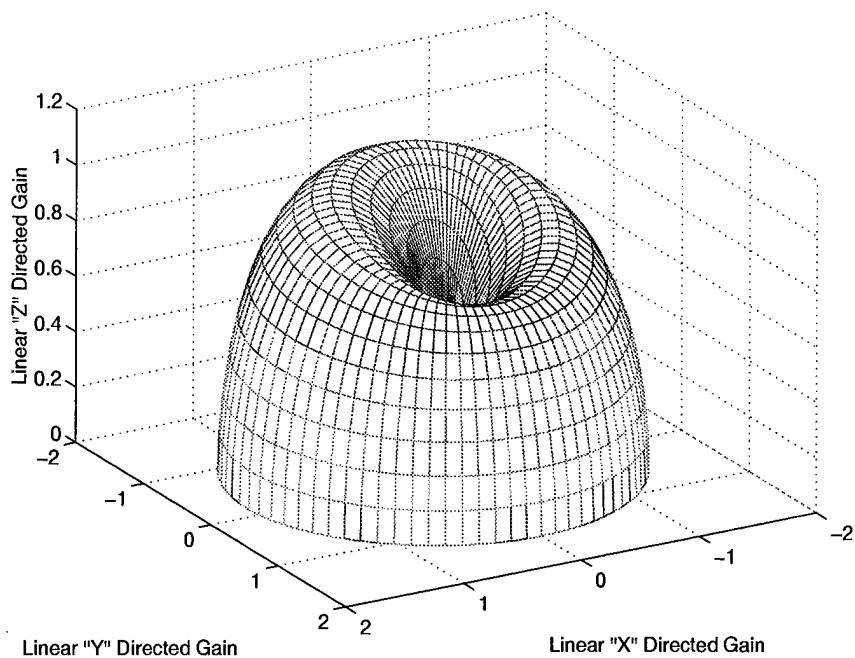


Figure 5.19 Optimized Antenna Design Radiation Pattern

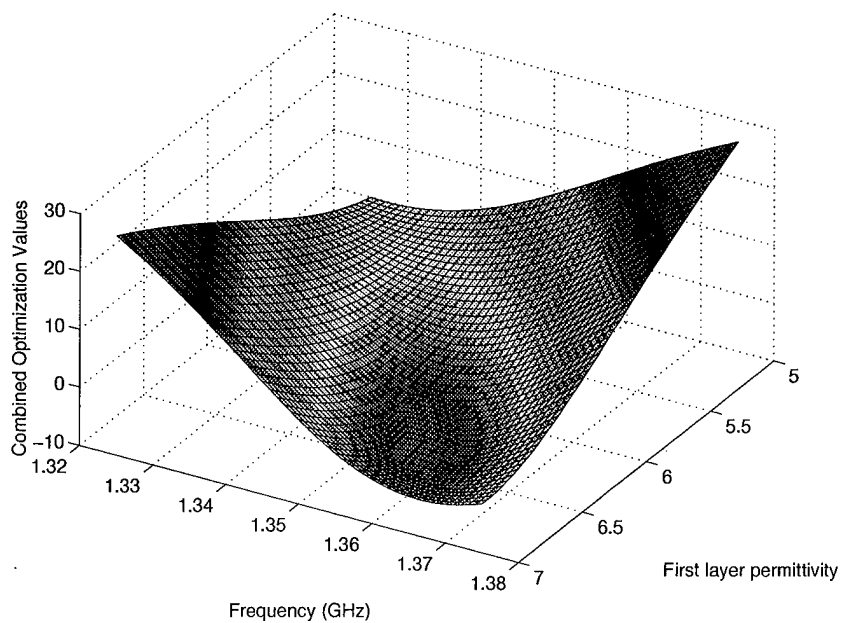


Figure 5.20 First Layer Relative Permittivity and Frequency Effects Near the Optimized Location

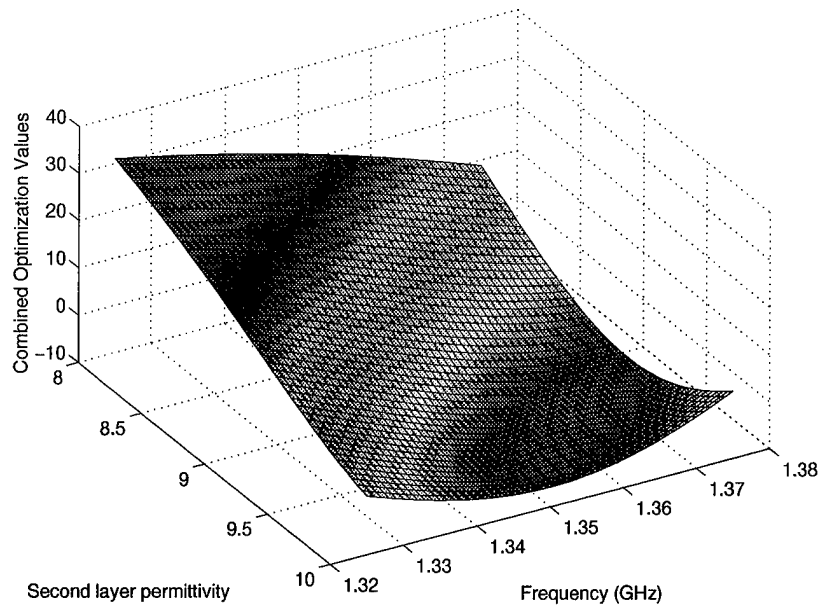


Figure 5.21 Second Layer Relative Permittivity and Frequency Effects Near the Optimized Location

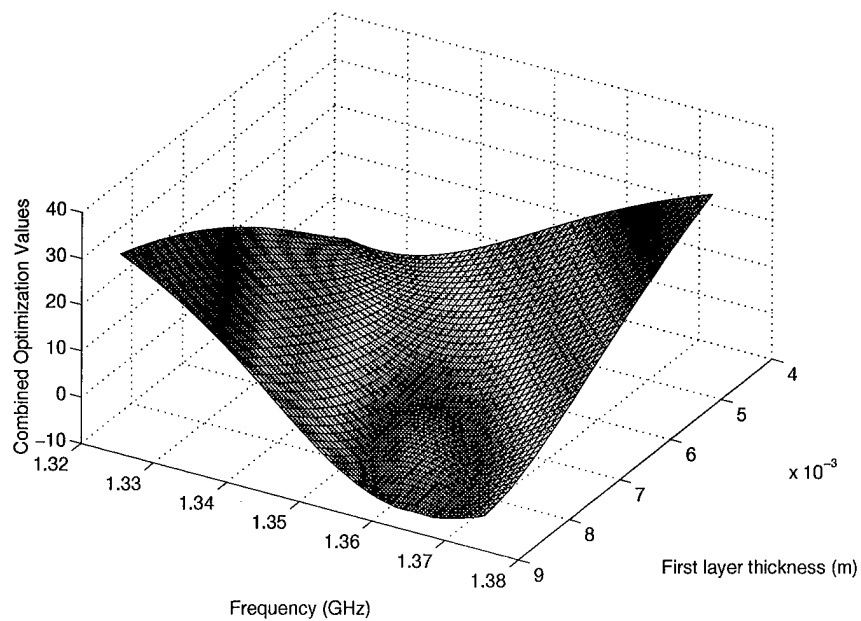


Figure 5.22 First Layer Thickness and Frequency Effects Near the Optimized Location

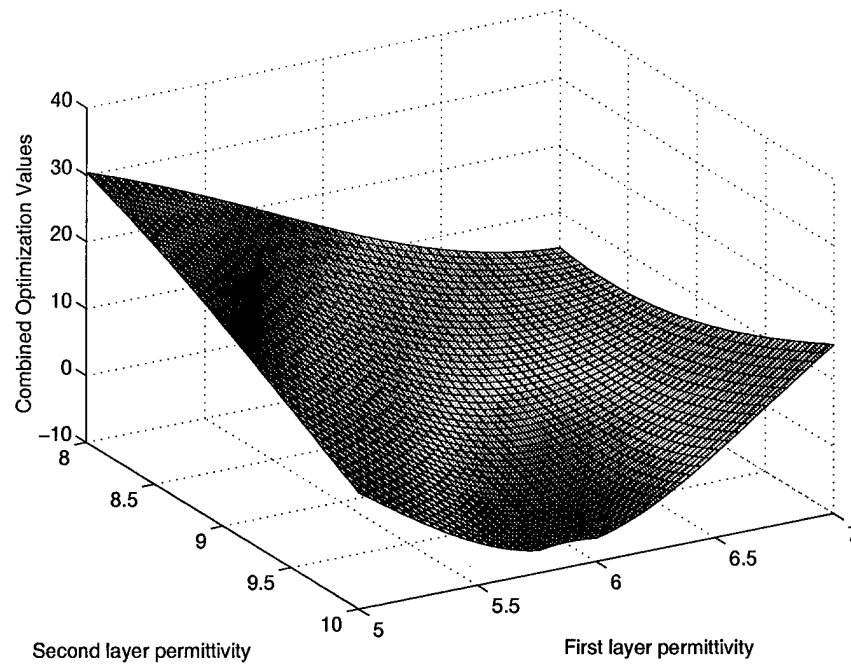


Figure 5.23 First and Second Layer Relative Permittivity Effects Near the Optimized Location

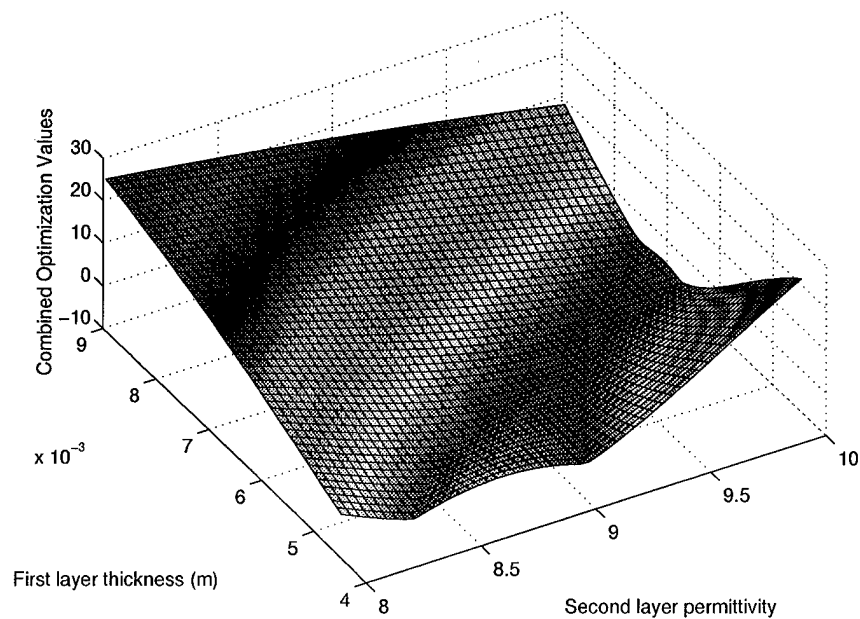


Figure 5.24 First Layer Thickness and Second Layer Relative Permittivity Effects Near the Optimized Location

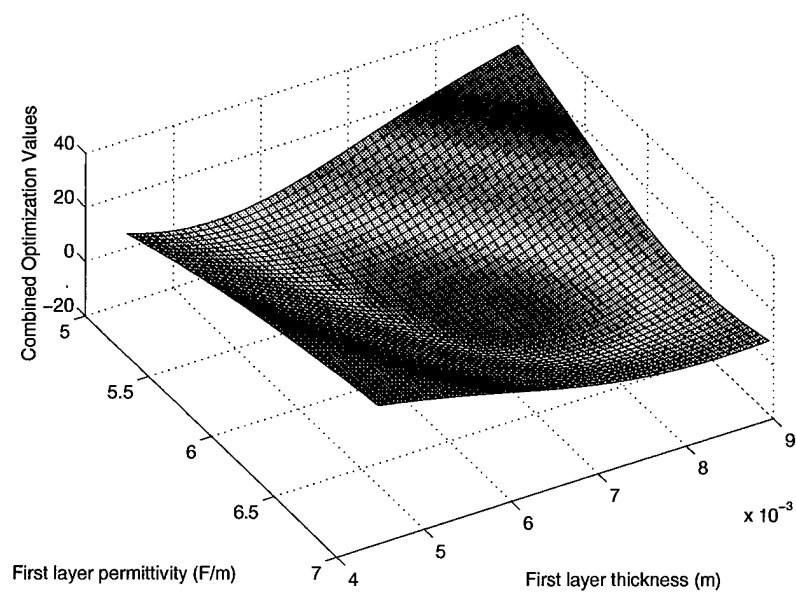


Figure 5.25 First Layer Relative Permittivity and Thickness Effects Near the Optimized Location

Scale Factor	3.5236
Frequency	4.768 GHz
First Superstrate Layer Relative Permittivity	6.15
First Superstrate Layer Thickness	0.075 inches (0.1905 cm)
Second Superstrate Layer Relative Permittivity	10.2
Second Superstrate Layer Thickness	0.075 inches (0.1905 cm)
Substrate Relative Permittivity	4.5
Substrate Thickness	0.10 inches (0.254 cm)
Cavity Dimensions:	
Length	1.2375 inches (3.1433 cm)
Width	1.2375 inches (3.1433 cm)
Height	0.250 inches (0.635 cm)
Patch Dimensions:	
Length	0.550 inches (1.397 cm)
Width	0.550 inches (1.397 cm)
Patch Location	Centered 0.075 inches (0.1905 cm) Above Cavity Bottom
Feed Pin Location	0.0687 inches (0.175 cm) Off Center
Predicted average gain (HFEM)	-6.582 dB
Predicted input impedance (HFEM)	$45.324 + j25.694$ ohms
Measured Input Impedance	$51.439 + j3.045$ ohms

Table 5.10 Constructed Antenna Design Parameters

5.4 Compact Range Validation of Designed Cavity-Backed Microstrip Antenna With Dielectric Overlays

Using the optimized design of Table 5.9, the completed optimized design methodology requires a constructed antenna for methodology verification. Unfortunately, exact dielectric materials with the permittivity values of Table 5.9 are not readily available. Therefore, the available dielectric materials for superstrate layers one and two are 6.15 and 10.2 respectively. Table 5.10 lists the antenna design parameters including the new antenna scale factor, the new antenna dimensions, and predicted antenna responses. Figure 5.26 shows the new scaled antenna design and Figure 5.27 shows the HFEM predicted radiation pattern with a predicted average antenna gain of -6.582 dB and a predicted input impedance of $45.324 + j25.694$ ohms. The resulting differences between the predicted average antenna gain and input impedance values listed in Table 5.10 for the constructed antenna and Table 5.9 for the optimized antenna design are directly due to using the available dielectric materials for the first and second superstrate layers rather than the exact optimized dielec-

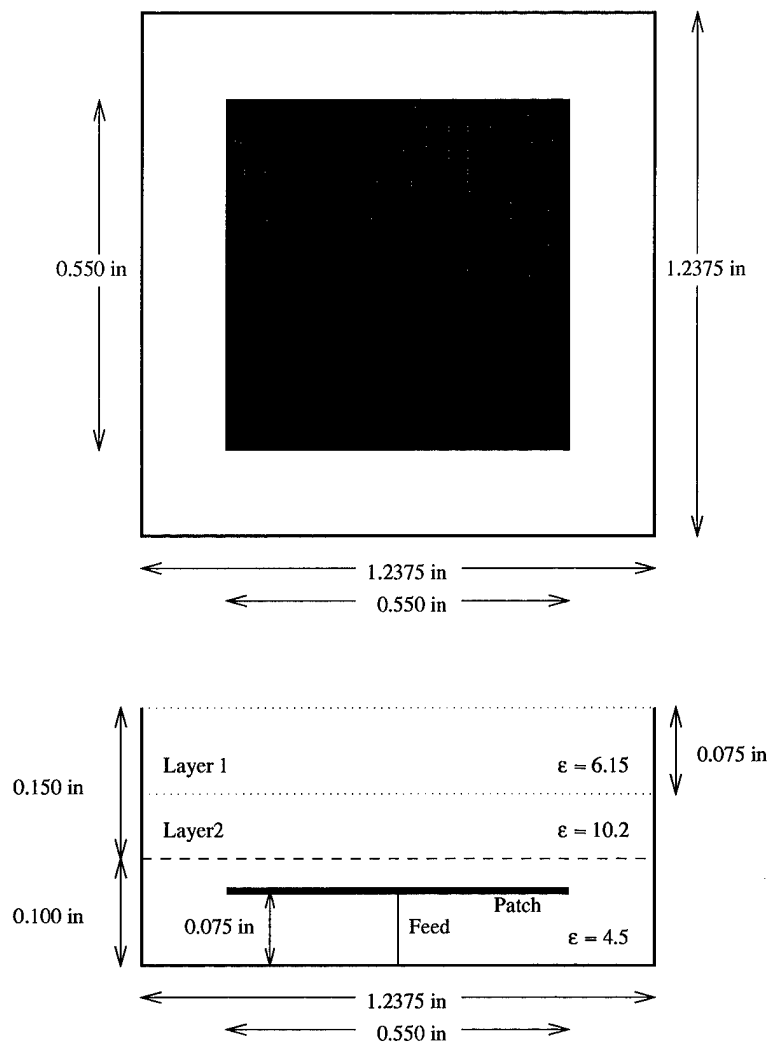


Figure 5.26 Constructed Antenna

tric values. In fact, the measured input impedance from the constructed antenna measured $51.439 + j3.045$ ohms, where the difference is due to the antenna radiation aperture's feed pin location.

Measurement of the constructed antenna using a compact anechoic antenna chamber to verify the optimized design methodology and HFEM predictions produced the electric field patterns shown in Figures 5.28, 5.29, 5.30, and 5.31 where the smooth curves are predicted electric field patterns and the rough curves are the measured electric field patterns. In general, the measured fields closely match the predicted fields with only minor differences. In Figures 5.29 and 5.31, two differences exist. The first, a small hump in

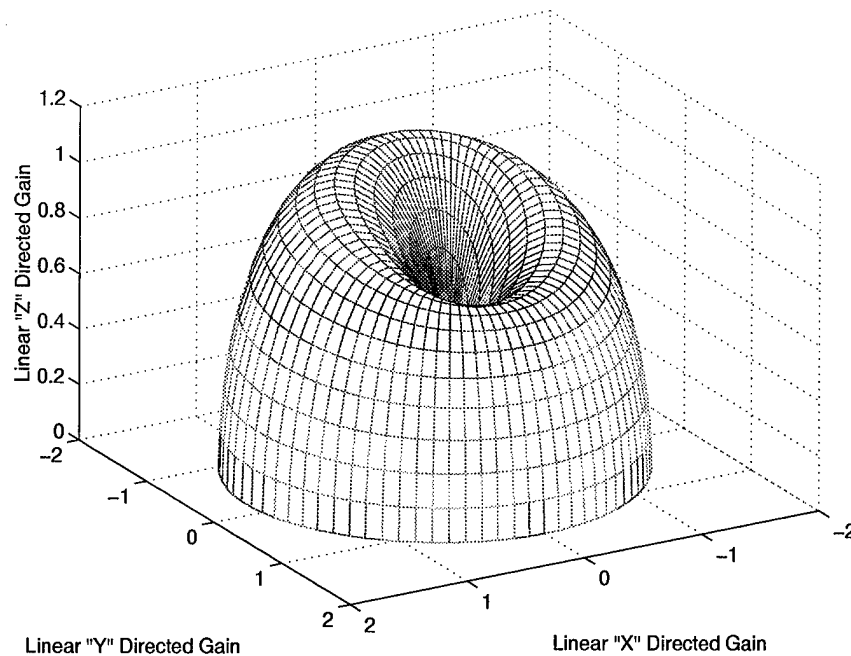


Figure 5.27 Predicted Radiation Pattern for the Constructed Antenna Design

the electric field pattern near the zero degree angle, is caused by uneven mounting of the constructed antenna into a measurement test body. The second, electric field round off at the field extremities, is caused by the finite ground plane used for antenna measurements instead of the ideal infinite ground plane used in antenna field predictions. In Figure 5.30, the expected electric field was approximately -80 dB, where the measured electric field was in the general range between -20 dB and -40 dB. The difference is attributed to cross polarization effects due to misalignment of the test body during field pattern measurements.

5.5 Closing Comments

Using the optimized design methodology of Chapter IV and a combined optimization constraint equation composed of minimum average antenna gain and a target input impedance of 50 ohms, this chapter located, built, and verified a realizable optimized antenna design. Despite increased variations in the average antenna gain and input impedance empirical models, the optimized antenna design compared well with HFEM results and

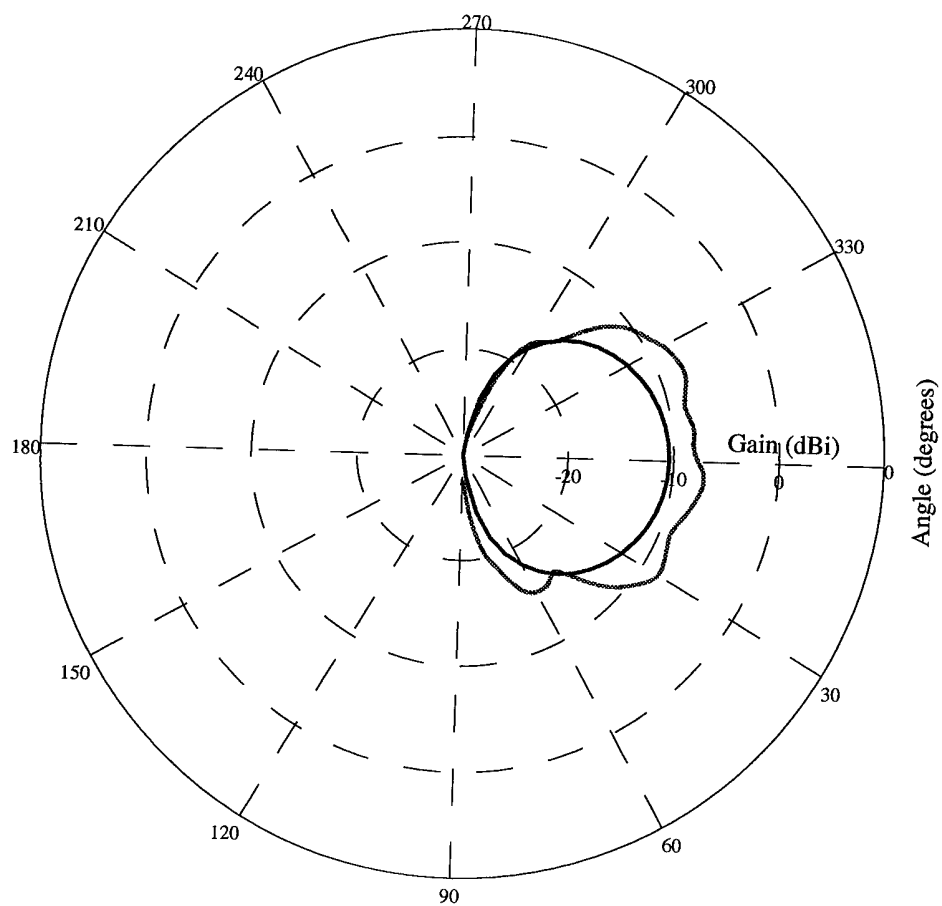


Figure 5.28 Electric Field with Phi Polarization ($\phi = 0$ degrees)

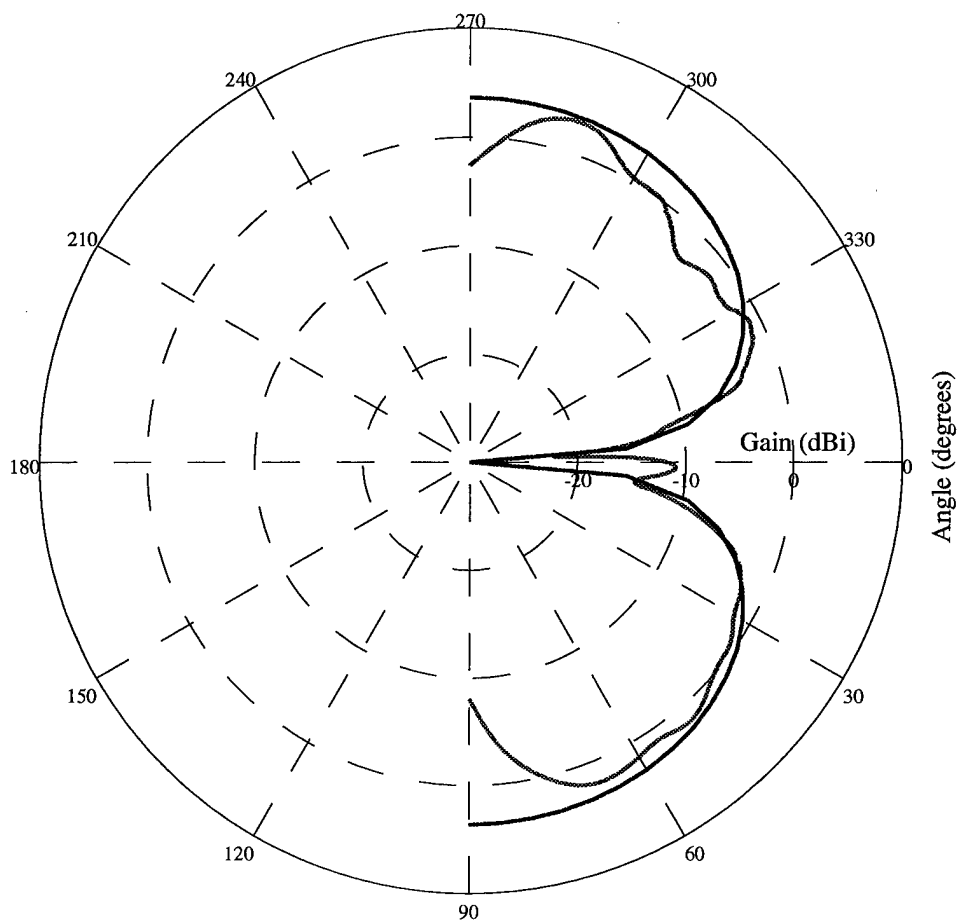


Figure 5.29 Electric Field with Theta Polarization ($\phi = 0$ degrees)

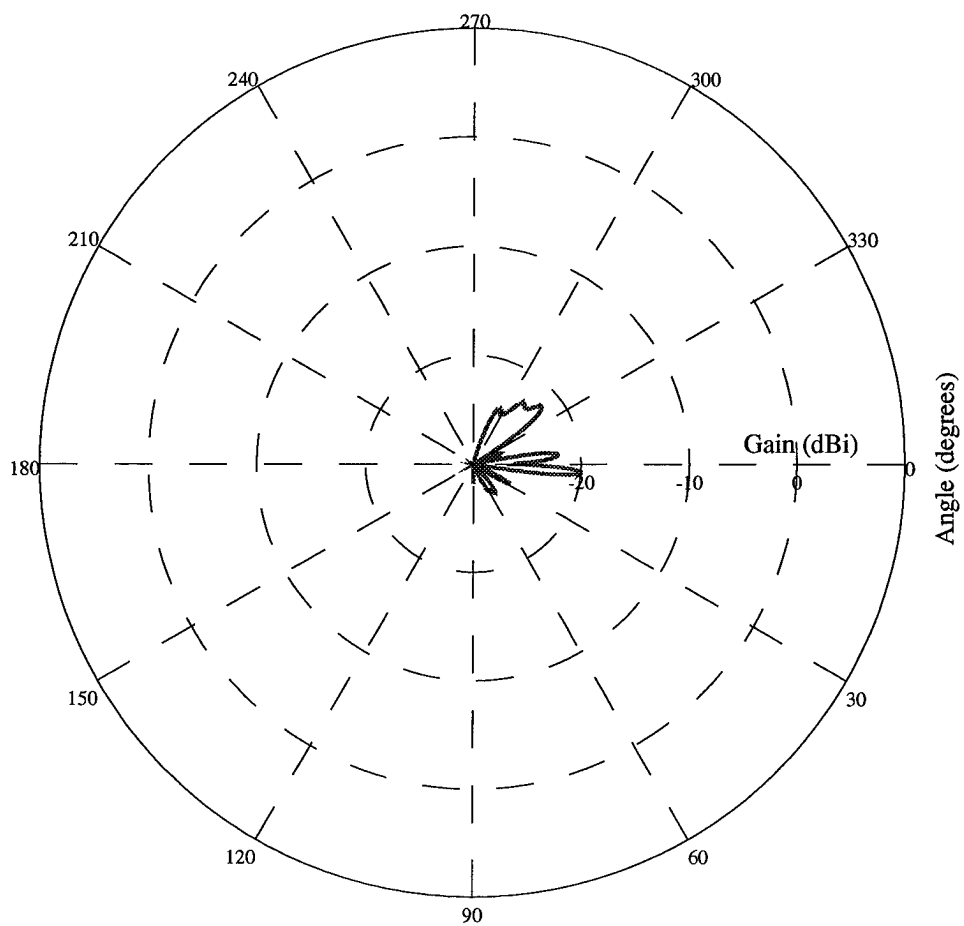


Figure 5.30 Electric Field with Phi Polarization ($\phi = 90$ degrees)

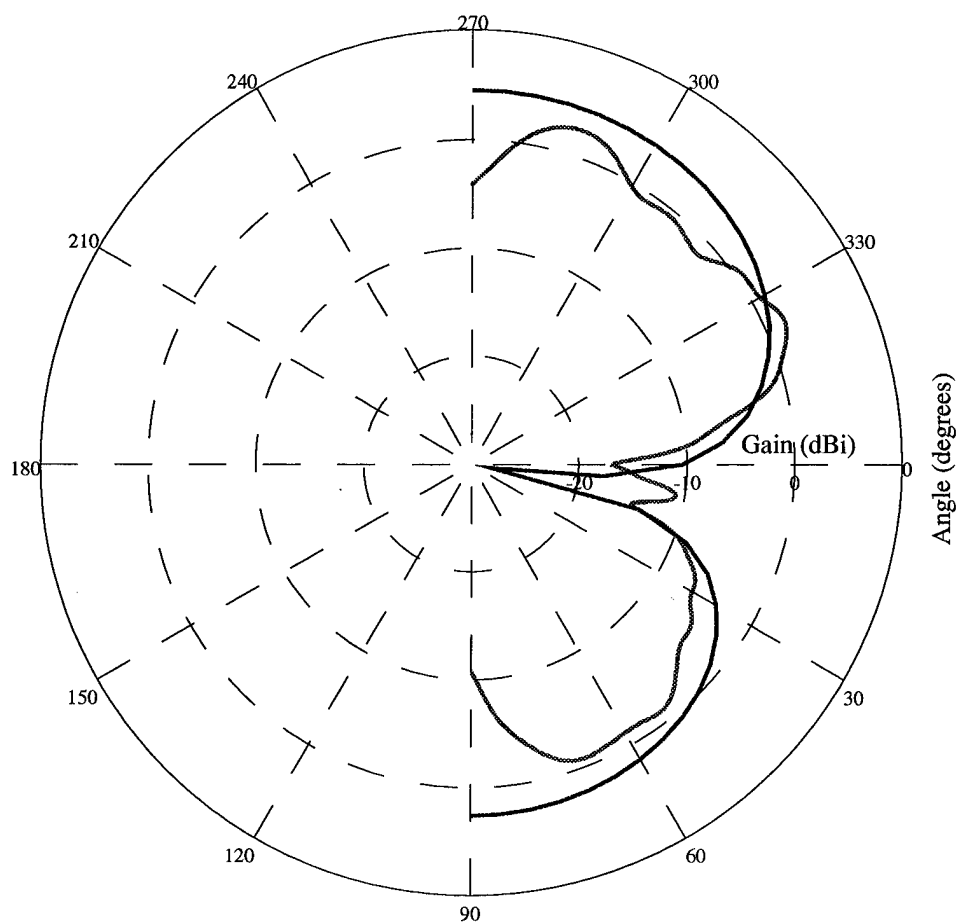


Figure 5.31 Electric Field with Theta Polarization ($\phi = 90$ degrees)

measured results. The constructed antenna used to verify the optimized antenna design used existing dielectric materials that closely matched the optimized dielectric materials and produced electric field patterns that closely resembled the predicted electric fields. As a result this RSM based design methodology is an excellent design tool for this antenna configuration.

VI. Conclusion

This thesis introduced a relatively new approach to the design of cavity-backed microstrip antennas that uses RSM techniques to determine an optimized antenna design. Section 6.1 states some specific conclusions found using the design methodology of Chapter IV and its implementation in Chapter V and summarizes some of the key impacts found. Section 6.2 lists some areas where further use or extension of this design methodology is possible.

6.1 Summary and Conclusions

From this research, several key conclusions are drawn that highlight the utility of this design methodology and the individual RSM techniques used to design an optimized cavity-backed microstrip antenna with dielectric overlays. The conclusions include:

1. The RSM based design methodology quickly and accurately predicted an optimized antenna design for this particular antenna configuration where the design methodology results closely agreed with HFEM comparison results and antenna range measurements. In general, all optimized results were within 4.0 percent of the HFEM results, and the predicted electric field patterns closely resembled actual antenna range field pattern measurements with only slight range measurement differences.
2. The full factorial designed experiment along with the design variables and variable levels suited this design methodology well. The full factorial designed experiment allowed for the drastically changing average antenna gain and antenna input impedance values to be sampled throughout the entire region of design interest where each design variable strongly impacted the overall design problem. Due to the cavity configuration of this antenna, antenna operating frequency directly influenced the resulting antenna performance, and due to dielectric loading effects, the relative permittivity variables of superstrate layers one and two as well as the thickness variable of superstrate layer one directly impacted the resulting antenna gain, input impedance, and antenna radiation pattern shape.

3. The cubic spline empirical model used throughout this research quickly and accurately determined average antenna gain with relatively small residual means and residual standard deviations but had difficulty accurately modeling and predicting antenna input impedance. As mentioned in Chapter II, dielectric loading reduces the antenna input impedance bandwidth and causes the impedance bandwidth to become even more restrictive than the frequency bandwidth [17,18]. In other words, slight changes in the relative permittivity of either superstrate layer one or layer two greatly impacted the resulting antenna input impedance for this antenna design causing the input impedance to have sharp changes in value.
4. The ANOVA tests performed in Chapter IV not only indicated the impacts that each design variable and each variable interaction factor had on the resulting average antenna gain performance for the antenna of Figure 4.1 but also provided a design tool indicating where design sensitivities were the strongest. Using ANOVA testing in this manner shows manufacturers and engineers where manufacturing tolerances should be the tightest. From Section 4.3.2, the antenna operating frequency and the second dielectric superstrate layer relative permittivity factors were the two design factors with the largest impact on the average antenna gain therefore requiring the tightest manufacturing control. This type of statistical analysis is only feasible because of the efficiency of the cubic spline empirical model.
5. The application of the simplex optimization method to the cubic spline empirical models in both Chapter IV and Chapter V quickly determined an optimized antenna design that compared well with verification results. In Chapter IV during the design methodology development phase, the simplex optimization method used the cubic spline empirical model to determine an optimized antenna design in an elapsed time interval of approximately one minute using 180 design iterations. The HFEM optimized design results verification test took approximately three hours. Assuming each simplex iteration would have taken as long, it would have taken 23 days to come up with the optimized design using HFEM testing rather than empirical modeling. The time savings found using empirical model based optimization is the power of RSM and designed experiments.

6.2 Recommendations

The results found in this research indicate that the design methodology developed here is extendible to other electromagnetic design problems with the proper selection of design variables, designed experiment, and empirical model. To build confidence in the validity of using this design methodology, several areas for continued research and design are listed below:

1. Optimize for a maximum antenna gain using the antenna configuration of Figure 4.1 in a designated angular region for a more directive antenna radiation pattern.
2. Explore the usefulness of other less time-expensive designed experiments such as the central composite design or the Latin squares design since the full factorial designed experiment required such a large number of antenna response measurements.
3. Compare this design methodology with other design approaches in recent antenna design literature such as those using genetic algorithms or quadratic optimization.
4. Perform rigorous ANOVA test comparisons between the HFEM and the empirical model results for design parameters other than frequency to build confidence in the validity of using an empirical model in ANOVA testing.
5. Apply the design methodology to other antenna designs such as a spiral antenna design.
6. Apply the design methodology to other electromagnetic problems such as periodic surfaces.

Bibliography

1. Adams, Arlon T. "Flush Mounted Rectangular Cavity Slot Antennas - Theory and Design." *IEEE Transactions on Antennas and Propagation* AP-15. 342-351. May 1967.
2. Alexopoulos, Nicolaos G. and David R. Jackson. "Fundamental Superstrate (Cover) Effects on Printed Circuit Antennas." *IEEE Transactions on Antennas and Propagation* 32. 807-815. August 1984.
3. Bahl, Inder J., et al. "Design of Microstrip Antennas Covered with a Dielectric Layer." *IEEE Transactions on Antennas and Propagation* AP-30. 314-317. March 1982.
4. Biebl, Erwin M. and Gerhard L. Friedsam. "Cavity-Backed Aperture Antennas with Dielectric and Magnetic Overlay." *IEEE Transactions on Antennas and Propagation* 43. 1226-1231. November 1995.
5. Box, George E. P. and Norman R. Draper. *Empirical Model-Building and Response Surfaces*. Wiley Series in Probability and Mathematical Statistics, New York: John Wiley and Sons, 1987.
6. Cheng, Jui-Ching, et al. "Theoretical Modeling of Cavity-Backed Patch Antennas Using a Hybrid Technique." *IEEE Transactions on Antennas and Propagation* 43. 1003-1013. September 1995.
7. Floyd, Jr., Victor M. *A Response Surface Methodology Study of Radar Cross Section Data Compression and Reconstruction*. MS thesis, Air Force Institute of Technology, Wright Patterson AFB, Dec 1995.
8. Froberg, Carl-Erik. *Numerical Mathematics Theory and Computer Applications*. Mento Park: The Benjamin Cummings Publishing Company, 1985.
9. Gerald, Curtis F. and Patrick O. Wheatley. *Applied Numerical Analysis* (third Edition). Massachusetts: Addison Wesley Publishing Company, 1984.
10. Jin, Jianming. *The Finite Element Method in Eleectromagnetics*. New York: John Wiley and Sons, 1993.
11. Lee, Jind-Yeh, et al. "Analysis of Cavity-Backed Aperture Antennas with a Dielectric Overlay." *IEEE Transactions on Antennas and Propagation* 42. 1556-1562. November 1994.
12. Long, Stuart A. "Experimental Study of the Impedance of Cavity-Backed Slot Antennas." *IEEE Transactions on Antennas and Propagation* AP-23. 1-7. January 1975.
13. Mason, Robert L., et al. *Statistical Design and Analysis of Experiments with Applications to Engineering and Science*. New York: John Wiley and Sons, 1989.
14. Montgomery, Douglas C. *Design and Analysis of Experiments*. New York: John Wiley and Sons, 1991.
15. Moosbrugger, Peter J., et al. "Experimental Design of a Two Layer Electromagnetically Coupled Rectangular Patch with a Global Response Surface Modeling Technique." *IEEE Transactions on Antennas and Propagation* 45. 781-787. May 1997.

16. Nielson, Kaj L. *Methods in Numerical Analysis*. New York: MacMillan Company, 1964.
17. Shen, Xiao-Hai, et al. "Study of Gain Enhancement Method for Microstrip Antennas Using Moment Method." *IEEE Transactions on Antennas and Propagation* 43. 227–231. March 1995.
18. Soares, Antonio J. M., et al. "The Effect of a Dielectric Cover on the Current Distribution and Input Impedance of Printed Dipoles." *IEEE Transactions on Antennas and Propagation* AP-32. 1149–1153. November 1984.
19. Strang, Gilbert. *Linear Algebra and its Applications*. San Diego: Harcourt Brace Jovanovich, 1988.
20. Wilson, Kelce. Interview, June 1997. Query technique for cubic splines.
21. Yang, H. Y. and Nicolaos G. Alexopoulos. "Gain Enhancements for Printed Circuit Antennas Through Multiple Superstrates." *IEEE Transactions on Antennas and Propagation* AP-35. 860–863. July 1987.

Vita

First Lieutenant Douglas J. Hermes was born on 28 December 1964 in Sherman, TX and graduated from Sherman High School in May 1983. In January of the following year, he enlisted into the United States Air Force at Lackland AFB, TX. Upon completion of Basic Training, he began Air Force Specialty training at Lowery AFB, CO as a Precision Measurement Equipment Specialist. In October 1984, he arrived at Bergstrom AFB, TX and served in the Precision Measurement Equipment Laboratory (PMEL), 67 Component Repair Squadron, 67 Reconnaissance Wing. His duties included calibration and maintenance of mission-critical metrology equipment, quality assurance of all PMEL calibrated equipment, and PMEL Laboratory Chief. In August 1990 after receiving an Air Force ROTC scholarship, he entered the University of Texas and graduated with a Bachelor of Science Degree in Electrical Engineering in December 1993. Upon graduation, he was commissioned into the United States Air Force. His first active-duty assignment after commissioning was to the 2d Space Operations Squadron, 50 Space Operations Group, 50 Space Wing, Falcon AFB, CO. His duties included serving as a Navstar Global Positioning System (GPS) Satellite Analysis Officer (SAO) and as the Squadron Executive Officer. As an SAO, he guaranteed satellite constellation accuracy for all GPS users by maintaining precise timing and navigation data availability. In May 1996, he entered the Air Force Institute of Technology (AFIT) and graduated with a Masters of Science Degree in Electrical Engineering in December 1997 specializing in Electromagnetic Field Theory. His follow-on assignment is to Wright Laboratory, Wright Patterson AFB, OH.

Permanent address: 1403 Finger Lakes
Dayton, Ohio 45458

REPORT DOCUMENTATION PAGE			Form Approved OMB No. 0704-0188	
Public reporting burden for this collection of information is estimated to average 1 hour per response, including the time for reviewing instructions, searching existing data sources, gathering and maintaining the data needed, and completing and reviewing the collection of information. Send comments regarding this burden estimate or any other aspect of this collection of information, including suggestions for reducing this burden, to Washington Headquarters Services, Directorate for Information Operations and Reports, 1215 Jefferson Davis Highway, Suite 1204, Arlington, VA 22202-4302, and to the Office of Management and Budget, Paperwork Reduction Project (0704-0188), Washington, DC 20503.				
1. AGENCY USE ONLY (Leave blank)		2. REPORT DATE December 1997		3. REPORT TYPE AND DATES COVERED Master's Thesis
4. TITLE AND SUBTITLE Optimized Design Methodology of Cavity-Backed Microstrip Antennas with Dielectric Overlays			5. FUNDING NUMBERS	
6. AUTHOR(S) Douglas J. Hermes, First Lieutenant, USAF				
7. PERFORMING ORGANIZATION NAME(S) AND ADDRESS(ES) Air Force Institute of Technology WPAFB, OH, 45433-6583			8. PERFORMING ORGANIZATION REPORT NUMBER AFIT/GE/ENG/97D-04	
9. SPONSORING/MONITORING AGENCY NAME(S) AND ADDRESS(ES) Dr. Stephen Schneider Wright Laboratories (WL/AAMP) 2241 Avionics Circle WPAFB OH, 45433-7318			10. SPONSORING/MONITORING AGENCY REPORT NUMBER	
11. SUPPLEMENTARY NOTES				
12a. DISTRIBUTION AVAILABILITY STATEMENT Distribution Unlimited			12b. DISTRIBUTION CODE	
13. ABSTRACT (Maximum 200 words) The optimized design methodology implemented in this research employs a design methodology, namely Response Surface Methodology (RSM), that is relatively new to the electromagnetics field. The design methodology used a full factorial designed experiment, a Hybrid Finite Element Method (HFEM) analysis code, a cubic spline empirical model, an Analysis of Variance (ANOVA) test, and a simplex optimization code to successfully measure, predict, analyze, and optimize average antenna gain and antenna input impedance for a cavity-backed microstrip antenna with dielectric overlays.. Based on HFEM results from the full factorial designed experiment, a cubic spline empirical model successfully predicted average antenna gain and input impedance values for variable combinations within the experiment variable limits.. The ANOVA test determined the impact each design variable introduced on the average antenna gain and indicated the areas of greatest concern during manufacturing and testing phases. Using simplex optimization, an optimized, realizable antenna design with minimum average antenna gain above the antenna bore sight and a target input impedance of 50 ohms was located within two minutes that agreed within approximately 4.0 percent to HFEM values determined from design validation tests, while measured results from the constructed optimized antenna design closely replicated the predicted antenna patterns and the predicted input impedance value. The design methodology eliminated numerous antenna builds by applying straight-forward RSM techniques and saved countless man hours. The significant time savings found using this optimized design methodology demonstrates the power of RSM and motivates its application to other electromagnetic design problems.				
14. SUBJECT TERMS Response Surface Methodology, microstrip antenna, optimization, Analysis of Variance, design methodology, empirical modeling, full factorial designed experiment			15. NUMBER OF PAGES 135	
			16. PRICE CODE	
17. SECURITY CLASSIFICATION OF REPORT UNCLASSIFIED	18. SECURITY CLASSIFICATION OF THIS PAGE UNCLASSIFIED	19. SECURITY CLASSIFICATION OF ABSTRACT UNCLASSIFIED	20. LIMITATION OF ABSTRACT UL	

GENERAL INSTRUCTIONS FOR COMPLETING SF 298

The Report Documentation Page (RDP) is used in announcing and cataloging reports. It is important that this information be consistent with the rest of the report, particularly the cover and title page. Instructions for filling in each block of the form follow. It is important to *stay within the lines* to meet *optical scanning requirements*.

Block 1. Agency Use Only (Leave blank).

Block 2. Report Date. Full publication date including day, month, and year, if available (e.g. 1 Jan 88). Must cite at least the year.

Block 3. Type of Report and Dates Covered. State whether report is interim, final, etc. If applicable, enter inclusive report dates (e.g. 10 Jun 87 - 30 Jun 88).

Block 4. Title and Subtitle. A title is taken from the part of the report that provides the most meaningful and complete information. When a report is prepared in more than one volume, repeat the primary title, add volume number, and include subtitle for the specific volume. On classified documents enter the title classification in parentheses.

Block 5. Funding Numbers. To include contract and grant numbers; may include program element number(s), project number(s), task number(s), and work unit number(s). Use the following labels:

C - Contract	PR - Project
G - Grant	TA - Task
PE - Program Element	WU - Work Unit Accession No.

Block 6. Author(s). Name(s) of person(s) responsible for writing the report, performing the research, or credited with the content of the report. If editor or compiler, this should follow the name(s).

Block 7. Performing Organization Name(s) and Address(es). Self-explanatory.

Block 8. Performing Organization Report Number. Enter the unique alphanumeric report number(s) assigned by the organization performing the report.

Block 9. Sponsoring/Monitoring Agency Name(s) and Address(es). Self-explanatory.

Block 10. Sponsoring/Monitoring Agency Report Number. (If known)

Block 11. Supplementary Notes. Enter information not included elsewhere such as: Prepared in cooperation with....; Trans. of....; To be published in.... When a report is revised, include a statement whether the new report supersedes or supplements the older report.

Block 12a. Distribution/Availability Statement.

Denotes public availability or limitations. Cite any availability to the public. Enter additional limitations or special markings in all capitals (e.g. NOFORN, REL, ITAR).

DOD - See DoDD 5230.24, "Distribution Statements on Technical Documents."

DOE - See authorities.

NASA - See Handbook NHB 2200.2.

NTIS - Leave blank.

Block 12b. Distribution Code.

DOD - Leave blank.

DOE - Enter DOE distribution categories from the Standard Distribution for Unclassified Scientific and Technical Reports.

NASA - Leave blank.

NTIS - Leave blank.

Block 13. Abstract. Include a brief (*Maximum 200 words*) factual summary of the most significant information contained in the report.

Block 14. Subject Terms. Keywords or phrases identifying major subjects in the report.

Block 15. Number of Pages. Enter the total number of pages.

Block 16. Price Code. Enter appropriate price code (*NTIS only*).

Blocks 17. - 19. Security Classifications. Self-explanatory. Enter U.S. Security Classification in accordance with U.S. Security Regulations (i.e., UNCLASSIFIED). If form contains classified information, stamp classification on the top and bottom of the page.

Block 20. Limitation of Abstract. This block must be completed to assign a limitation to the abstract. Enter either UL (unlimited) or SAR (same as report). An entry in this block is necessary if the abstract is to be limited. If blank, the abstract is assumed to be unlimited.